High-speed Coherent Optical Orthogonal Frequency-Division Multiplexing Design and Implementation

by

Qi Yang

Submitted in total fulfilment of
the requirements for the degree of
Doctor of Philosophy

Department of Electrical & Electronic Engineering

The University of Melbourne

Australia

August, 2010

Abstract

High-speed Coherent Optical Orthogonal Frequency-Division Multiplexing Design and Implementation

by **Qi Yang**

We have witnessed a dramatic increase of interest in orthogonal frequency-division multiplexing (OFDM) from optical communication community in recent years. The number of publications on optical OFDM has grown dramatically since it was proposed as an attractive modulation format for long-haul transmission either in coherent detection or direct-detection. Over the last few years, net transmission data rates grew at a factor of 10 per year at the experimental level. These progresses may eventually lead to realization of commercial transmission products based on optical OFDM in the future, with the potential benefits of high spectral efficiency and flexible network design.

As the IP traffic continues to grow at a rapid pace, 100 Gb/s Ethernet is being considered as the new generation transport standard for IP networks. As the data rate approaches 100 Gb/s and beyond, the electrical bandwidth required for CO-OFDM would be at least 15 GHz and may not be cost-effective to implement even with the best commercial digital-to-analog converters (DAC) and analog-to-digital converters (ADC) in silicon integrated circuit (IC). To overcome this electrical bandwidth bottleneck, we propose and demonstrate the concept of OBM-OFDM to divide the entire OFDM spectrum into multiple orthogonal bands. Due to the inter-band orthogonality, the multiple OFDM bands with zero or small guard bands can be multiplexed and de-multiplexed without inter-band interference. With this scheme, transmission of 107 Gb/s CO-OFDM signal over 1000 km (10×100 km) standard single mode fiber (SSMF) has been realized using only erbium-doped fiber amplifier (EDFA) and without a need for optical dispersion compensation.

Large amount of optical OFDM studies are reported based on offline processing using high-speed sampling scope which show many advantages of optical OFDM systems achieving over 100 Gb/s aggregated data rate and over thousands of km in transmission distance. However, many lack discussion on the potential implementation difficulties. Special requirements of optical communication systems such as several order of magnitude higher data rate than wireless counterpart requires careful studies in feasible real-time implementation. We demonstrate a field-programmable gate array (FPGA) based real-time

CO-OFDM receiver at a sampling speed of 2.5 GS/s, and show its performance in receiving a subband of a 53.3 Gb/s multi-band signal. Additionally, by taking advantage of the multi-band structure of the OFDM signal, we successfully characterize a 53.3 Gb/s CO-OFDM signal in real-time by measuring one of its subbands at a time (3.55 Gb/s).

Transmission bandwdith of ever-advacing optical transport is one of the important cost-drivers. To save the transmission bandwidth, using advanced coding to improve system performance without the bandwidth extension is a promising technique. We show two approaches with different coding scheme for CO-OFDM - trellis coded modulation (TCM) and low-density-parity-check (LDPC). Both schemes are demonstrated using CO-OFDM with higher order moulation format for long haul transmission. The superior system performance of these two schemes shows that the combination of advanced coding with high-level modulation may be a promising technique to support high-spectral-efficiency and high-performance CO-OFDM transmission.

This is to certify that

(i) the thesis comprises only my original work,

(ii) due acknowledgement has been made in the text to all other material used,

(iii) the thesis is less than 100,000 words in length, exclusive of table, maps, bibliographies, appendices and footnotes.

Signature

Date

Declaration

I hereby declare that this thesis comprises only my original work. No material in this thesis has been previously published and written by another person, except where due reference is made in the text of the thesis. I further declare that this thesis contains no material which has been submitted for a degree or diploma or other qualifications at any other university. Finally, I declare that the thesis is less than 100,000 words in length, exclusive of tables, figures, bibliographies, appendices and footnotes.

Acknowledgments

This dissertation would not have been possible without the support and encouragement of many people throughout my education, whether explicitly mentioned here or not, and to these people I express my deep appreciation.

Firstly, I would like to express my deepest gratitude to my supervisor Associate Professor William Shieh, and co-supervisor Professor Efstratios Skafidas, for the high quality of their academic advice and direction, and for their generous help and constant support throughout my Ph.D study. I would also like to acknowledge Dr Noriaki Kaneda, Dr Young-Kai Chen at Bell Laboratories in Murray Hill, US, for giving me the opportunity to undertake an unforgettable and productive internship. Special thanks go to Dr. Xiang Liu at Bell Laboratories for his academic and personal supports.

I feel grateful to the Victoria Research Laboratory, National ICT Australia, for providing my PhD top-up scholarship, conference and internship travel expenses. I also appreciate the support I have received from the University of Melbourne through IPRS and MIRS scholarships. Many thanks go to my colleagues around me for providing a friendly and entertaining working environment.

My special thanks to my research partners within Associate Professor William Shieh's research group. We had many productive and insightful discussions. I am grateful to Dr. Xingwen Yi for guidance in various aspects of the experimental studies. I appreciate the collaboration opportunity with Yan Tang, Yiran Ma, Abdullah Al Amin, Xi Chen, Simin Chen, An Li, and Prof. Zhengrong Tong on several projects.

On a personal level, I am forever indebted to my parents for the love they provided me through my entire life.

Contents

List of Figures

1 Introduction

1.1 Overview

The Internet traffic from data, voice and video services is driving the bandwidth demand of telecommunication networks dramatically. This in turn has put much pressure on core networks. Figure 1 (a) shows the evolution of data traffic where the traffic increases about 5 times within every 3 years [1]. Figure 1(b) and (c) show the fast increase in traffic growth from Corning [2] and [3]. The 100G Ethernet has been recognized a necessary in the end of the last decade. Moreover, driven by the rapid advances of CMOS digital signal processing technologies, 100 Gb/s Ethernet (100 GbE) has become increasingly a commercial reality [4].

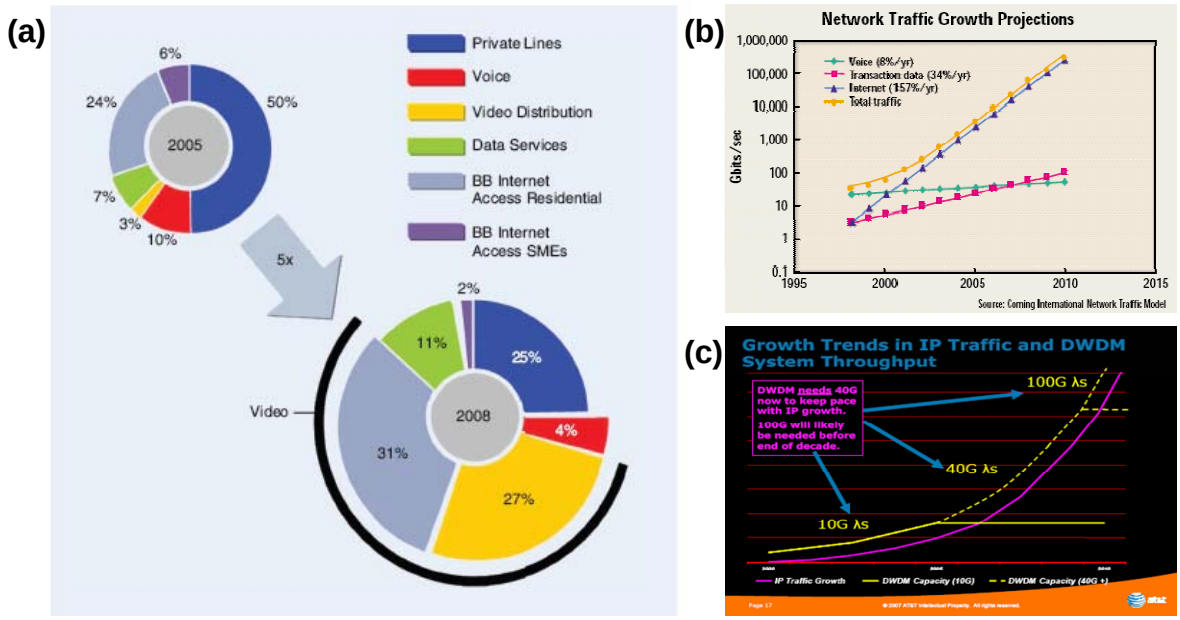

Figure 1. Growth of the Internet traffic: (a) Evolution of data traffic composition. BB: broadband; SME: small and medium-sized enterprises; (b) Network traffic growth projections from Corning. (c) Growth trends in IP traffic and DWDM system throughput.

In order to meet the demands of high capacity transport network, especially for 100G Ethernet and beyond, worldwide research and development effort on high-speed transmission is in full swing. To increase the data rate per wavelength to 100 Gb/s and beyond, the main issues are identified as follows：

- Bandwidth expansion

One straightforward approach to enhancing the capacity is to increase the transmission bandwidth per wavelength, electrically or optically. In optical fiber communications, two techniques for increasing the transmission capacity are widely used: (1) extending the

bandwidth by adding multiple optical carriers, and (2) extending the electronic bandwidth per wavelength. The former has already been widely studied and is well known as wavelength division multiplexing (WDM). Using WDM, the transmission bandwidth can be easily extended by adding more transceivers for the existing fiber links without installation and alternation of the fiber link. Such an approach can be considered as one of the most cost efficient ways to increase the optical link throughput [5]. The latter relies on the state-of-art CMOS technology. However, the current commercial digital-to-analog converters (DACs) / analog-to-digital converters (ADCs) in silicon integrated circuit (IC) can only run at a bandwidth of 6 GHz [6], indicating that to realize 100 Gb/s transmission directly is challenging in a cost-effective manner [7]. Nevertheless, most recently the high speed DAC/ADC has achieved more than 30 giga-sample per second (GS/s) with > 20GHz analog bandwidth, which potentially can support 100 Gb/s transmission [8].

- Spectral efficiency enhancement

One of the most critical figure-of-merits in optical communications is spectral efficiency, which is defined as the information capacity per unit bandwidth. The existing optical network mainly utilizes intensity modulation and direct detection (IM/DD) for the transmission. Most of them use binary modulation, which reduces the complexity of transmitter and receiver. However, using binary modulation, regardless of detection techniques, spectral efficiency cannot exceed 1 bit/s/Hz [9]. Recently, in order to increase the system capacity, many advanced modulation formats in amplitude, phase, and polarization of the signal have been widely studied. With advanced modulation formats combined with the coherent detection technology, spectral efficiency with several bit/s/Hz can be easily achieved [10]. The recent surge of the interests in advanced modulation formats began from multilevel phase/amplitude modulation to polarization division multiplexing. Although the research on optical OFDM can be traced back ten years ago [11], it only started to receive great attention after it was proposed as an attractive modulation format for long-haul transmission either in coherent detection [12] or direct-detection [13, 14]. The synergies between coherent optical communications and OFDM are two-fold. The coherent system brings OFDM a much needed linearity in RF-to-optical (RTO) upconversion and optical-to-RF (OTR) downconversion. OFDM brings coherent system computation efficiency and ease of channel and phase estimation [15]. In spite of the fact that all the current coherent optical OFDM (CO-OFDM) experimental demonstrations use off-line signal processing [16-21], the complementary metal–oxide semiconductor (CMOS) application-specific integrated circuit (ASIC) chips

recently have demonstrated for single carrier coherent systems [22,23] signify that the current silicon speed can support 40 Gbit/s OFDM transmission systems. Because of its superior scalability with the bit rate of the transmission systems, CO-OFDM is well-positioned to be an attractive choice of modulation format for the next generation of 100 Gb/s transmission.

Although great number of optical OFDM studies are reported based on offline processing using high-speed sampling scopes demonstrating many advantages of optical OFDM systems at 100 Gb/s aggregated data rate over thousands of kilometers in transmission distance [16-21], many lack discussion on the possible implementation difficulties. Special requirement of optical communication system such as several order of magnitude higher data rate than wireless counterpart requires careful study on feasible real-time implementation of the high-speed optical OFDM systems. As of the time of this writing, several demonstrations of real-time reception have been reported for both coherent single-carrier [6,24,25] and CO-OFDM signals [26-29]. With the state-of-art ASIC technology, 40 Gb/s and 100 Gb/s optical OFDM transceivers are foreseeable in the near future.

As the line rate has reached up to 1 Tb/s using off-line signal processing, and real-time demonstration has shown to support beyond 40 Gb/s, many other attractive research topics are currently being investigated, such as nonlinearities of optical OFDM, high spectral efficiency, etc. Among these topics, the advanced coding is a promising technique to achieve enhanced optical transmission performance. Traditionally, forward error correction (FEC) requires extending the signal bandwidth to fill the coding overhead. As signal spectrum efficiency (SE) becomes greatly valuable nowadays, researchers are seeking some approaches to improve the system performance while main the SE.

Therefore, this thesis will be laid out according to the above-mentioned aspects: (i) demonstration of 107 Gb/s optical OFDM over 1000 km standard signal mode fiber (SSMF); (ii) implementation of real-time optical OFDM; (iii) advanced coding for coherent optical OFDM. Additionally, some other techniques to improve the optical OFDM performance based on channel estimation will be also discussed in a separate section.

1.2 Motivations of the Thesis

In this section, the motivations for the research in the thesis are shown, organized into four parts. Firstly, the motivations for the 100 Gb/s optical transmission aided by the electronic DSP is presented. So far, the research on optical OFDM has achieved up to 10 Tb/s transmission data rate over tens of thousands kilometers reaches [30]. However, most of the

reports are based on offline processing. Thus the real-time investigation is highly desired, which is discussed in the 1.2.2. In section 1.2.3, the aim of using advanced coding to improve the system performance is presented. In the last section 1.2.4, some advanced techniques for CO-OFDM will be presented, such as bit and power loading, and a special channel estimation algorithm.

1.2.1 100 Gb/s coherent optical OFDM transmission

Optical fiber communications has several advantages over the RF counterpart, such as low transmission loss and enormous bandwidths, etc. However, when the optical signal is transmitted or received in the electrical domain, the limitation of the RF bandwidth will dominate. For instance, a 107 Gb/s optical OFDM signal needs ~30-GHz optical bandwidth including the 7% FEC overhead. Using coherent detection, the minimum required electrical bandwidth is ~15 GHz [7]. However, by the year of 2008, the best commercial DACs/ADCs in silicon integrated circuit were only run at a bandwidth of 6 GHz [6]. Thus, to implement 100 Gb/s OFDM transmission is challenging in a cost-effective manner. Therefore, the following questions need to be answered for 100 Gb/s CO-OFDM implementation and transmission:

- Can 100 Gb/s signals be generated/received using the state-of-art electronic DSP?
- What is the impact of multiband portioning on CO-OFDM generation and detection?

1.2.2 Multi-gigabit/s real-time coherent optical OFDM transmission

Real-time coherent optical single carrier demonstration was first proposed in 2006 [31,32]. In the single-carrier scheme, the main digital signal processing is based on constant-modulus algorithm (CMA) and finite impulse response (FIR) digital filters. Such filters can be easily implemented on ASICs. In contrast, OFDM is based on frame and symbol structure. Time-domain and frequency-domain conversion are essential for OFDM. Like FFT, some digital signal processing procedures require complex computation in ASIC design, such as complex number multiplication. Consequently, to implement real-time optical OFDM, the following three restricts must be carefully considered:

- Optical OFDM transmitter and receiver setup

Unlike single-carrier counterpart, OFDM requires DAC to generate OFDM time-domain signal like an arbitrary wave generation (AWG) at the transmitter part. Compared to offline processing, the real-time requires that signal be processed in multiple ‘channels’. Currently,

the digital signal processor only can run at a few hundreds of megahertz, while the fast DAC/ADC can be operated at a few Gigahertzes. Thus signal has to be parallel processed within multiple channels in the processor. The high speed signal has to be firstly multiplexed into high speed serial data in the transmitter, and lastly de-multiplexed for the digital signal processing in the receiver. Furthermore, precise alignment in the high speed interface is essential.

- Efficient digital signal processing algorithms

In OFDM scheme, there are several main signal processing procedures, such as window synchronization, (inverse) discrete Fourier transform, channel estimation, phase estimation, etc. To implement those procedures into one chip, the algorithms have to be efficient in resource consumption, and suitable for parallel channel processing.

- Resource consumption

In addition to the DSP algorithms that can be implemented, other important considerations for real-time optical OFDM are the hardware limitation, resource usage, and FPGA/ASIC capacity. For instance, the resolution of ADC has the influences on the system performance, and also affects the entire hardware resources. Some limited resources, such as number of multipliers, must be carefully considered. It is the main limitation for the real-time CO-OFDM implementation using FPGA.

1.2.3 Advanced coding for CO-OFDM transmission without bandwidth extension

One of the main advantages of coherent optical OFDM is the high spectral efficiency. In 2009, the transmission with QPSK modulation has achieved 1-Tb/s net rate with spectrum efficiency of 3.3 bit/s/Hz [19,20]. To further increase the transmission rate, two approaches are widely used: (i) to occupy wider optical bandwidth; (ii) to use higher order modulation, and increase the spectrum efficiency. As the fiber transmission bandwidth is constrained by the EDFA bandwidth, only a small fraction of the overall fiber bandwidth can be used (~70 nm). Thus, approach (ii) is becoming more attractive. Nowadays researches have started to employ the whole C and L band in the fiber communication with up to 32-QAM constellation mapping [33,34]. Up to now, the optical spectrum efficiency has broken 10 bit/s/Hz with 128-QAM in dual polarizations [35]. However, higher order modulation leads to sacrifice of the OSNR. In a nutshell, to improve the system performance with the same bandwidth has

become a promising technique.

1.2.4 Some advanced techniques for CO-OFDM based on channel estimation

In CO-OFDM, channel estimation is essential as it affects the transmission system performance. The information transmission can also be adapted according to the channel characteristics. Traditionally, time-domain channel estimation algorithm requires several training symbols to obtain the channel transfer function. This will introduce a small overhead over the entire net rate. Consequently, a channel estimation algorithm that can have the same performance while reducing the overhead from training symbols will be desirable for CO-OFDM transmission. Moreover, when the channel information is feedback to the transmitter, the transmit signal can be modified to fit the channel transmission characteristics. The subcarriers with better performance can be loaded with higher modulation. By doing so, the net rate can be increased. Suitable power loading adjustment can help to further improve the transmission performance.

1.3 Thesis outline

The organization of this thesis is laid out as follows:

Chapter 1: Introduction

Overview of coherent optical OFDM development and introduction of the thesis is presented in this chapter.

Chapter 2: Basics of Optical OFDM

Before discussing the designs and implementations, the basics of optical OFDM are firstly shown in this chapter. Several main aspects in optical OFDM are discussed, such as orthogonality, discrete Fourier transform, and cyclic prefix. Two flavors of optical OFDM are briefly discussed: direct-detection optical OFDM (DDO-OFDM) and Coherent optical OFDM (CO-OFDM).

Chapter 3: 107 Gb/s CO-OFDM long haul transmission

In this chapter, the implementation of 107 Gb/s CO-OFDM over 1000 km is fully discussed. Using orthogonal-band-multiplexing, the electrical bandwidth limitation can be overcome. The influence of multi-band detection for CO-OFDM will also be discussed.

Chapter 4: Real-time CO-OFDM Implementation

This chapter shows the implementation of real-time CO-OFDM based on FPGA. Several digital signal processing algorithms for real-time implementation are discussed. Moreover, some important implementation issues, such as resource restrictions will be shown in this chapter.

Chapter 5: Advanced Coding for CO-OFDM Without Bandwidth Extending

In this chapter, two schemes based on advanced coding for CO-OFDM are presented. The transmission performances are much improved for both back-to-back and long haul transmission cases while the signal bandwidth remains the same.

Chapter 6: Some Advanced Techniques for CO-OFDM Based On Channel Estimation

Two advanced techniques for CO-OFDM based on channel estimation are shown in this chapter. Firstly, a channel estimation based on frequency-domain averaging algorithm is discussed. Secondly, the bit and power loading algorithms for optical OFDM are proposed, which can increase the transmission net rate or improve the receiver sensitivity.

Chapter 7: Conclusion

This chapter summaries the described design and implementation for coherent optical OFDM in this thesis. All the demonstrations show that the coherent optical OFDM is being an attractive modulation format, which may be widely used for next generation networks. .

1.4 Contribution of the thesis

The contributions of the thesis are listed as follows:

Chapter 3

- We propose a novel approach, namely orthogonal-band-multiplexed (OBM) OFDM, which can subdivide the entire OFDM spectrum into multiple orthogonal bands in order to avoid the electrical bandwidth bottleneck.

- We show the world-first experiment of 107 Gb/s coherent optical OFDM through optical realization of OBM-OFDM. A numerical simulation for both single channel and WDM transmission is conducted to verify the feasibility of the demonstrated OBM-OFDM experiment system.

- Guard band influence of OBM-OFDM is discussed. It is observed that when the orthogonality between OFDM subcarriers or sub-bands is maintained, no penalties are observed for OBM-OFDM signals.

Chapter 4

- We experimentally demonstrate the world-first experiment of real-time demonstration with 3.6 Gb/s per single subband for optical OFDM. Additionally, using the concept of OBM-OFDM, net rate up to 54 Gb/s can be achieved.

- We analyze various practical optical OFDM algorithms for real-time implementation.

- Several practical considerations over real-time CO-OFDM are shown, such as bit-resolution and hardware resource, etc.

Chapter 5

- We theoretically study the trellis coded modulation for CO-OFDM transmission, and experimentally demonstrate the CO-OFDM with trellis coded 32-QAM. The system sensitivity is much improved by expanding the constellation, while the transmission bandwidth remains the same.

- We also demonstrate 428 Gb/s low-density-parity-check coded 16-QAM. Combined with rate ½ low-density parity-check (LDPC) coding, both high spectrum efficiency and improved sensitivity are achieved without the signal bandwidth extension.

Chapter 6

- We experimentally demonstrate the effectiveness of the CO-OFDM transmission based on frequency-domain averaging channel estimation algorithm. Compared to time-domain averaging, frequency-domain averaging channel estimation algorithm shows comparable performance with much reduced overhead.

- We show the experiment demonstration of CO-OFDM systems with bit and power loading. The net rate can be increased without modifying the channel bandwidth and launch power. The system performance is further improved through optimal power loading into each modulation band.

1.5 Publications arising from the work completed in this thesis

1. Qi Yang, Yiran Ma, and William Shieh "107 Gb/s Coherent Optical OFDM Reception Using Orthogonal Band Multiplexing", in Proc. Optical Fiber Communication (OFC) Conference 2008, PDP 7, 2008
2. Qi Yang, Noriaki Kaneda, Xiang Liu, Sethumadhavan Chandrasekhar, William Shieh, and Young-Kai Chen, "Real‐Time Coherent Optical OFDM Receiver at 2.5-GS/s for Receiving a 54 Gb/s Multi‐Band Signal" in Proc. Optical Fiber Communication (OFC) Conference 2009, PDPC5, 2009.
3. Qi Yang, Noriaki Kaneda, Xiang Liu, Sethumadhavan Chandrasekhar, William Shieh, and Young-Kai Chen, "Towards Real-Time Implementation of Optical OFDM Transmission", in Proc. Optical Fiber Communication (OFC) Conference 2010, Invited paper No.826, 2010.
4. Qi Yang, Yan Tang, Yiran Ma, and William Shieh "Experimental Demonstration and Numerical Simulation of 107 Gb/s High Spectral Efficiency Coherent Optical OFDM", Journal of Lightwave Technology, vol. **27**, issue 3, pp. 168-176, 2009.
5. Qi Yang, Simin Chen, Yiran Ma, and William Shieh, "Real-time reception of multi-gigabit coherent optical OFDM signals," Opt. Express **17**, 7985-7992, 2009.
6. Q. Yang, N. Kaneda, X. Liu, and W. Shieh, "Demonstration of frequency-domain averaging based channel estimation for 40 Gb/s CO-OFDM with high PMD," in Proc. Optical Fiber Communication (OFC) Conference 2009, paper OWM6, 2009.
7. Qi Yang, Kaneda, N., Xiang Liu, and Shieh, W., "Demonstration of Frequency-Domain Averaging Based Channel Estimation for 40 Gb/s CO-OFDM With High PMD," Photonics Technology Letters, IEEE , vol.**21**, no.20, pp.1544-1546, 2009.
8. Qi Yang, Yiran Ma, and William Shieh, "1-Tb/s Signal-channel Coherent Optical OFDM Transmission with Trellis-coded Modulation", Electronics Letters, pp 1045-1047, 2009.
9. Qi Yang, Yiran Ma, and William Shieh, "1-Tb/s Signal-channel Coherent Optical OFDM Transmission with Trellis-coded Modulation", in Opto-Electronics and Communications (OECC) Conference 2009, paper ThJ3, 2009.
10. Qi Yang, William Shieh, and Yiran Ma, "Guard-band influence on orthogonal-band-multiplexed coherent optical OFDM", Optics Letters, vol. **33**, issue 19, pp. 2239-224, 2008.
11. Qi Yang, William Shieh, and Yiran Ma, "Bit and Power Loading for Coherent Optical OFDM", Photonics Technology Letters, volume 20, issue **15**, pp 1305-1307, 2008.

12. Qi Yang, William Shieh, and Yiran Ma, "Bit and Power Loading for Coherent Optical OFDM", in Opto-Electronics and Communications (OECC) Conference 2008.
13. Qi Yang, Xiang Liu, S. Chandrasekhar, and William Shieh, "Experimental Demonstration of 44 Gb/s Coherent. Optical OFDM with Trellis-Coded 32-QAM", in Opto-Electronics and Communications Conference (OECC) 2010, paper 8B4-2, 2010.
14. Qi Yang, Abdullah Al Amin, Xi Chen, Yiran Ma, Simin Chen, and William Shieh, "428 Gb/s single-channel coherent optical OFDM transmission over 960 km SSMF with constellation expansion and LDPC coding," Opt. Express **18**, 16883-16889, 2010
15. W. Shieh, Q. Yang, and Y. Ma, "107 Gb/s coherent optical OFDM transmission over 1000 km SSMF fiber using orthogonal band multiplexing," Opt. Express **16**, 6378-6386, 2008
16. W. Shieh, X. Yi, Y. Ma, and Q. Yang, "Coherent optical OFDM: has its time come? [Invited]," J. Opt. Netw. **7**, 234-255, 2008
17. William Shieh, Yiran Ma, Qi Yang, Simin Chen, and Yan Tang, "Transmission Channel Rate for Coherent Optical OFDM - Is the Sky the Limit?", IEEE annual meeting 2009, invited paper.
18. Xiang Liu, Qi Yang, S. Chandrasekhar, and William Shieh, "Transmission of 44 Gb/s Coherent Optical OFDM Signal with Trellis-Coded 32-QAM Subcarrier Modulation", in Proc. Optical Fiber Communication (OFC) Conference 2010, OMR3, 2010.
19. Kaneda, N., Qi Yang, Xiang Liu, Chandrasekhar, S., Shieh, W., and Young-Kai Chen, "Real-Time 2.5 GS/s Coherent Optical Receiver for 53.3 Gb/s Sub-Banded OFDM", Journal of Lightwave Technology, vol.**28**, no.4, pp.494-501, 2010.
20. Noriaki Kaneda, Xiang Liu, Young-Kai Chen, Qi Yang, William Shieh, "Realizing Real-Time Implementation of Coherent Optical OFDM Receiver with FPGAs", in Opto-Electronics and Communications (OECC) Conference 2009, invited paper, 5.4.4, 2010.
21. Yiran Ma, Qi Yang, Yan Tang, Simin Chen, William Shieh, "1-Tb/s per Channel Coherent Optical OFDM Transmission with Subwavelength Bandwidth Access", in Proc. Optical Fiber Communication (OFC) Conference 2009, PDPC1.
22. Yiran Ma, Qi Yang, Yan Tang, Simin Chen, and William Shieh, "1-Tb/s Single-Channel Coherent Optical OFDM Transmission With Orthogonal-Band Multiplexing and Subwavelength Bandwidth Access", J. Lightwave Technol. **28**, 308-315, 2010.

23. Yiran Ma, Qi Yang, Yan Tang, Simin Chen, and William Shieh, "1-Tb/s Single-Channel Coherent Optical OFDM Transmission over 600 km SSMF Fiber with Subwavelength Bandwidth Access", Optics Express, vol. **17**, issue 11, pp. 9421-9427, 2009.
24. Yiran Ma, Qi Yang, Simin Chen, and William Shieh, "Multi-tone generation using a recirculating frequency shifter and its application to 1-Tb/s coherent optical OFDM signal", in Opto-Electronics and Communications (OECC) Conference 2009, paper ThLP75, 2009.
25. Yiran Ma, William Shieh, and Qi Yang, "Bandwidth-Efficient 21.4 Gb/s Coherent Optical 2x2 MIMO OFDM Transmission", in Proc. Optical Fiber Communication (OFC) Conference 2008, JWA59, 2008.
26. Zhengrong Tong, Qi Yang, Yiran Ma, and William Shieh, "21.4 Gb/s Coherent Optical OFDM Transmission over 200 km Multimode Fiber", in Optoelectronics and Communications Conference (OECC), 2008, postdeadline paper PDP5, 2008.
27. Zhengrong Tong, Qi Yang, Yiran Ma, and William Shieh, "21.4 Gb/s Coherent Optical OFDM Transmission over 200 km Multimode Fiber", Electrical Letters, vol. **44**, issue 23, pp:1373-1374, 2008.
28. Simin Chen, Qi Yang, Yiran Ma, and William Shieh, "Multi-gigabit Real-time Coherent Optical OFDM Receiver", in Proc. Optical Fiber Communication (OFC) Conference 2009, OTuO4, 2009.
29. Simin Chen, Qi Yang, Yiran Ma and William Shieh, "Real-Time Coherent Optical MIMOOFDM Reception up to 6.67 Gbps", in Opto-Electronics and Communications (OECC) Conference 2009, paper ThJ2, 2009.
30. Simin Chen, Qi Yang, and William Shieh, "Demonstration of 12.1 Gb/s Single-Band Real-Time Coherent Optical OFDM Reception", in Opto-Electronics and Communications (OECC) Conference 2010, paper 8B4-2, 2010.
31. Simin Chen, Qi Yang, Yiran Ma, and William Shieh, "Real-Time Multi-Gigabit Receiver for Coherent Optical MIMO-OFDM Signals", Journal of Lightwave Technology, vol. **27**, issue 16, pp. 3699-3704, 2009.

2 Basics of Optical OFDM

Before discussing the main designs and implementations in the thesis, it is necessary to conduct some literature review and basics of coherent optical OFDM. In recent years, we have witnessed a dramatic increase of interest in orthogonal frequency-division multiplexing (OFDM) from optical communication community. The number of publications on optical OFDM has grown dramatically since it was proposed as an attractive modulation format for long-haul transmission either in coherent detection [7] or direct-detection [36,37]. Over the last few years, net transmission data rates grew at a factor of 10 per year at the experimental level. To date, experimental demonstration of up to 10 Tb/s transmission in a single channel [30] has been accomplished whereas demonstration of real-time optical OFDM with digital signal processing has surpassed 40 Gb/s [28]. These progresses may eventually lead to the realization of commercial transmission products based on optical OFDM in the future, with the potential benefits of high spectral efficiency and flexible network design.

2.1 Historical perspective of OFDM

OFDM plays a significant role in the modem telecommunications for both wireless and wired communications. The history of frequency division multiplexing (FDM) began in 1870s when the telegraph was used to carry information through multiple channels [38]. The fundamental principle of orthogonal frequency division multiplexing was proposed by Chang [39] as a way to overlap multiple channel spectra within a limited bandwidth without interference, considering the effects of both filter and channel characteristic. Since then, many researchers have investigated and refined the technique over the years and it has been successfully adopted in many standards. Table 1 shows some of the key milestones of the OFDM technique in RF domain.

Table 1. Historical development of RF-domain OFDM.

1966	R. Chang, foundation work on OFDM [39]
1971	S. B. Weinstein and P. M. Ebert, DFT implementation of OFDM [40]
1980	R. Peled and A. Ruiz, Introduction of cyclic prefix [41]
1985	L. Cimini, OFDM for mobile communications [42]
1995	DSL formally adopted Discrete Multi-tone (DMT), a variation of OFDM.
1995 (1997)	ETSI Digital Audio (Video) Broadcasting Standard, DAB(DVB)

1999 (2002)	Wireless LAN standard, 802.11 a (g), Wi-Fi
2004	Wireless MAN standard, 802.16, WiMax
2009	Long Time Evolution (LTE), 4 G Mobile standard

Although OFDM has been studied in RF domain for over four decades, the research of OFDM in optical communication began only in the late 1990s [11]. The fundamental advantages of OFDM in an optical channel were first disclosed in [43]. In the late 2000s, long-haul transmission by optical OFDM has been investigated by a few groups. Two major research directions appeared, direct-detection optical OFDM (DDO-OFDM) [44,45] looking into a simple realization based on low-cost optical components and coherent optical OFDM (CO-OFDM) [7] aiming to achieve high spectral efficiency and receiver sensitivity. Since then, the interest in optical OFDM increases dramatically. In 2007, the world's first coherent optical OFDM experiment with line rate of 8 Gb/s was reported [46]. In the last few years, the transmission capacity continued to grow about 10 times per year. In 2009, up to 1 Tb/s optical OFDM was successfully experimentally demonstrated [19,20,21]. Table 2 shows the development of optical OFDM in the last two decades.

Table 2 Progress of optical OFDM

1996	Pan and Green, OFDM for CATV [11]
2001	You and Kahn, OFDM in direct modulation (DD) systems [47] Dixon et al., OFDM over multimode fiber [43]
2005	Jolley et al., experiment of 10 Gb/s optical OFDM over multimode fiber (MMF) [48] Lowery and Armstrong, power efficient optical OFDM in DD systems [49]
2006	Lowery and Armstrong [44], and Djordjevic and Vasic [45], long-haul direct-detection optical OFDM (DDO-OFDM) Shieh and Athaudage, long-haul coherent optical OFDM (CO-OFDM) [46]
2007	Shieh et al.[46], 8 Gb/s CO-OFDM transmission over 1000 km
2008	Yang et al., [16], Jansen et al., [17], Yamada et al., [18], >100 Gb/s per single channel CO-OFDM transmission over 1000 km
2009	Ma et al., [19], Dischler et al., [20], Chandrasekhar et al [21] , >1Tb/s CO-OFDM long-haul transmission

Besides offline digital signal processing, from 2009 onwards, a few research groups started to investigate real-time optical OFDM transmission. The first real-time optical OFDM demonstration took place in 2009 [26], three years later than real-time single-carrier coherent optical reception [24,25]. The pace of real-time OFDM development is fast, with the net rate crossing 10 Gb/s and 40Gb/s within one year [28,29]. Moreover, by using orthogonal-band-multiplexing (OBM), which is a key advantage for OFDM, up to 54 Gb/s [26] and 110 Gb/s [50] over 600 km standard signal mode fiber (SSMF) was successfully demonstrated. Most recently, 41.25 Gb/s per single-band was reported in [28]. As evidenced by the commercialization of single-carrier coherent optical receivers, it is foreseeable that real-time optical OFDM transmission with much higher net rate will materialize in the near future based on state-of-the-art ASIC design.

2.2 OFDM fundamentals

Before moving onto the description of optical OFDM transmission, this section will review the basics of OFDM itself, including some fundamental concepts and mathematic expressions. It is well known that OFDM is a special class of multi-carrier modulation (MCM), a generic implementation of which is depicted in Figure 2. The structure of a complex multiplier (I/Q modulator/demodulator), which is commonly used in MCM systems, is also shown in the Figure 2. The key concept of OFDM is the orthogonality of the individual subcarriers.

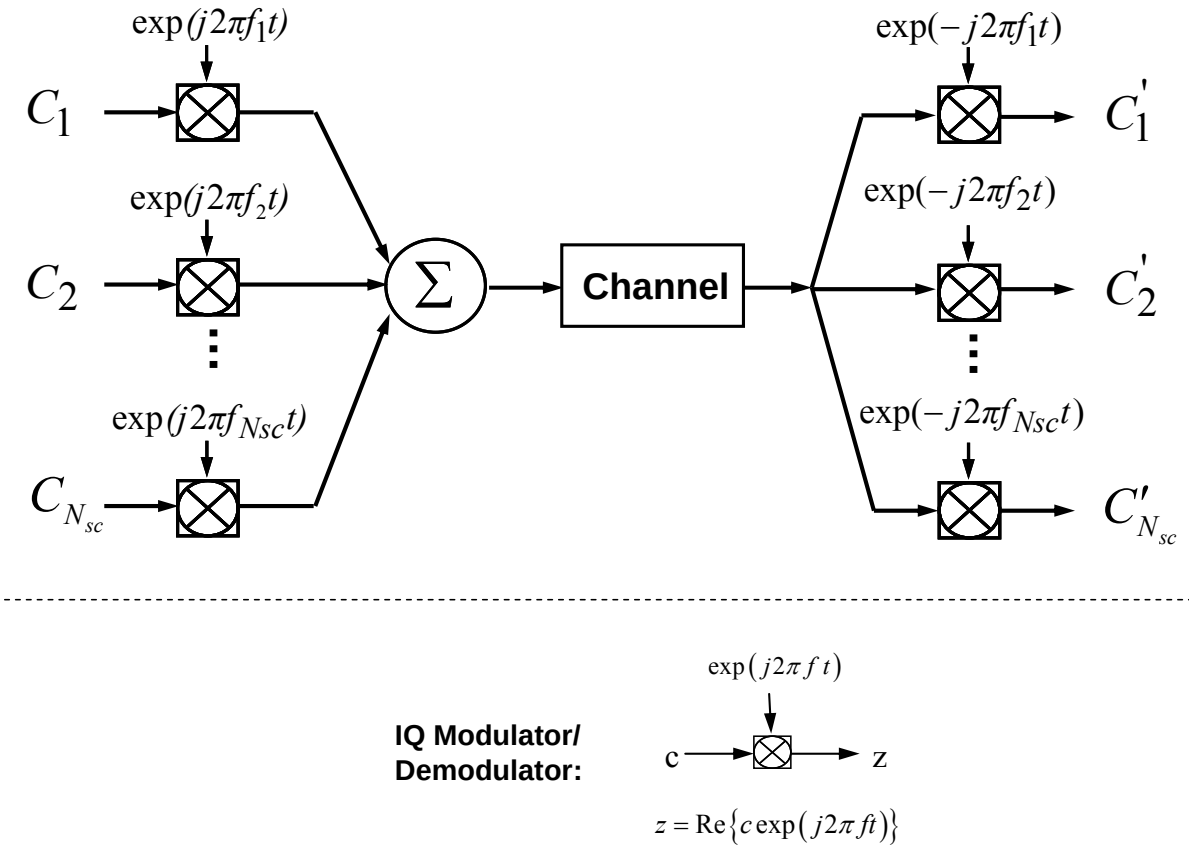

Figure 2. Conceptual diagram for a multi-carrier modulation (MCM) system, such as OFDM.

2.2.1 Orthogonality between OFDM subcarriers and subbands

The MCM transmitted signal $s(t)$ is represented as

$$s(t) = \sum_{i=-\infty}^{+\infty} \sum_{k=1}^{N_{sc}} c_{ki} s_k \left(t - iT_s\right) \tag{1}$$

$$s_k\left(t\right) = \Pi(t)\, \mathrm{e}^{j2\pi f_k t} \tag{2}$$

$$\Pi\left(t\right) = \begin{cases} 1, & \left(0 < t \le T_s\right) \\ 0, & \left(t \le 0, t > T_s\right) \end{cases} \tag{3}$$

where c_{ki} is the ith information symbol at the kth subcarrier, s_k is the waveform for the kth subcarrier, N_{sc} is the number of subcarriers, f_k is the frequency of the subcarrier, and T_s is the symbol period, $\Pi(t)$ is the pulse shaping function. The optimum detector for each subcarrier could use a filter that matches the subcarrier waveform, or a correlator matched to the subcarrier as shown in Figure 2. Therefore, the detected information symbol c'_{ik} at the output of the correlator is given by

$$c'_{ki} = \frac{1}{T_s}\int_0^{T_s} r\left(t - iT_s\right)s^*{}_k dt = \frac{1}{T_s}\int_0^{T_s} r\left(t - iT_s\right)e^{-j2\pi f_k t}dt \tag{4}$$

where $r(t)$ is the received time-domain signal. The classical MCM uses non-overlapped band-limited signals, and can be implemented with a bank of large number of oscillators and filters at both transmit and receive end [51,52]. The major disadvantage of MCM is that it requires excessive bandwidth. This is because in order to design the filters and oscillators cost-effectively, the channel spacing has to be multiple of the symbol rate, greatly reducing the spectral efficiency. A novel approach called orthogonal frequency-division multiplexing (OFDM) was investigated by employing overlapped yet orthogonal signal set [53]. This orthogonality originates from straightforward correlation between any two subcarriers, given by

$$\begin{aligned}\delta_{kl} &= \frac{1}{T_s}\int_0^{T_s} s_k s^*{}_l dt = \frac{1}{T_s}\int_0^{T_s} \exp\left(j2\pi\left(f_k - f_l\right)t\right)dt \\ &= \exp\left(j\pi\left(f_k - f_l\right)T_s\right)\frac{\sin\left(\pi\left(f_k - f_l\right)T_s\right)}{\pi\left(f_k - f_l\right)T_s}\end{aligned} \tag{5}$$

It can be seen that if the following condition

$$f_k - f_l = m\frac{1}{T_s} \tag{6}$$

is satisfied, then the two subcarriers are orthogonal to each other. This signifies that these orthogonal subcarrier sets, with their frequencies spaced at multiple of inverse of the symbol rate can be recovered with the matched filters in (5) without inter-carrier interference (ICI), in spite of strong signal spectral overlapping.

This shows that the orthogonality condition holds for any pair of subcarriers within in an OFDM signal. Moreover, the concept of this orthogonality can be extended to combine multiple OFDM bands into a signal with much larger spectral width. Such approach was first introduced by [16] to flexibly multiply the capacity of a single wavelength. This method of sub-dividing OFDM spectrum into multiple orthogonal bands is so called 'orthogonal-band-multiplexed OFDM' (OBM-OFDM), which will be fully discussed in chapter 3.

2.2.2 Discrete Fourier transform (DFT) implementation of OFDM

We change the expression of (1) as:

$$\tilde{s}(t) = \sum_{i=0}^{N-1} A_i \exp(j2\pi \frac{i}{T} t + \phi_i), \qquad 0 \le t \le T \tag{7}$$

which is the complex form of the OFDM baseband signal.

If we sample the complex signal with a sample rate of 1/T, and add a normalizing factor 1/N, then

$$S_n = \sum_{i=0}^{N-1} A_i \exp(j2\pi \frac{i}{N} n), \qquad n = 0,1,...,N-1 \tag{8}$$

This is exactly the expression of inverse discrete Fourier transform (IDFT). It means that the OFDM baseband signal can be implemented by IDFT. The pre-coded signals are in the frequency domain, and output of the IDFT is in the time domain. In contrast, at the receiver side, the data is recovered by discrete Fourier transform (DFT), which is given by:

$$A_i = \sum_{i=0}^{N-1} S_n \exp(-j2\pi \frac{i}{N} n), \qquad n = 0,1,...,N-1 \tag{9}$$

There are two fundamental advantages of DFT/IDFT implementation of OFDM. First, because they can be very efficiently implemented by (inverse) fast Fourier transform (I)FFT, algorithm, the number of complex multiplications for (I)DFT/IDFT is reduced from N^2 to $(N/2)\cdot \log_2(N)$, almost linearly with the number of subcarrier, N [54]. Second, a large number of orthogonal subcarriers can be generated and demodulated without resorting to very complex RF oscillators and filters. This leads to a relatively simple architecture for OFDM implementation when large number of subcarriers is required.

2.2.3 Cyclic prefix for OFDM

In addition to modulation and demodulation of many orthogonal subcarriers via (I)FFT, one has to mitigate dispersive channel effects such as chromatic and polarization mode dispersions for good performance. In this respect, one of the enabling techniques for OFDM is the insertion of cyclic prefix [55,56]. Let us first consider two consecutive OFDM symbols that undergo a dispersive channel with a delay spread of t_d. For simplicity, each OFDM

symbol includes only two subcarriers with the fast delay and slow delay spread at t_d, represented by 'fast subcarrier' and 'slow subcarrier', respectively. Figure 3 (a) shows that inside each OFDM symbol, the two subcarriers, and 'fast subcarrier' and 'slow subcarrier' are aligned upon the transmission. Figure 3 (b) shows the same OFDM signals upon the reception where the 'slow subcarrier' is delayed by t_d against the 'fast subcarrier'. We select a DFT window containing a complete OFDM symbol for the 'fast subcarrier'. It is apparent that due to the channel dispersion, the 'slow subcarrier' has crossed the symbol boundary leading to the interference between neighboring OFDM symbols, formally, the so-called inter-symbol-interference (ISI). Furthermore, because the OFDM waveform in the DFT window for 'slow subcarrier' is incomplete, the critical orthogonality condition for the subcarriers is lost, resulting in an inter-carrier-interference (ICI) penalty.

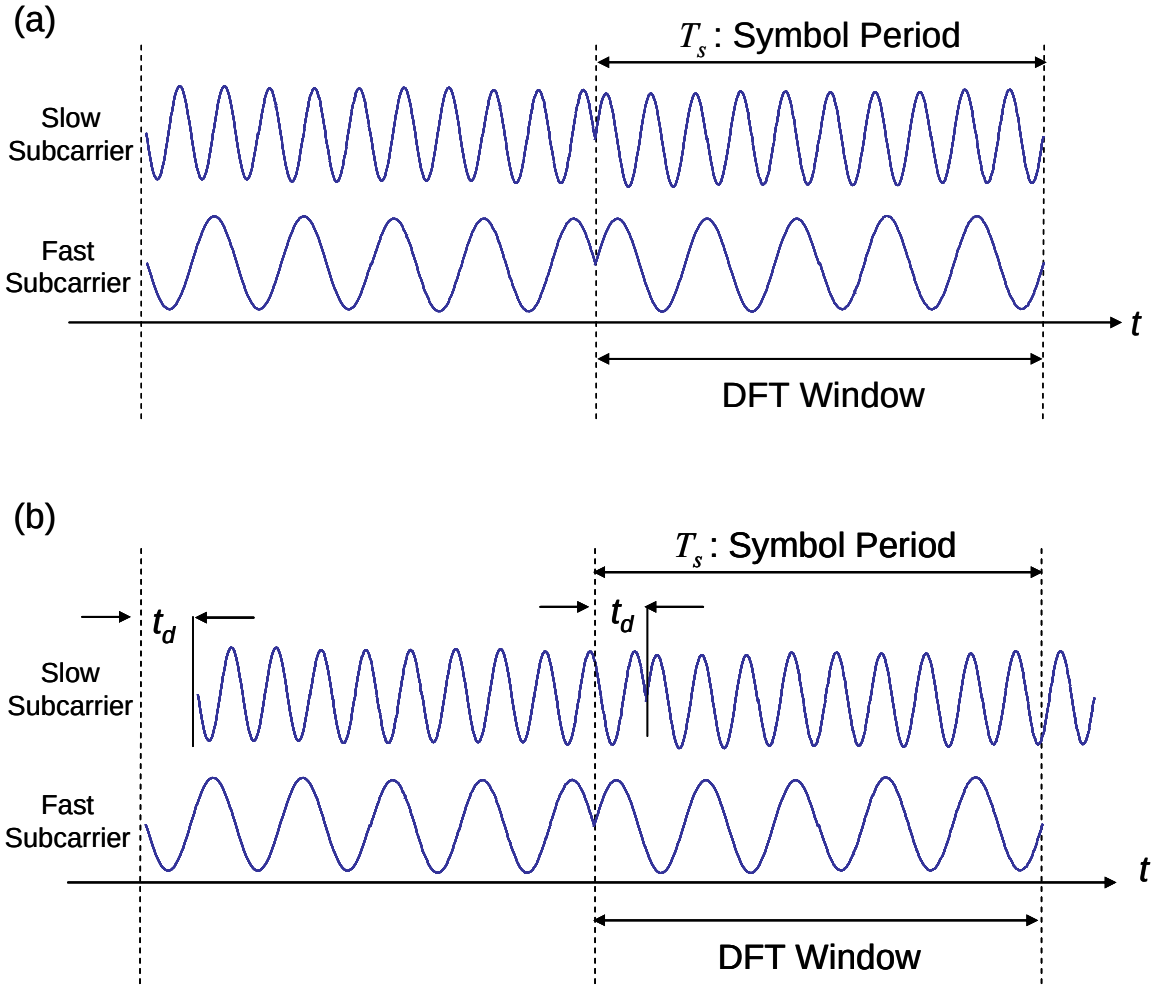

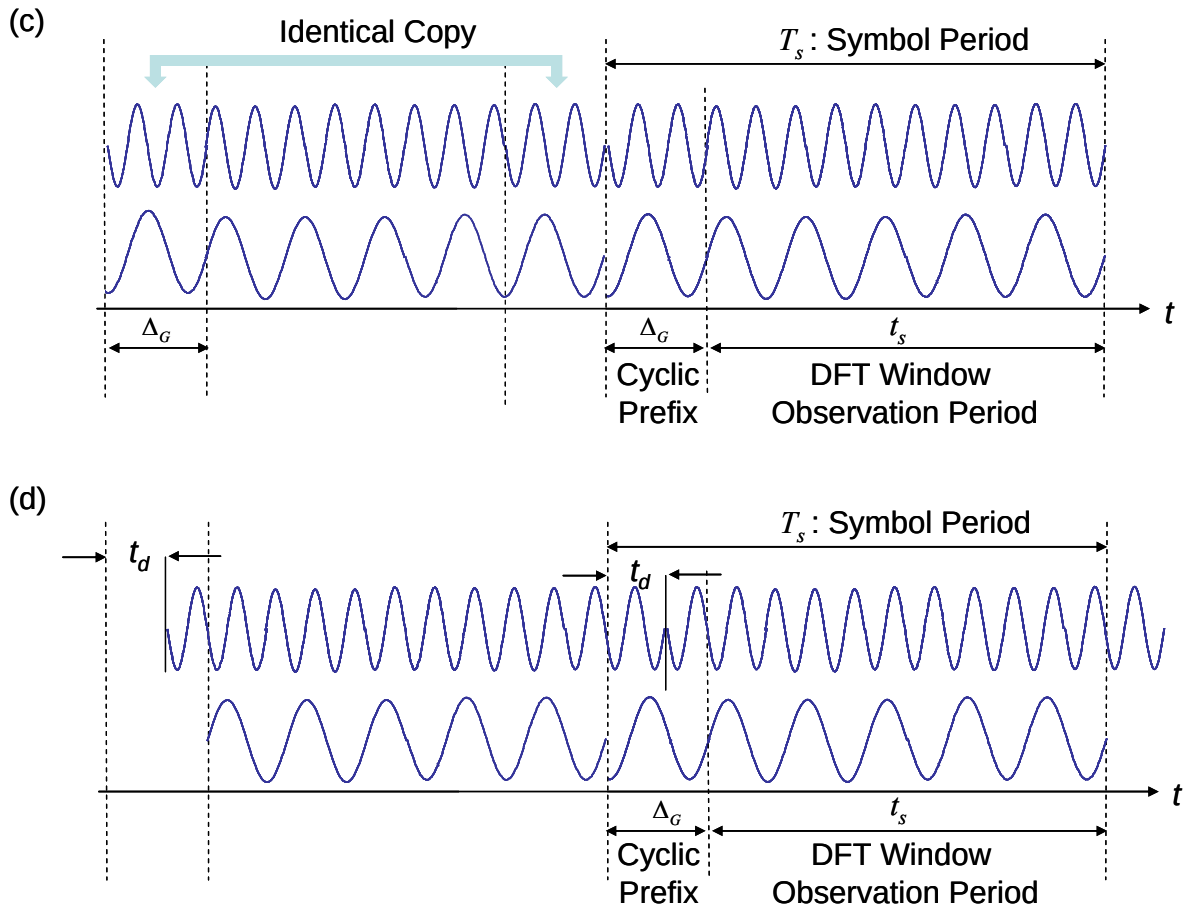

Figure 3. OFDM signals (a) without cyclic prefix at the transmitter, (b) without cyclic prefix at the receiver, (c) with cyclic prefix at the transmitter, and (d) with cyclic prefix at the receiver.

Cyclic prefix was proposed to resolve the channel dispersion induced ISI and ICI [57]. Figure 3 (c) shows insertion of a cyclic prefix by cyclic extension of the OFDM waveform into the guard interval Δ_G. As shown in Figure 3 (c), the waveform in the guard interval is essentially an identical copy of that in the DFT window, with time-shifted by 't_s' forward. Figure 3 (d) shows the OFDM signal with the guard interval upon reception. Let us assume that the signal has traversed the same dispersive channel, and the same DFT window is selected containing a complete OFDM symbol for the 'fast subcarrier' waveform. It can be seen from Figure 3 (d), a complete OFDM symbol for 'slow subcarrier' is also maintained in the DFT window, because a proportion of the cyclic prefix has moved into the DFT window to replace the identical part that has shifted out. As such, the OFDM symbol for 'slow subcarrier' is an 'almost' identical copy of the transmitted waveform with an additional phase shift. This phase shift is dealt with through channel estimation and will be subsequently removed for symbol decision. The important condition for ISI-free OFDM transmission is given by:

$$t_d < \Delta_G \tag{10}$$

It can be seen that after insertion of the guard interval greater than the delay spread, two critical procedures must be carried out to recover the OFDM information symbol properly, namely, (i) selection of an appropriate DFT window, called DFT window synchronization, and (ii) estimation of the phase shift for each subcarrier, called channel estimation or subcarrier recovery. Both signal processing procedures are actively-pursued research topics, and the research on these topics can be found in both books and journal papers [57,58].

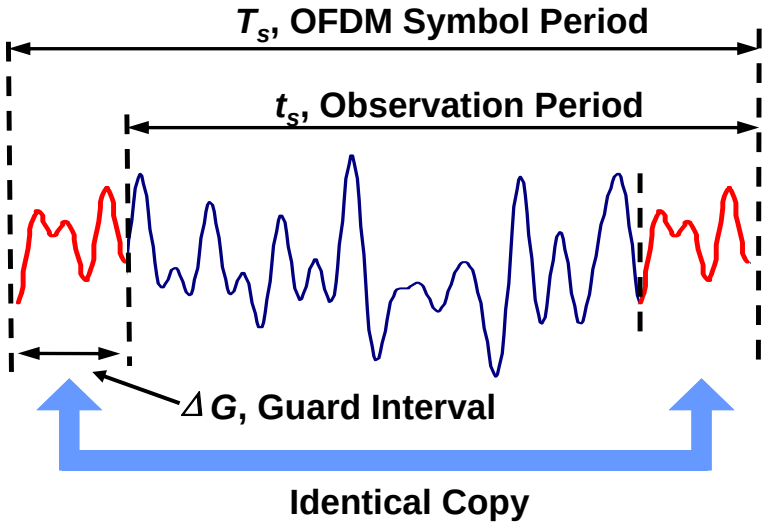

Figure 4. Time-domain OFDM signal for one complete OFDM symbol.

The corresponding time-domain OFDM symbol is illustrated in Figure 4, which shows one complete OFDM symbol comprised of observation period and cyclic prefix. The waveform within the observation period will be used to recover the frequency-domain information symbols.

2.3 Flavors of optical OFDM

One of the major strengths of OFDM modulation format is its rich variation and ease of adaption to a wide range of applications. In wireless systems, OFDM has been incorporated in wireless LAN (IEEE 802. 11a/g, or better known as WiFi), wireless WAN (IEEE 802.16e, or better known as WiMax), and digital radio/video systems (DAB/DVB) adopted in most parts of the world. In RF cable systems, OFDM has been incorporated in Asymmetric Digital Subscriber Line (ADSL) and very-high-rate digital subscriber line (VDSL) broadband access via telephone copper wiring or power line. This rich variation has something to do with the intrinsic advantages of OFDM modulation including dispersion robustness, ease of dynamic

channel estimation and mitigation, high spectral efficiency and capability of dynamic bit and power loading. Recent progress in optical OFDM is of no exception. We have witnessed many novel proposals and demonstrations of optical OFDM systems from different areas of the applications that aim to benefit from the afore-mentioned OFDM advantages. Despite the fact that OFDM has been extensively studied in the RF domain, it is rather surprising that the first report on optical OFDM in the open literature only appeared in 1998 by Pan et al. [11] where they presented in-depth performance analysis of hybrid AM/OFDM subcarrier-multiplexed (SCM) fiber-optic systems. The lack of interest in optical OFDM in the past is largely due to the fact the silicon signal processing power had not reached the point where sophisticated OFDM signal processing can be performed in a CMOS integrated circuit.

Optical OFDM is mainly classified into two main categories: coherent detection and direct detection according to their underlying techniques and applications. While direct detection has been the mainstay for optical communications over the last two decades, the recent progress in forward-looking research has unmistakably pointed to the trend that the future of optical communications is the coherent detection.

Direct-detection optical OFDM (DDO-OFDM) has much more variants than the coherent counter part. This mainly stems from the broader range of applications for direct-detection optical OFDM due to its lower cost. For instance, the first report of the DDO-OFDM [11] takes advantage of that the OFDM signal is more immune to the impulse clipping noise in the (Cable TV) CATV network. Other example is the single-side-band (SSB)-OFDM which has been recently proposed by Lowery et al. and Djordjevic et al. for long-haul transmission [36, 37]. Tang et. al. have proposed an adaptively modulated optical OFDM (AMOOFDM) that uses bit and power loading showing promising results for both multimode fiber and short-reach SMF fiber link [59, 60]. The common feature for DDO-OFDM is of course using the direct-detection at the receiver, but we classify the DDO-OFDM into two categories according to how optical OFDM signal is being generated: (i) linearly-mapped DDO-OFDM (LM-DDO-OFDM) where \the optical OFDM spectrum is a replica of baseband OFDM, and (ii) nonlinearly-mapped DDO-OFDM (NLM-DDO-OFDM) where the optical OFDM spectrum does not display a replica of baseband OFDM [61].

Coherent optical OFDM (CO-OFDM) represents the ultimate performance in receiver sensitivity, spectral efficiency and robustness against polarization dispersion, but yet requires the highest complexity in transceiver design. In the open literature, CO-OFDM was first

proposed by Shieh and Authaudage [12], and the concept of the coherent optical MIMO-OFDM was formalized by Shieh et al. in [62]. The early CO-OFDM experiments were carried out by Shieh et al. for a 1000 km SSMF transmission at 8 Gb/s [46], and by Jansen et al. for 4160 km SSMF transmission at 20 Gb/s [63]. Another interesting and important development is the proposal and demonstration of the no-guard interval CO-OFDM by Yamada et. al. in [64] where optical OFDM is constructed using optical subcarriers without a need for the cyclic prefix. Nevertheless, the fundamental principle of CO-OFDM remains the same, which is to achieve high spectral efficiency by overlapping subcarrier spectrum yet avoid the interference by using coherent detection and signal set orthogonality. This thesis focuses on coherent optical OFDM.

2.4 Conclusion

In this chapter, we first reviewed the historical perspective of OFDM. It starts with literature overview of OFDM in wireless research area. The development of OFDM in optical research area is then listed. Moreover, we reviewed the real-time optical OFDM demonstrations in the recent a few years. In the section 2.2, the fundamentals of OFDM are given. There are three key points in the OFDM structure: (a) orthogonality, (b) discrete Fourier transforms, and (c) usage of cyclic prefix. These three points are fully discussed using mathematic models and expressions. Two flavors of optical OFDM are listed in the following section, direction detection optical OFDM and coherent optical OFDM. Due to benefits of coherent detection, in the thesis, coherent optical OFDM is mainly discussed.

3 107 Gb/s CO-OFDM Long Haul Transmission

3.1 Overview

Orthogonal frequency-division multiplexing has been extensively studied to combat RF microwave multipath fading and has emerged as the leading modulation technology for the wireless and wire-line systems in RF domain. An optical equivalent of RF OFDM called coherent optical OFDM has been proposed [12] and has become a promising technique for high spectral efficiency and dispersion resilient transmission [63, 65]. As the IP traffic continues to grow at a rapid pace, the 100 Gb/s Ethernet is being the transport standard for IP networks [4]. As the data rate approaches 100 Gb/s and beyond, the electrical bandwidth required for CO-OFDM would be at least 15 GHz [7] and is not cost-effective to implement even with the best commercial DAC and ADC in silicon integrated circuit[6]. To overcome this electrical bandwidth bottleneck, we propose and demonstrate the concept of OBM-OFDM to divide the entire OFDM spectrum into multiple orthogonal bands. Due to the inter-band orthogonality, the multiple OFDM bands with zero or small guard bands can be multiplexed and de-multiplexed without inter-band interference. With this scheme, transmission of 107 Gb/s CO-OFDM signal over 1000 km (10×100 km) SSMF has been realized using only erbium-doped fiber amplifier (EDFA) and without a need for optical dispersion compensation. Although several transmission experiments at 100 Gb/s and above have been demonstrated at longer distance relying on dispersion compensation module and Raman Amplification (RA) in each span [66,67], our work has achieved the 1000 km transmission without optical dispersion compensation and without RA beyond 100 Gb/s. The 107 Gb/s OBM-OFDM can be also considered as 5×21.4 Gb/s WDM channels without frequency guard band, occupying 32 GHz optical bandwidth, implying a high spectral efficiency of 3.3 bit/s/Hz using only 4-QAM encoding.

By multiplexing and demulitpelxing multiple OFDM bands, OBM-OFDM has the following advantages: (i) high spectral efficiency can be achieved by allowing for zero or small guard band, (ii) OBM-OFDM offers the flexibility of demodulating two OFDM sub-bands simultaneously with just one FFT whereas three (I)FFTs would be otherwise needed for the same purpose, (iii) OBM-OFDM can be readily partitioned with electrical anti-alias filters,

and subsequently processed with lower-speed DAC/ADCs , and (iv) the required cyclic prefix length is shortened due to the sub-banding of the overall spectrum.

In this chapter, we show implementation of 107 Gb/s OBM-OFDM transmission experiment, and substantiate the experiment with numerical simulation. This chapter is organized as follows. In Section 3.2, the principle of OBM-OFDM is presented where a complete OFDM spectrum is partitioned into multiple orthogonal bands. In Section 3.3, two implementations of OBM-OFDM in RF domain and optical domain are illustrated. The RF implementation can be realized in a mixed-signal CMOS ASIC design. A detailed description of OBM-OFDM experimental setup is described in Section 3.4. In Section 3.5, we discuss the experimental results with a focus on the OSNR sensitivity and nonlinearity performance. In Section 3.6, the influence of frequency guard band is investigated by varying the amount of the guard band up to 10 times of the subcarrier spacing. Insignificant penalty is observed when the guard band equals to multiple times of the subcarrier spacing, namely, when the condition of the orthogonality is satisfied. To corroborate the experimental results, numerical simulation is conducted to investigate 107 Gb/s CO-OFDM transmission in both single-channel and WDM systems in Section 3.7. Finally, in Section 3.8 we draw the conclusions.

3.2 Principle of orthogonal-band-multiplexed OFDM

The basic principle of OBM-OFDM is to partition the OFDM into multiple sub-bands, while maintaining their orthogonal property. As shown in Figure 5, the entire OFDM spectrum comprises N OFDM bands, each with the subcarrier spacing of Δf , and band frequency guard spacing of Δf_G . The subcarrier spacing Δf is identical for each band due to using the same sampling clock within one circuit. From the equation (6), the orthogonal condition between the different bands is given by

$$\Delta f_G = m\Delta f \tag{11}$$

Namely, the guard band is multiple (m times) of subcarrier spacing. In doing so, the orthogonality condition is satisfied for any two subcarriers inside the complete OFDM spectrum. For instance, the subcarrier f_i in band 1 is orthogonal to another subcarrier f_j in different OFDM band (band 2). Especially, when m equals to 1 in (11) the OFDM bands can be multiplexed/de-multiplexed even without guard band, despite the fact that they originate from different bands. We call this method of sub-dividing OFDM spectrum into multiple orthogonal bands as ‘orthogonal-band-multiplexed OFDM’ (OBM-OFDM). An identical

bandwidth-scalable and spectral-efficient multiplexing scheme for CO-OFDM has been first proposed in [68] where it is called cross-channel OFDM (XC-OFDM). We adopt the term of OBM-OFDM to stress the bandwidth reduction through sub-banding the OFDM spectrum.

Using such a scheme, each OFDM sub-band can be de-multiplexed using an anti-alias filter slightly wider than the signal band. To detect OBM-OFDM, two approaches can be used. First, the receiver laser is tuned to the center of each band. Each band is detected separately by using an 'anti-alias filter I' that low-passes only one-band RF signal. Second, the local laser is tuned to the center of the guard band. Two bands are detected by using an 'anti-alias filter II' that low-passes two-band RF signal simultaneously. In either case, the inter-band interference can be avoided because of the orthogonality between the neighboring bands, despite the leakage of the subcarriers from neighboring bands.

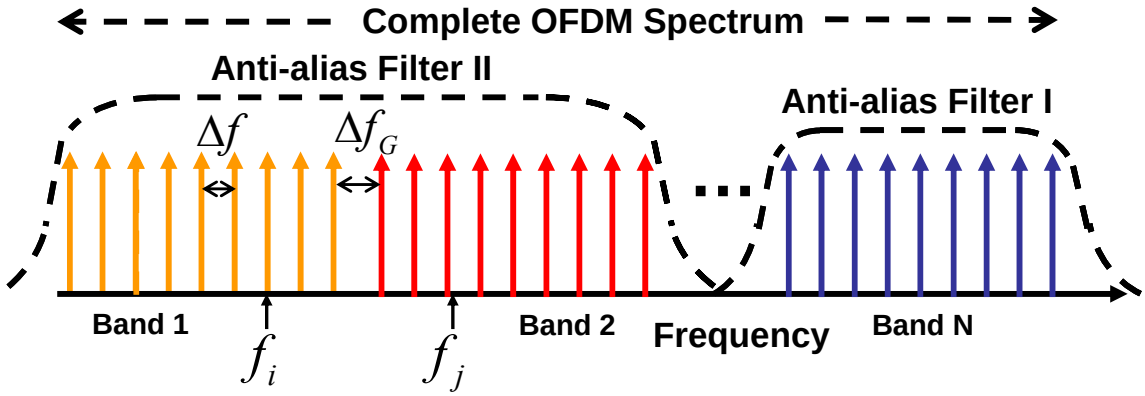

Figure 5. Conceptual diagram of OBM-OFDM. Anti-alias filters *I* and *II* correspond to two detection approaches illustrated in Section II.

3.3 Implementation of OBM-OFDM

OBM-OFDM can be implemented either in electrical or optical domain. As mentioned earlier, OBM-OFDM is particularly suitable to realize with mixed-signal ICs to resolve ADC/DAC bandwidth bottleneck, while the optical realization of OBM-OFDM serves as an alternative to the other spectrally efficient multiplexing schemes including coherent WDM [69], all-optical OFDM [70] and electro-optically subcarrier-multiplexed OFDM [71].

3.3.1 Electrical implementation of OBM-OFDM

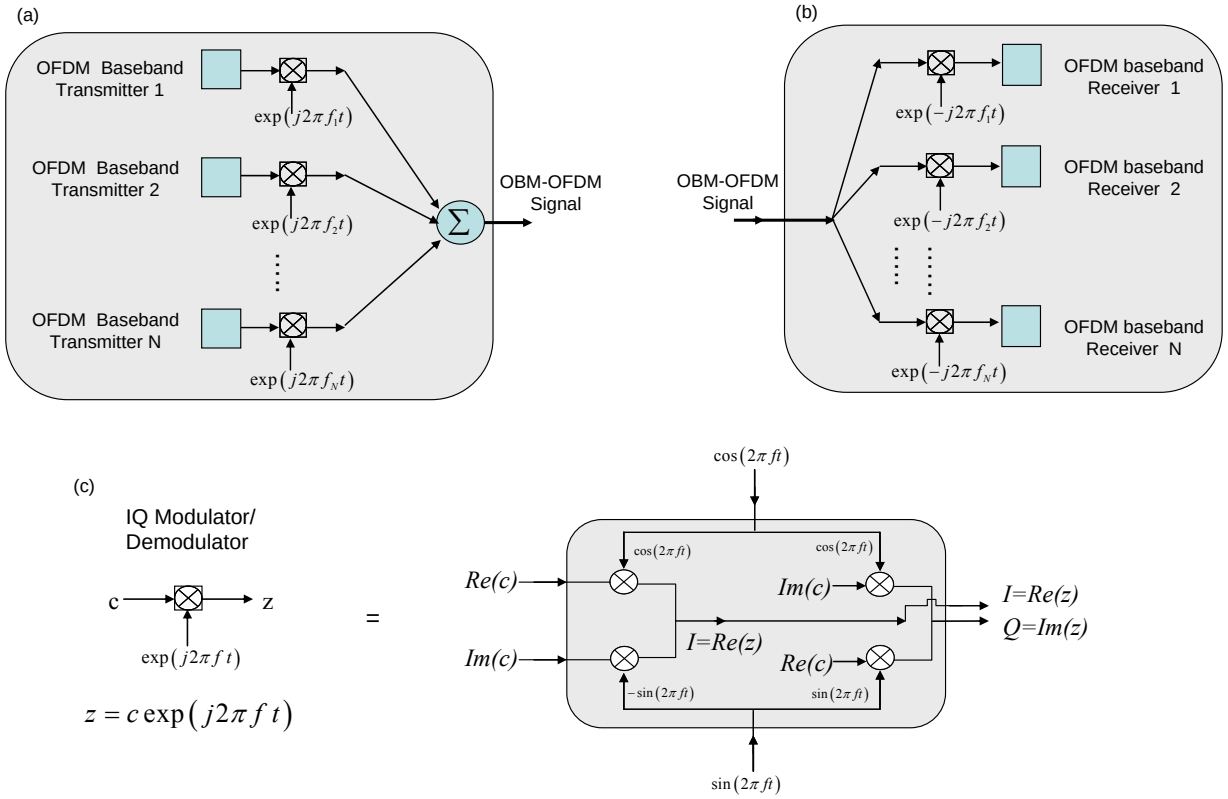

Figure 6. Schematic of OBM-OFDM implementation in mixed-signal circuits for (a) the transmitter, (b) the receiver, and (c) the I/Q modulator/demodulator. Both the output from the transmitter in (a) and the input to the receiver in (b) are complex signals with real and imaginary components.

Figure 6 shows the conceptual diagrams for implementing the OBM-OFDM using mixed-signal circuits. In Figure 6 (a), each OFDM baseband transmitter is implemented using digital IC design. The subsequent up-conversion, band-filtering and RF amplification can be implemented in RF IC design. The output of the OFDM baseband transmitter will be filtered through an anti-alias filter and up-convert to appropriate RF band with the center frequency from f_1 to f_N using an I/Q modulator or a complex multiplexer, the structure of which is shown in Figure 6 (c). The range of f_1 to f_N is centered around zero, given by

$$f_l = l \cdot \Delta f_b \qquad l \in [-L, L] \tag{12}$$

where f_l is the center frequency of the *l*th OFDM band, Δf_b is the band spacing, L is the maximum band number. The output of each I/Q modulator is a complex value that has real and imaginary parts as shown in Figure 6 (c). These complex signals are further summed up at the output, namely, real and imaginary parts are added up in separate parallel paths. The combined complex OFDM signal will be used to drive an optical I/Q modulator to be up-converted to optical domain [68, 72]. At the receive end as shown in Figure 6 (b), the

incoming signal is split into multiple sub bands and down-converted to baseband using I/Q demodulators. Anti-alias filters should be used to remove unwanted high frequency components at the output of the demodulators. In such a way, the DAC/ADC only needs to operate at the bandwidth of each OFDM band, which is approximately scaled down by a factor equal to the number of sub bands from the original complete OFDM spectrum. For instance, the bandwidth of 107 Gb/s data rate with QPSK modulation and polarization multiplexing is around 35GHz. If the number of sub bands is five, each OFDM band will only need to cover about 7 GHz optical bandwidth. The electrical bandwidth required is 3.5 GHz, or half of the OFDM band spectrum if direct conversion is used at transmit and receive ends. The DAC/ADC with bandwidth of 3.5 GHz can be implemented in today's technology [6] and using a wider bandwidth for each OFDM band will reduce the number of the OFDM bands further down to two or three.

3.3.2 Optical implementation of OBM-OFDM

The OBM-OFDM could be realized using either subcarrier multiplexing [73] or wavelength multiplexing to patch multiple orthogonal bands into a complete OFDM spectrum (Figure 5). The OBM-OFDM can be also optically implemented by transmitting OFDM data through many WDM channels and locking all the lasers to the common optical standard such as an optical comb [74]. In doing so, the orthogonality condition is satisfied for all subcarriers across the entire WDM channels. This form of OFDM transmission is called XC-OFDM[68]. An optical filter with bandwidth slightly larger than the channel bandwidth can be used to select the desired channel. Consequently, no frequency guard band is necessary between neighboring WDM channels.

3.4 Experimental setup and description

Although the electronic OBM-OFDM is more cost-effective solution, the related research work will involve expensive high-speed mixed signal design, foundry run, and chip testing. We choose optical multiplexing to obtain OBM-OFDM for proof-of-concept demonstration at 107 Gb/s. Figure 7 shows the experimental setup for 107 Gb/s CO-OFDM transmission.

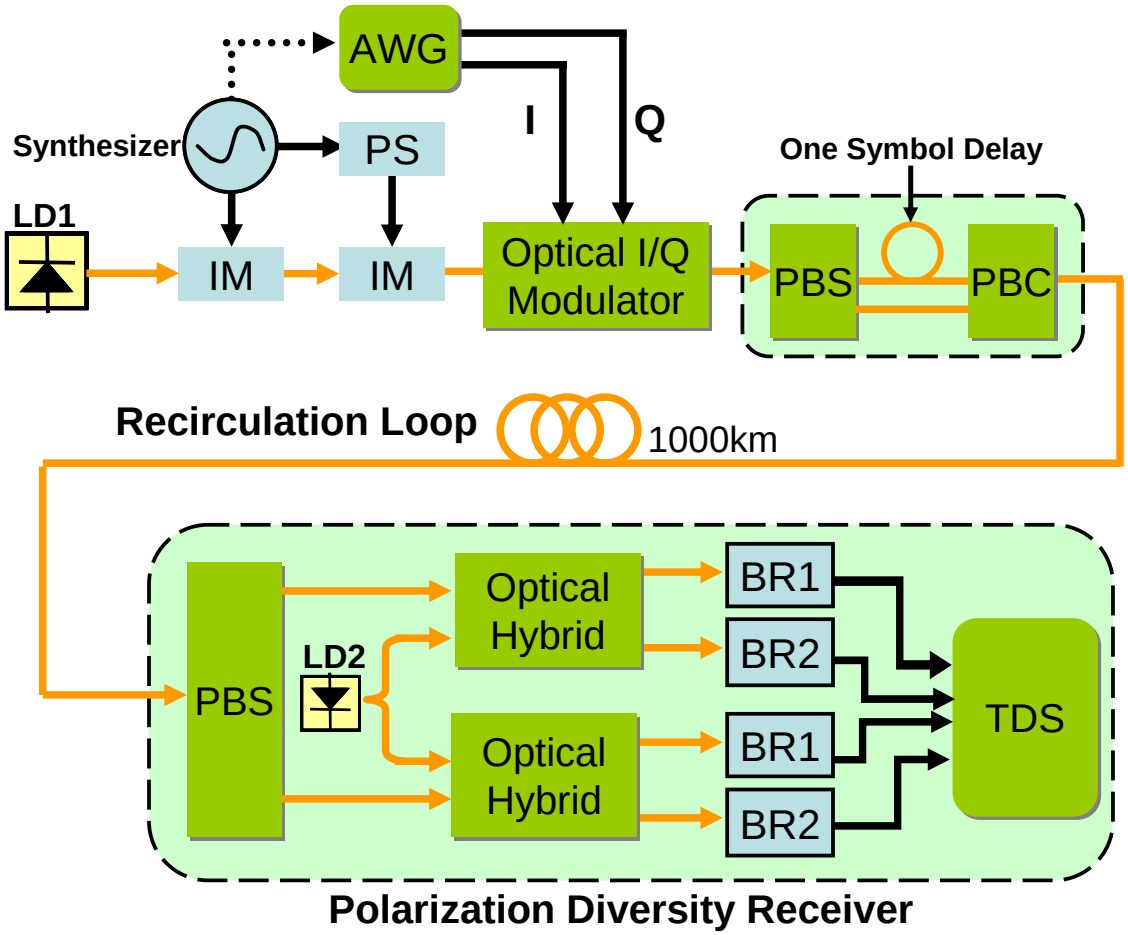

IM: Intensity Modulator PS: Phase Shifter LD: Laser Diode
AWG: Arbitrary Waveform Generator TDS: Time-domain Sampling Scope
PBS/C: Polarization Splitter/Combiner BR: Balanced Receiver

Figure 7. Experimental setup for 107 Gb/s OBM-OFDM systems.

3.4.1 CO-OFDM transmitter

The 107 Gb/s OBM-OFDM signal is generated by multiplexing 5 OFDM (sub) bands. In each band, 21.4 Gb/s OFDM signals are transmitted in both polarizations. The multi-frequency optical source spaced at 6406.25MHz is generated by cascading two intensity modulators (IM). When a single frequency RF signal with certain power is fed into the intensity modulator, it can be used to generate three tones, in which the middle tones are un-suppressed carrier, while the two-side optical tones are generated due to double sideband modulation. So if such tones are fed into the next intensity modulator or phase modulator, more tones will expanded. By properly tuning the bias voltage, five tones with even power can be produced. The guard band equals to just one subcarrier spacing (m=1 in (11)). Figure 8 shows the multiple tones generated by this cascaded architecture using two IMs which is different than previous setup using one IM and one phase modulator (PM) [7,75]. The new setup enables

better flatness across the five bands, and less leakage spectrum out of the intended five bands. Only the middle five tones with large and even power are used for performance evaluation. The transmitted signal is generated off-line by MATLAB program with a length of 2^{15}-1 PRBS and mapped to 4-QAM constellation. The digital time domain signal is formed after IFFT operation. The total number of OFDM subcarriers is 128, and guard interval is 1/8 of the observation window. The middle 82 subcarriers out of 128 are filled, from which 4 pilot subcarriers are used for phase estimation. The I and Q components of the time domain signal is uploaded onto Tektronix Arbitrary Waveform Generator (AWG), which provides the analog signals at 10 GS/s for both I and Q parts. Figure 9 (a) shows the electrical spectrum of the I/Q channel at the output of AWG. It can be seen that the aliasing components of OFDM signal are present above 6 GHz. When combining multiple OFDM sub-bands, such aliasing frequency components will degrade the signals in the adjacent bands. A 3-GHz low-pass electrical filter is used to eliminate the aliasing OFDM components. Figure 9 (b) shows the electrical spectrum after low-pass filtering, where the aliasing spectrum components are removed.

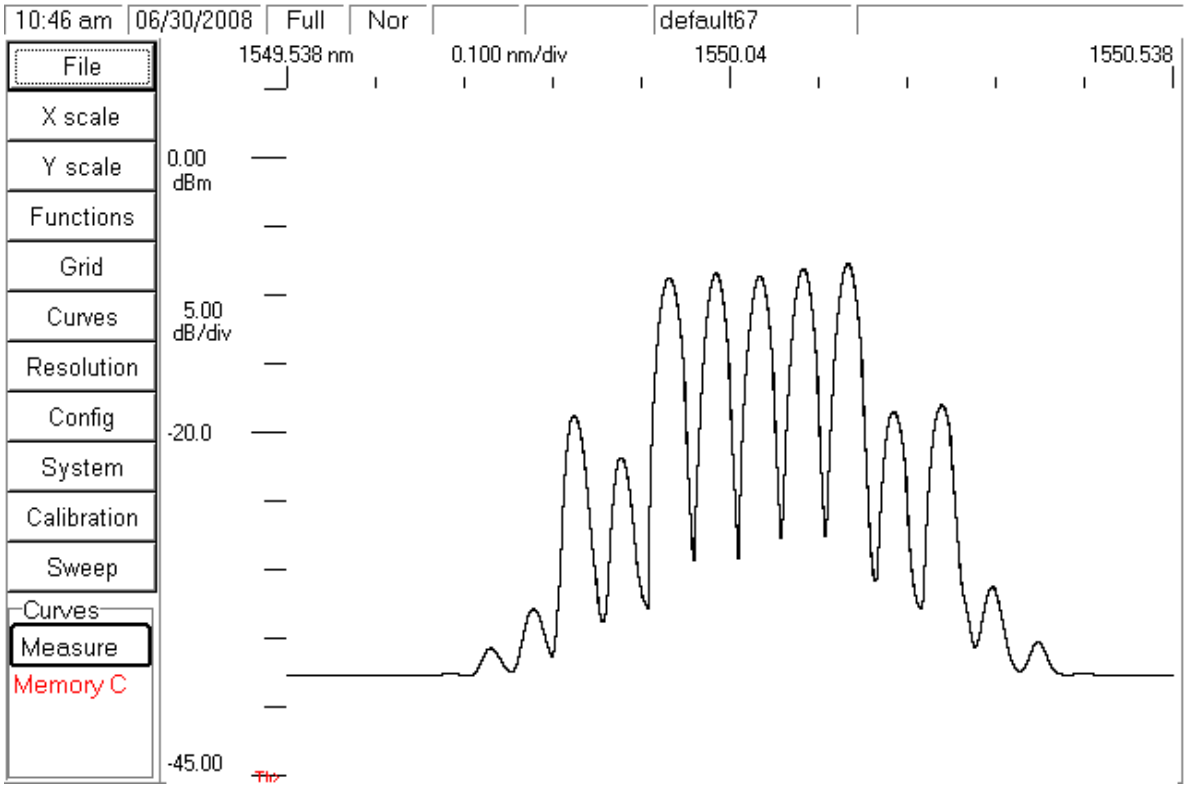

Figure 8. Multiple tones generated by two cascaded intensity modulators.

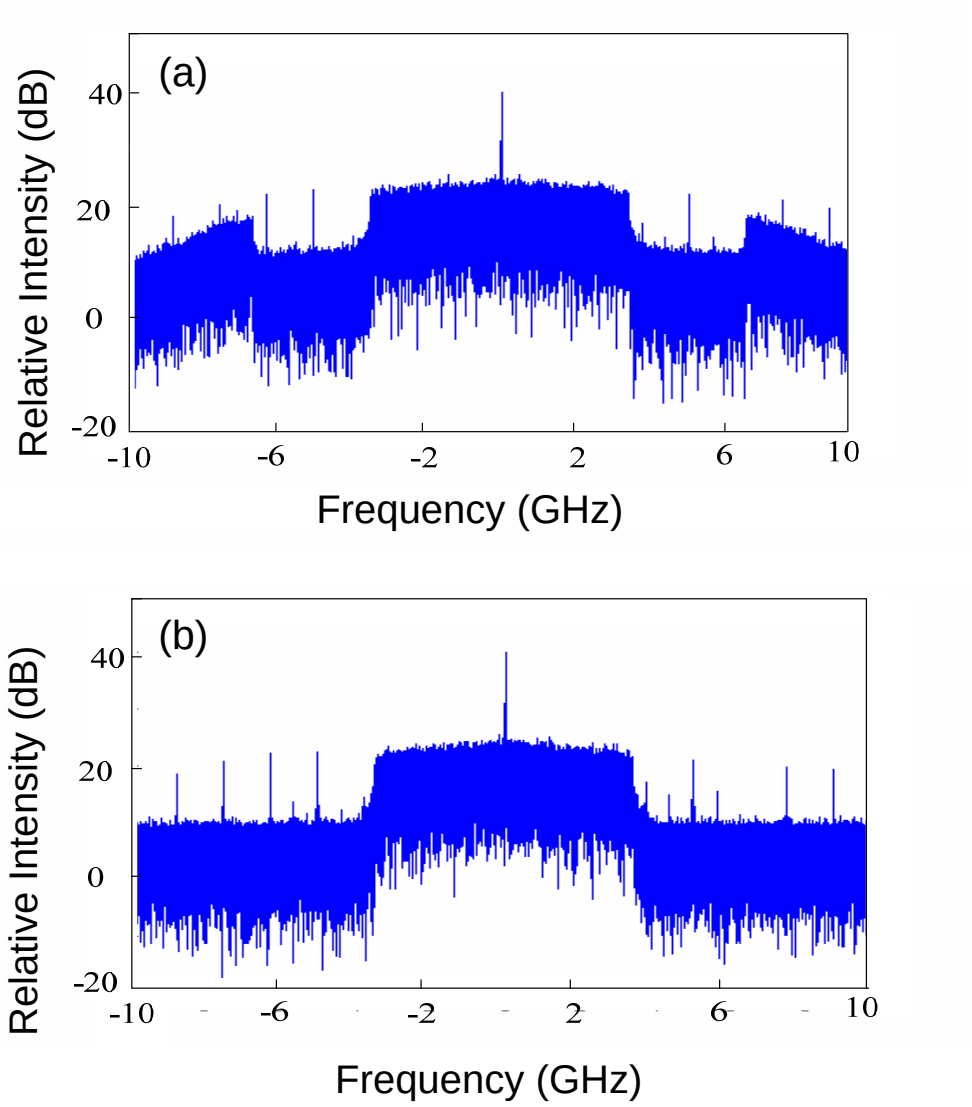

Figure 9. The electrical spectrum for (a) directly at the output of the AWG, and (b) after 3 GHz anti-aliasing filters.

The AWG is phase locked to the synthesizer through 10 MHz reference. The optical I/Q modulator comprising two MZMs with 90^0 phase shift is used to directly impress the baseband OFDM signal onto five optical tones. The modulator is biased at null point to completely suppress the optical carrier and perform linear RF-to-optical up-conversion [72]. The optical output of the I/Q modulator consists of five-band OBM-OFDM signals. Each band is filled with the same data at 10.7 Gb/s data rate and is consequently called 'uniform filling' in this section. To improve the spectrum efficiency, 2x2 MIMO-OFDM is employed, that is, two OFDM transmitters are needed to send two independent data into each polarization, which are then detected by two OFDM receivers one for each polarization.

A cost-effective method is adopted to emulate the two transmitters as shown below: The single-polarization optical OFDM signal at the output of the I/Q modulator is first evenly

spitted into two polarization branches with a polarization-beam splitter (PBS), with one branch delayed by one OFDM symbol period, i.e., 14.4 ns in this experiment, which equals to one OFDM symbol length. The two polarization branches are subsequently combined, emulating two independent transmitters, one on each polarization, resulting in a composite data rate of 21.4 Gb/s. The two polarization components are completely independent due to the delay of 14.4 ns for each OFDM symbol.

3.4.2 Fiber link

A multi-span fiber link is emulated with a recirculation loop, which consists of 100 km SSMF fiber and an EDFA to compensate the link loss. Neither optical dispersion compensation nor Raman amplification is used for the transmission.

3.4.3 CO-OFDM receiver

The signal is coupled out of the loop and received with a polarization diversity coherent receiver [76,77] comprising a polarization beam splitter, a local laser, two hybrids and four balanced receivers. The complete OFDM spectrum, comprised of 5 sub-bands, is shown in Figure 10 (a). The entire bandwidth for 107 Gb/s OFDM signal is only 32 GHz, about 5 GHz tighter than that shown in experiment [7]. This is because (i) the guard band is reduced from 8 to 1 times of the subcarrier spacing, and (ii) the number of the pilot subcarriers is reduced from 8 to 4.

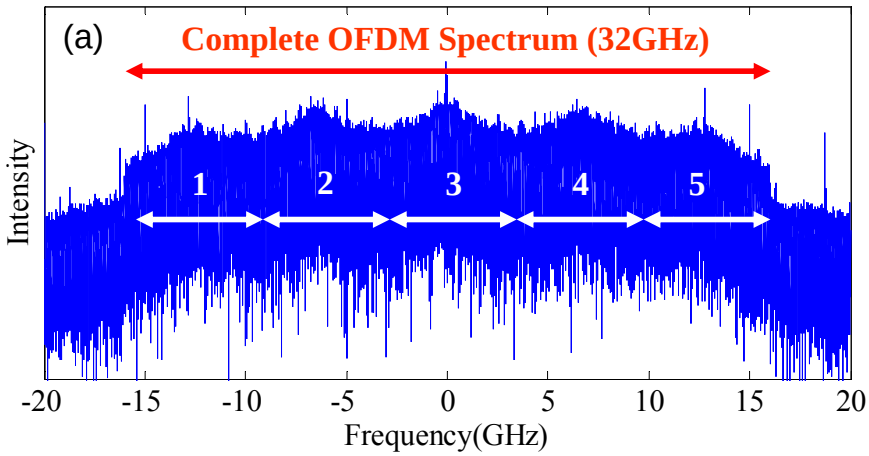

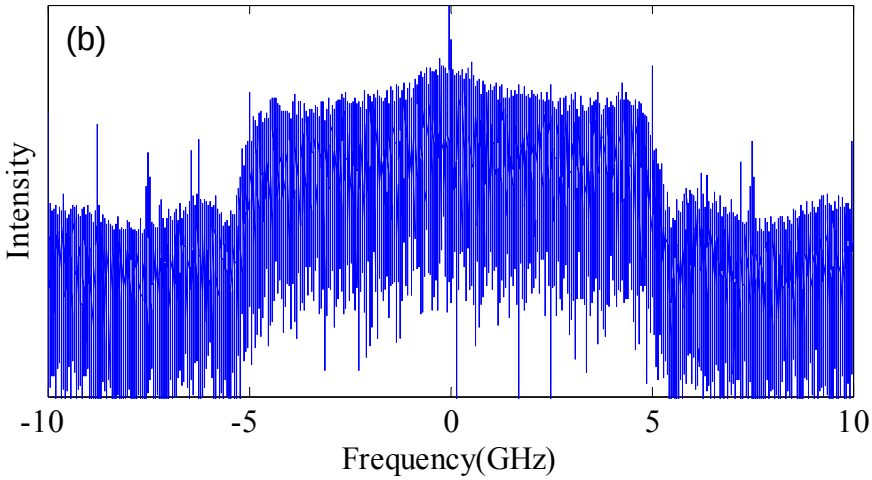

Figure 10. (a) RF Spectrum for the 107 Gb/s signal using a polarization diversity coherent receiver. The band numbers are depicted next to the corresponding bands. (b) The RF spectrum at the receiver after the 3.8 GHz anti-alias filter.

The local laser is tuned to the center of each band, and the RF signals from the four balanced detectors is firstly passed through the anti-aliasing low-pass filters with a bandwidth of 3.8 GHz, such that only a small portion of the frequency components from other bands is passed through, which can be easily removed during OFDM signal processing. The performance of each band is measured independently. The detected RF signals are then sampled with a Tektronix Time Domain-sampling Scope (TDS) at 20 GS/s. The sampled data is processed with a MATLAB program to perform 2x2 MIMO-OFDM processing. The receiver signal processing [76,77] involves (1) FFT window synchronization using Schmidl format to identify the start of the OFDM symbol, (2) software estimation and compensation of the frequency offset, (3) channel estimation in terms of Jones Matrix H, (4) phase estimation for each OFDM symbol, and (5) constellation construction for each carrier and BER computation.

The channel matrix H is estimated by sending 30 OFDM symbols using alternative polarization launch. The total number of OFDM symbol evaluated is 500 symbols. Mathematically, the transmitter information symbol of the two polarizations in the forms of Jones vector are given by

$$c = \begin{pmatrix} c_1 \\ c_2 \end{pmatrix} \tag{13}$$

where c_1 and c_2 are transmitted OFDM information symbols for two polarizations, Assume the fiber transmission Jones Matrix H is

$$H = \begin{pmatrix} h_{11} & h_{12} \\ h_{21} & h_{22} \end{pmatrix} \tag{14}$$

Ignoring the additive noise, the two received OFDM symbol is thus given by

$$c' = \begin{pmatrix} c'_1 \\ c'_2 \end{pmatrix} = H \cdot c \tag{15}$$

Or equivalently

$$\begin{cases} c'_1 = h_{11}c_1 + h_{12}c_2 \\ c'_2 = h_{21}c_1 + h_{22}c_2 \end{cases} \tag{16}$$

From (16), the transmitted information symbols can be recovered from the received signals by inverting H:

$$c = H' \begin{pmatrix} c'_1 \\ c'_2 \end{pmatrix}, \quad H' = \begin{pmatrix} h_{11} & h_{12} \\ h_{21} & h_{22} \end{pmatrix}^{-1} \tag{17}$$

The training symbols are generated by filling the odd symbols with known random data, while nulling the even symbols. After the polarization multiplexing emulator, the training symbols form a pattern of alternative polarization launch for two consecutive OFDM symbols. Using odd training symbols, the associated channel estimation can be expressed as

$$\begin{bmatrix} c'_1 \\ c'_2 \end{bmatrix} = \begin{bmatrix} h_{11} & h_{12} \\ h_{21} & h_{22} \end{bmatrix} \begin{bmatrix} c_1 \\ 0 \end{bmatrix} \Rightarrow \begin{cases} h_{11} = c'_1 / c_1 \\ h_{21} = c'_2 / c_1 \end{cases} \tag{18}$$

and using even training symbols as

$$\begin{cases} h_{12} = c'_1 / c_2 \\ h_{22} = c'_2 / c_2 \end{cases} \tag{19}$$

It can be seen from (18) and (19), by using alternative polarization training symbol, the full channel estimation of H can be obtained. Then using the inverse of this matrix in (17) and the received information symbols, the transmitted symbols in the two polarizations can be estimated. The estimated transmitted symbols will be mapped to the closest constellation points to recover the transmitted digital bits.

3.5 Measurement and discussion

Figure 10 (a) shows the RF spectrum after 1000 km transmission measured with the polarization diversity coherent receiver shown. No frequency guard band (m=1) is used in our transmission measurement. It can be seen that five OFDM bands each with 6.4 GHz bandwidth are closely patched together and the entire OFDM spectrum occupied is about 32 GHz. The out-band components are due to the multi-frequency source generation not tightly bounded at 5 tones. This artifact will not exist in the real application using either subcarrier multiplexing or optical multiplexing OBM-OFDM. Figure 10 (b) shows the detected electrical spectrum after using a 3.8 GHz electrical anti-alias filter for one-band detection. The anti-alias filter is critical for OBM-OFDM implementation. As is shown in Figure 10 (a), without electrical anti-alias filter, the electrical spectrum will be as broad as 16 GHz, indicating that at least 32 GS/s ADC has to be used. However, the filtered spectrum in Figure 10 (b) can be easily sampled with 20 GS/s, or even at a lower speed of 10 Gb/s. Additionally, despite the fact that there are some spurious components from neighboring band that is leaked at the edge of the 3.8 GHz filter, since they are orthogonal subcarriers to the interested OFDM subcarriers at the center, they do not contribute to the interference degradation. Compared with our previous work [7], the spectrum of 107 Gb/s CO-OFDM is reduced from 37 GHz to 32 GHz by using zero guard band and less pilot subcarriers in this experiment.

Table 3 (a) and 1(b) show the performance of five bands at both back-to-back and 1000 km transmission. It can be seen that both polarizations in each band can be recovered successfully, and this is done without a need for a polarization controller at receive. The difference of BER in each entry is attributed to the tone power imbalance and instability as well as the receiver imbalance for two polarizations. The nonlinearity tolerance of OBM-OFDM transmission is firstly measured by varying the launch power into the optical links.

Table 3. (a) BER distribution at back-to-back at an OSNR of 17.0 dB

Band	1	2	3	4	5
BER (x polarization)	4×10^{-4}	2.5×10^{-4}	4.63×10^{-4}	3.63×10^{-4}	2×10^{-4}
BER (y polarization)	4×10^{-4}	2.38×10^{-4}	3.88×10^{-4}	3.00×10^{-4}	3×10^{-4}

(b) BER distribution after 1000 km transmission at an OSNR of 18.9 dB

Band	1	2	3	4	5
BER (x polarization)	1.38×10^{-4}	1.0×10^{-4}	1.38×10^{-4}	1.5×10^{-4}	7.5×10^{-5}
BER (y polarization)	1.63×10^{-4}	1.3×10^{-4}	3.13×10^{-4}	2.5×10^{-4}	1.2×10^{-4}

Figure 11 shows the measured Q as a function of launch power at 1000 km. It can be seen that the optimal power for 107 Gb/s OBM-OFDM is around -1 dBm.

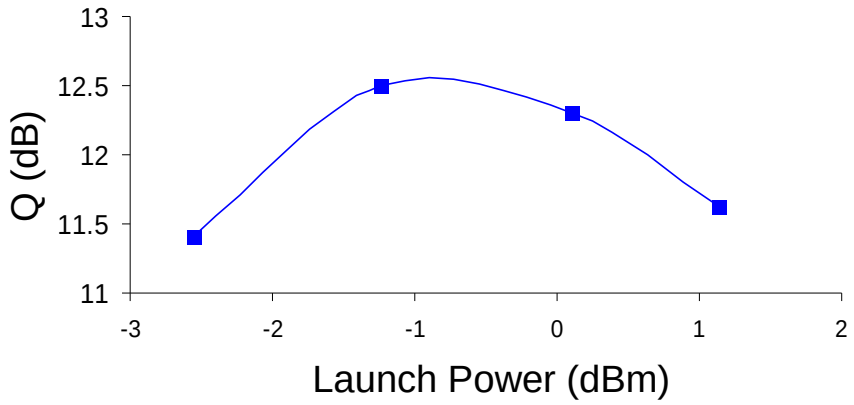

Figure 11. The system performance as a function of the launch power at the reach of 1000 km.

Figure 12 shows the BER sensitivity performance for the entire 107 Gb/s CO-OFDM signal at the back-to-back and 1000 km transmission with the launch power of -1 dBm. The BER is counted across all five bands and two polarizations. It can be seen that the OSNR required for a BER of 10^{-3} is respectively 15.8 dB and 16.8 dB for back-to-back and 1000 km transmission. The back-to-back 15.8 dB of OSNR sensitivity at 107 Gb/s is about 1.2 dB better than that reported in the previous publication [7]. This improvement is attributed to three factors: (i) the five tones generated in this chapter have much better flatness than those in [5], (ii) 4 pilot subcarriers are used instead 8 in [7], and (iii) the balance between the two arms of polarization diversity coherent receiver is improved.

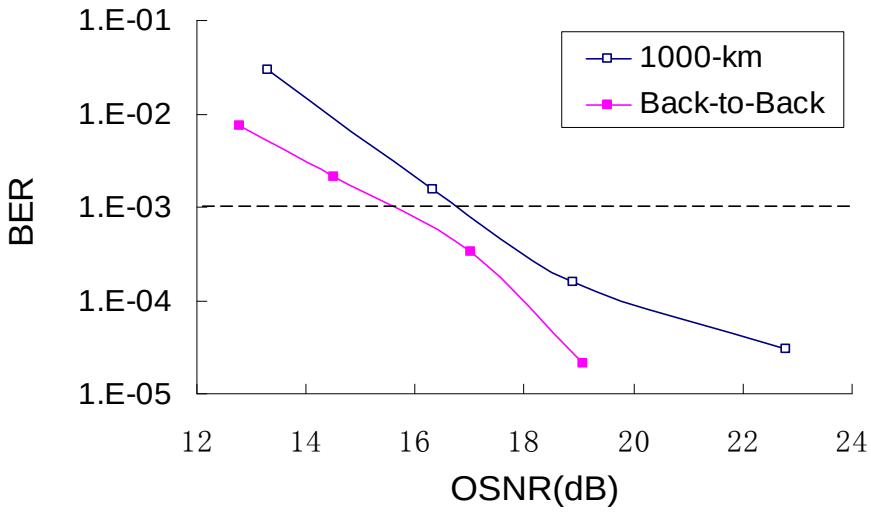

Figure 12. BER sensitivity of 107 Gb/s CO-OFDM signal at the back-to-back and 1000 km transmission.

Figure 13 shows the system Q performance of the 107 Gb/s CO-OFDM signal as a function of reach up to 1000 km. It can be seen that the Q reduces from 17.2 dB to 12.5 dB when reach increases from back-to-back to 1000 km transmission. By improving the balance between our polarization diversity coherent receivers, the disparity between the two polarizations has improved from 1.5 dB in [7] to 0.49 dB in this report.

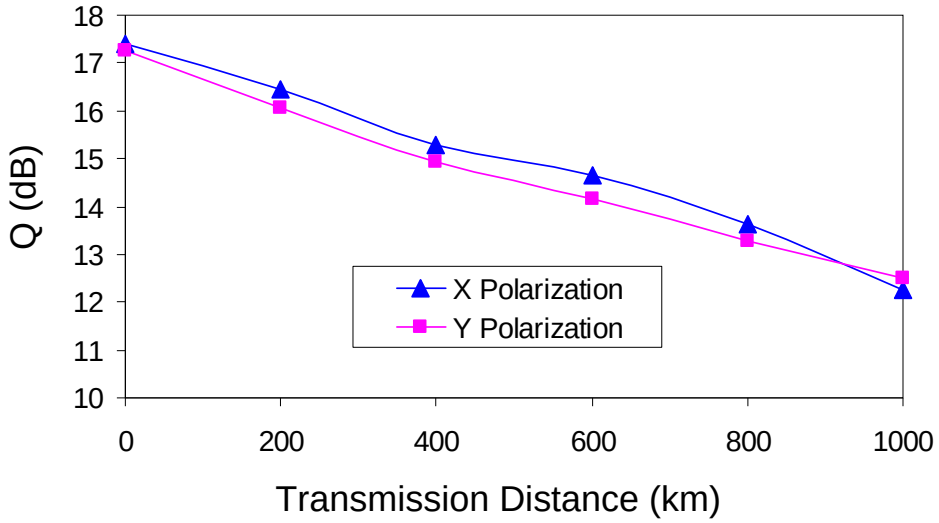

Figure 13. Q factor of 107 Gb/s CO-OFDM signal as a function of transmission distance.

3.6 Guard band influence on OBM-OFDM

As discussed in section 3.2, the orthogonality condition is satisfied when the guard band Δf_G is integer (m) times of subcarrier spacing Δf. In this section we show a generalized study of the influence of guard band to the system performance. We firstly verify through experiment the validity of the orthogonality condition that minimizes the inter-band interference (IBI).

The experiment set up is the same as Figure 7. Due to the inter-band interference the subcarriers at the two edges of each band bear the largest inter-band penalty. Figure 14 (a) and (b) show the SNR sensitivity performance of the 'edge subcarriers' (the first and the last subcarrier of the band) as a function of the guard band normalized to the subcarrier spacing, at the back-to-back and 1000 km transmission with -1 dBm launch power. For simplicity, only one polarization is presented. The system signal-to-noise ratio (SNR) oscillates as the guard spacing increases with a step size of half of the subcarrier spacing. It is shown in theory that ICI interference due to frequency spacing is a sinc function [78]. The SNR oscillation eventually stabilizes to a constant value around a 10.5 dB. By comparing with the stabilized constant, the system penalty as a function of the guard band can be investigated. Figure 14

shows the system penalty for both polarizations, when the guard band equals to a multiple of the subcarrier spacing, the Q penalty almost decreases to zero at 1000 km transmission, validating the orthogonal condition.

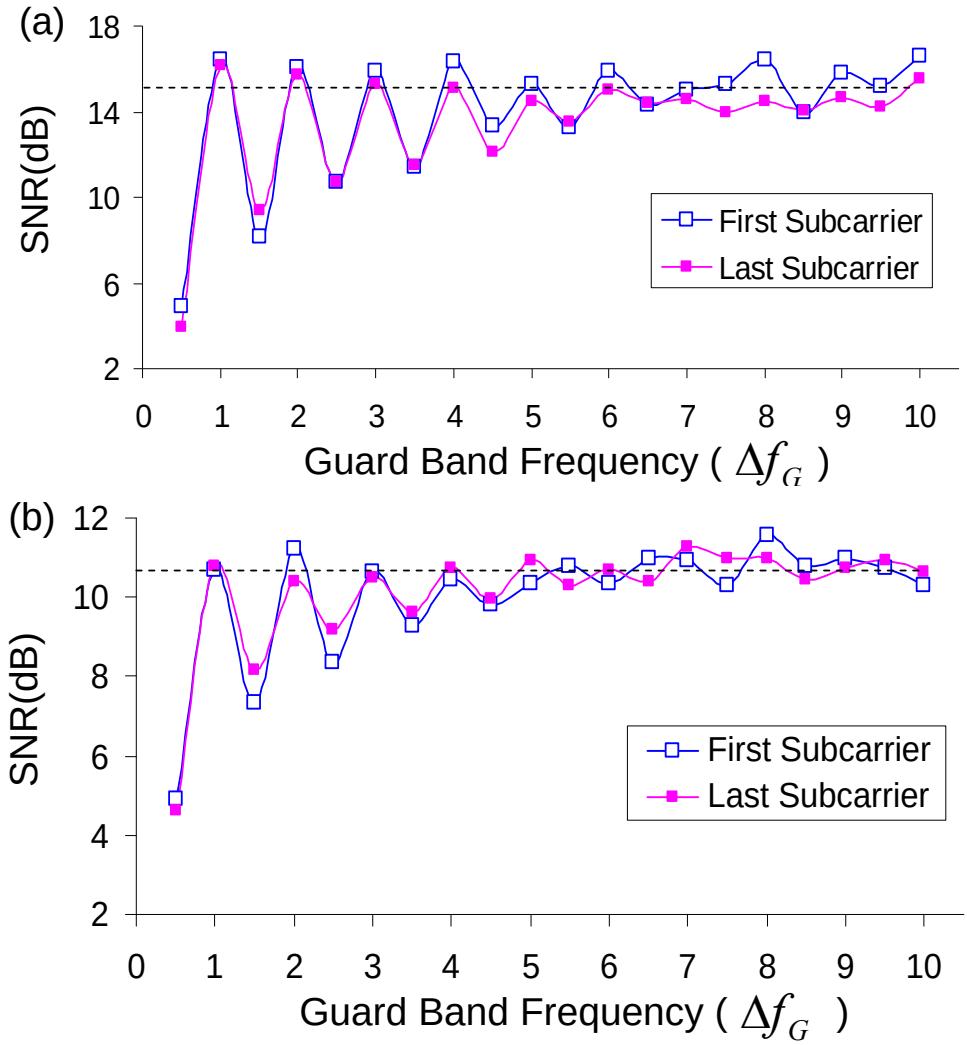

Figure 14. The SNR sensitivity performance of two edge subcarriers at (a) back-to-back transmission and (b) 1000 km transmission. The guard band frequency is normalized to the subcarrier spacing.

3.7 Simulation of 107 Gb/s OBM-OFDM transmission

In the experiment shown in Sections 3.4 and 3.5, five OFDM bands with the same data are multiplexed (uniform filling) to generate an OBM-OFDM signal. There is a concern whether this uniform filling will underestimate the nonlinearity such that our experiment may over-estimate the CO-OFDM transmission performance. Therefore it is important to compare the performance difference between the uniform filling used in the experiment and the scenario for which each band is filled with independent data (random filling). Furthermore, while the experiment is more convincing and will be the ultimate method of validation, the numerical simulation is more flexible and can carry out many more measurement scenarios with

relatively low cost. In this section, we intend to conduct the simulation to compare the nonlinearity performance difference between the uniformly filled OBM-OFDM and randomly filled OBM-OFDM, in both single-channel and WDM environments.

The basic CO-OFDM system with polarization multiplexed transmission is shown in Figure 15. We configure the simulation condition in the way such that it closely mirrors our experimental setup. Two optical OFDM signals are generated independently and combined with a polarization beam combiner. Multiple WDM channels with CO-OFDM modulation format are launched into the optical link. The optical link consists of multi-span SSMF fibers and an EDFA to compensate the loss. The output signal after transmission is detected using an optical coherent receiver which serves as an optical-to-RF OFDM direct down-converter. In the OFDM receiver, the signal is first sampled using an ADC, and demodulated by performing FFT to recover the data. We apply commonly used parameters for our simulation: 100 km span distance, fiber chromatic dispersion of 16 ps/nm/km, 0.2 dB/km loss, fiber effective area of 80 μ m^2, and a nonlinear coefficient of 2.6×10^{-20} m^2/W. The fiber span loss is compensated by an EDFA with a gain of 20 dB and noise figure of 6 dB. The linewidths of the transmit and receive lasers are assumed to be 100 kHz. 8 WDM channels are spaced at 50 GHz. Same OFDM parameters with that in experiment are used: OFDM symbol period of 12.8 ns. The number of OFDM subcarriers for each band is 128 (640 for 5 bands) and the middle 82 subcarriers out of 128 are filled. The payload is generated pseudo-random bit sequences (PRBS) of length 2^{15}-1. The guard interval is set to one eighth of the observation period, and 4-QAM encoding is used for each subcarrier. The bandwidth of each CO-OFDM signal is 32 GHz. The relative phase shift between subcarriers and channel estimation are calculated by using training sequences. The phase drift from the laser phase noise is also estimated and compensated using pilot subcarriers described in [79]. For the uniform filling, the user data is mapped onto 82 subcarriers and the same data block is repeatedly used to fill out the rest 328 subcarriers. In this way, the transmitted OFDM signal similar to that used in the experiment can be simulated, that is, the five bands are filled with the identical data. For the random filling, the data mapped onto each subcarrier has no correlation.

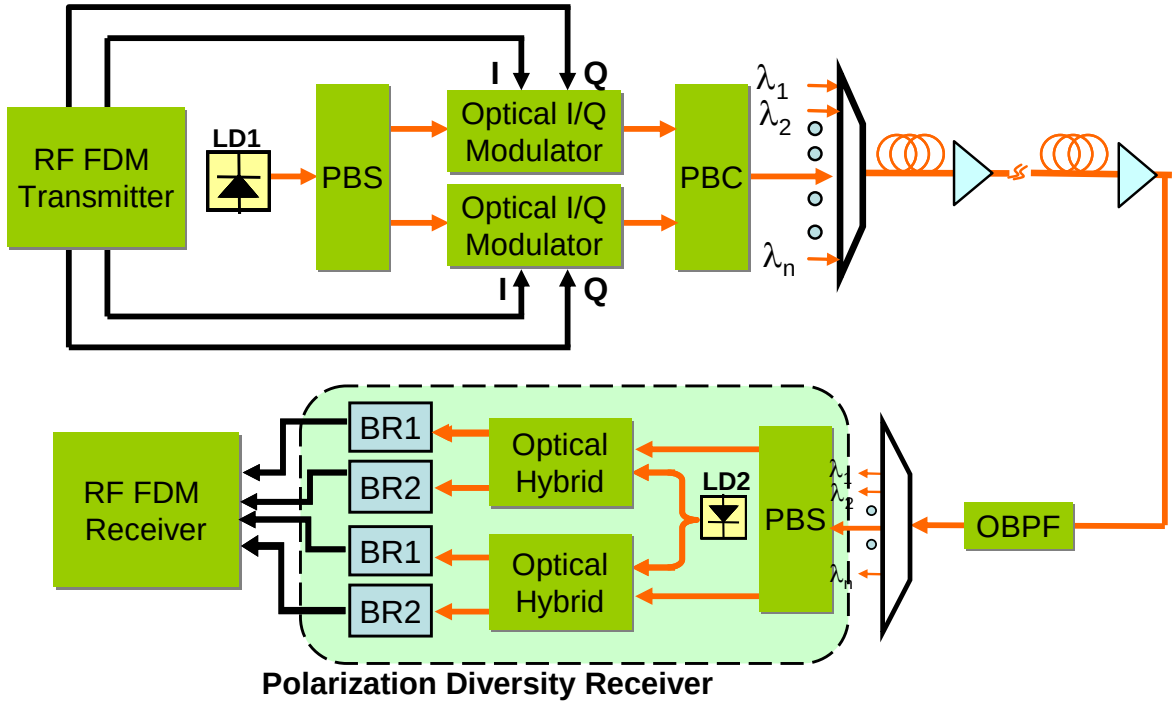

Figure 15. Conceptual diagram of simulated CO-OFDM system.

Figure 16 shows the Q factor as a function of launch power under the uniform filling and the random filling after 1000 km fiber for single-channel and WDM transmission. The single-channel optimal launch power is respectively 0 dBm and 1 dBm for uniform filling and random filling, whereas the optimal launch power for WDM systems is both 0 dBm for both uniform filling and random filling. We can see that if the power is increased beyond these optimal values, the nonlinearity of optical fiber will degrade the performance of system, resulting in a reduced Q. On the other hand, if the input power is reduced from these optimal values, the optical signal noise ratio (OSNR) of the received signal becomes lower, also resulting in a reduced Q. For both single-channel and WDM transmission, uniform filling shows worse nonlinearity performance. The reason is that the uniform filling increases the peak-to-average power ratio (PAPR) due to the correlation between the bands, which will severely degrade the signal at the high launch power. The phase walk-off and de-correlation between neighboring bands arising from the fiber dispersion helps reduce the nonlinearity after long distance fiber transmission. However, there is still residual Q difference after 1000 km transmission between uniform filling and random filling.

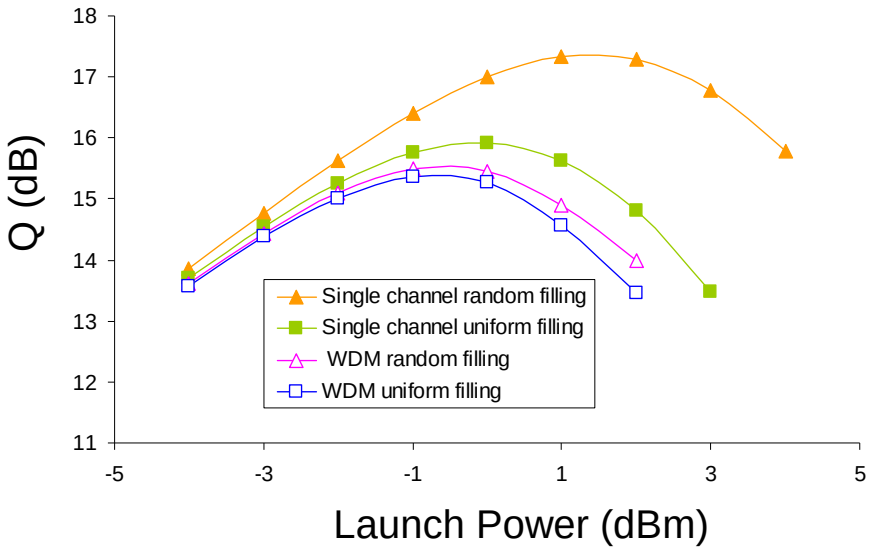

Figure 16 . System Q performance as a function of fiber launch power after 1000 km for both single-channel and WDM CO-OFDM transmission.

The slight system performance underestimation is observed by using the uniform filling in comparison with random filling due to enhanced nonlinearity in the uniform filling. For the single-channel transmission, the optimum launch power difference between uniform filling and random filling is 1dB and the optimum Q difference is about 1.2 dB. In the case of WDM, two filling schemes have the same optimum launch power of -1 dBm and the Q difference of 0.4 dB. It can be seen that at the fixed launch power of -1 dBm for the single-channel scenario, the Q difference between the random filling and uniform filling is only 0.5 dB, which agrees with the discussion in [7]. Most importantly, the simulation signifies that for single channel transmission, the true (random filled) 107 Gb/s OBM-OFDM system will have better system performance than what we have observed in Sections 3.4 and 3.5. The conclusion also applies to the WDM transmission. Therefore, OBM-OFDM with the uniform filling provides a conservative estimation of true OBM-OFDM system. This observation is important because to completely de-correlate the neighboring band data, multiple AWGs and band mixer have to be used, which in turn leads to a much more expensive proposition for constructing the experimental setup. It is observed that at the launch power of -1 dBm, the experimental Q of 12.5 dB (Figure 13) is about 3.3 dB below the simulated Q for the uniformly filled single channel at the reach of 1000 km. This difference is attributed to the imperfection of CO-OFDM transmitter and receiver, and OFDM signal processing involving non-ideal phase estimation and channel estimation.

3.8 Conclusion

We have proposed and elucidated the principle of orthogonal-band-multiplexed OFDM (OBM-OFDM) to subdivide the entire OFDM spectrum into multiple orthogonal bands. As a result, the DAC/ADCs do not need to operate at extremely high sampling rate. We show the proof-of-concept transmission experiment through optical realization of OBM-OFDM. A numerical simulation for both single channel and WDM transmission is conducted to verify the feasibility of the demonstrated OBM-OFDM experiment system. Back-to-back OSNR sensitivity of 15.8 dB at the data rate of 107 Gb/s for a BER of 10^{-3} was achieved. The demonstrated system employs 2×2 MIMO-OFDM signal processing and achieves high electrical spectral efficiency of 3.3 bit/s/Hz.

4 Real-time CO-OFDM Implementation

4.1 Overview

As the progress in high-speed electronic circuits ranging from analog-to-digital converters to digital signal processing application-specific integrated circuits (ASIC) continue to accelerate, the application of such electronic circuits and tools has stimulated and revived ideas of various multi-level modulation formats in fiber optic communications that had been mostly forgotten after active studies in 80s and 90s [80,81]. Multi-level modulation formats can be largely divided into time-domain modulation scheme such as single-carrier QPSK modulation [82,83] or frequency domain modulation scheme such as orthogonal frequency-division multiplexing (OFDM) [12]. Both approaches have attracted much research attention and have been demonstrated as viable solutions to significantly increase the data capacity in fiber optics communications as well as to enhance capabilities to mitigate various impairments of optical transmission system. While earlier studies of optical multi-level modulations scheme with digital signal processing focus on single-carrier time-domain modulation schemes, optical OFDM have simultaneously attracted much research interest for both coherent optical detection, i.e. CO-OFDM [12] and direct detection, i.e. DD-OFDM [36].

One of the previously discussed advantages of optical OFDM formats compared to single-carrier modulation formats is its computational efficiency in compensating optical transmission impairment such as chromatic dispersion (CD) and polarization mode dispersion (PMD) [7]. While single-carrier modulation formats often require multi-tap equalization for channel estimation and compensation to compensate for CD and PMD and other inter symbol interference (ISI) effects [84,85], OFDM with large number of subcarriers can take advantage of low OFDM symbol rate to afford time domain guard interval insertion between symbols realized by cyclic prefix (CP) to accommodate various ISI and consequently compensate for it with simple single-tap frequency domain equalization. This CP based ISI compensation, the training symbols and pilot subcarriers for symbol synchronization, channel estimation and frequency and phase estimation are commonly used techniques for optical OFDM. These techniques are the signatures of widely deployed OFDM systems in today's communication systems for example in wireless local area network [86], where the simplified equalization techniques are strongly desired mainly for the lower power consumption and portability. Since optical OFDM borrows such efficient techniques from copper wireline and wireless

communication systems, one argument can be that the implementation is straightforward or without major obstacles. In fact, although numerous amount of optical OFDM studies are reported based on offline processing using high-speed sampling scope and suggest many advantages of optical OFDM systems achieving over 100 Gb/s aggregated data rate and over thousands of km in transmission distance [16-18], many lack discussion on the possible implementation difficulties. Special requirements of optical communication system such as order of magnitude higher data rate than wireless counterpart demand additional attention and require careful studies in feasible real-time implementation of the high-speed optical OFDM systems.

A limited number of real-time demonstrations are demonstrated so far for both single-carrier coherent signal [24, 25] and CO-OFDM signal [26-29]. For CO-OFDM QPSK signal, net rate for single subband of 1.55 Gb/s was reported [26]. One of the advantages of OFDM data format is its scalability in the data structure to expand from orthogonal subcarriers structure to orthogonal subbands structure. The multi-band structure OFDM has been proposed to alleviate bandwidth constraint of DAC/ADC and it has been shown that upon the reception, a fraction of the OFDM spectrum can be carved out and detected at a fraction of the overall data rate.

In this chapter, we demonstrate a field-programmable gate array (FPGA) based real-time CO-OFDM receiver at a sampling speed of 2.5 GS/s, and show its performance in receiving a subband of a 53.3 Gb/s multi-band signal. Additionally, by taking advantage of the multi-band structure of OFDM signal, we successfully characterize a 53.3 Gb/s CO-OFDM signal in real-time by measuring one of its subbands at a time (3.55 Gb/s). An error floor as low as 3.7×10^{-8} is observed. The measurement of the low error-floor will facilitate the real-time margin measurement for CO-OFDM systems, which would be otherwise time-prohibitive for off-line processing. To the best of our knowledge, the sampling speed is the highest and the error floor is the lowest demonstrated so far for real-time CO-OFDM reception.

4.2 Experimental setup

Figure 17 shows the experimental setup of the 2.5 GS/s real-time CO-OFDM receiver. At the transmitter, a data stream consisting of pseudo-random bit sequences (PRBS) of length 2^{15}-1 was first mapped onto three OFDM subbands with QPSK modulation. 3 OFDM subbands were generated by an arbitrary waveform generator (AWG) at 10 GS/s, including pilot subcarriers each subband contained 115 subcarriers modulated with QPSK. Two unfilled gap

bands with 62 subcarrier-spacing were placed between the three subbands, which allowed them to be evenly distributed across the AWG output bandwidth. Subcarrier spacing therefore is therefore 10 GHz / 512 equals to 19.5 MHz. In each OFDM subband, the filled subcarriers, together with 8 pilot subcarriers and 13 adjacent unfilled subcarriers, were converted to the time domain via inverse fast Fourier transform (IFFT) with size of 128. The number of filled subcarriers was restricted by the 1.2 GHz RF low-pass filter, which was used to select the subband to be received. A cyclic prefix of length 16 sample point was used, resulting in an OFDM symbol size of 144 with the symbol interval of 57.6-ns (144×400-ps). The total number of OFDM symbols in each frame was 512. The first 1024 samples were used for symbol synchronization followed by 16 symbols that were used as training symbols for channel estimation. The time domain data representation is shown in Figure 18. Subtracting both symbol and subcarrier overhead, the spectral occupancy to the Nyquist limit (1.25-GHz) is about 71 % for each subband.

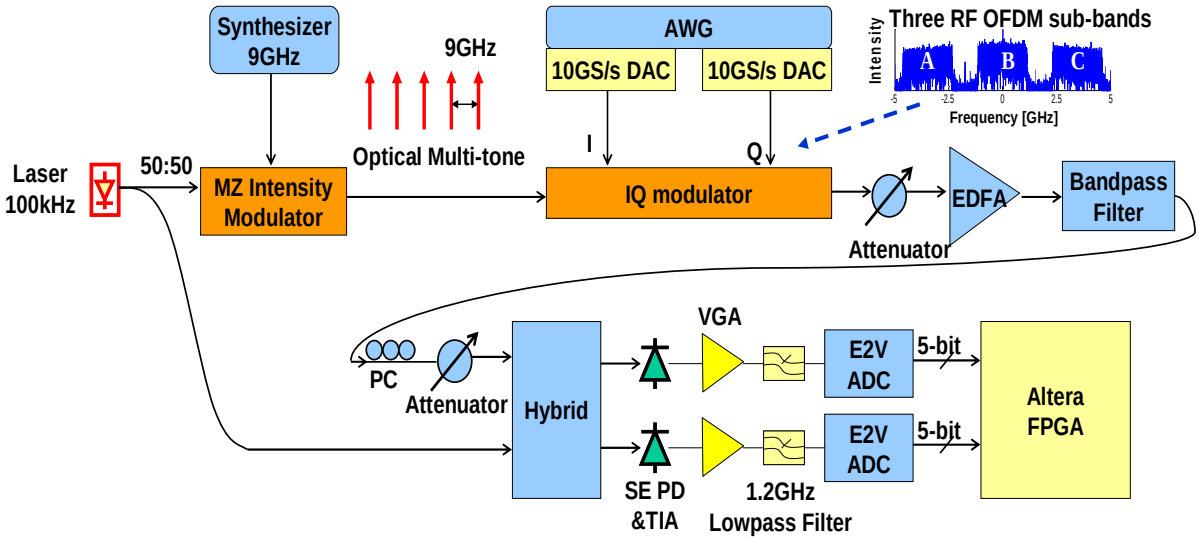

Figure 17. Real-time CO-OFDM transmission experimental setup. An external cavity laser is used as both transmit and LO laser. Subbands are created in both electrical (3 subbands) domain using AWG and optical domain (5 tones) using overdriven MZM.

Figure 18. OFDM frame structure in serial representation. The first 1024 samples are for symbol synchronization, followed by 16 pilot symbols for channel estimation and data payload of 496 symbols. Each symbol consists of 144 samples.

The real and imaginary parts of the OFDM symbol sequence were converted to analog waveforms via the AWG, before being amplified and used to drive an optical I/Q modulator that was biased at null. The transmitter laser and the receiver local laser were originated from the same external-cavity laser (ECL) with approximately 100-kHz linewidth through a 3-dB

coupler. By doing so, frequency estimation was not needed in this experiment. Only single-polarization of the light was modulated and polarization controller (PC) was placed before the hybrid to receive the right polarization. The maximum net data rate of the signal after the optical modulation was 3.55 Gb/s for each OFDM subband. The multi-frequency optical source contained 5 optical carriers at 9-GHz spacing, and was generated by a technique similar to [75,85], in which we use a Lithium Niobate Mach-Zehnder (MZ) intensity modulator driven by a high-power RF sinusoidal wave at 9 GHz. The synthesizer and the AWG are synchronized by a 10-MHz reference clock. The total number of subbands was then 15, resulting in a total net data rate of 54 Gb/s. Figure 19 shows the optical spectrum of 15-subband OFDM signal, the ripple is caused by the uneven power of 3 electrically created subbands. Unlike earlier works [85], the adjacent subbands in the multi-band OFDM signal contained independent data contents, more closely emulating an actual system. At the receiver, the OFDM signal in each subband was detected by a digital coherent receiver consisting of an optical hybrid and two single-ended input photodiode with a transimpedance amplifier (PIN-TIA). Two variable gain amplifiers (VGAs) are used to correct any amplitude difference between I/Q channels created by optical hybrid or optical front-ends as well as to amplify the signals to the full extent of available resolution of ADC which were sampling at a rate of 2.5 GS/s. The five most significant bits of each ADC (E2V AT84AS008) were fed into an Altera Stratix II GX FPGA. All the CO-OFDM digital signal processing was performed in the FPGA. The bit error rate was measured from the defined inner registers through embedded logic analyzer SignalTap II ports in Altera FPGA.

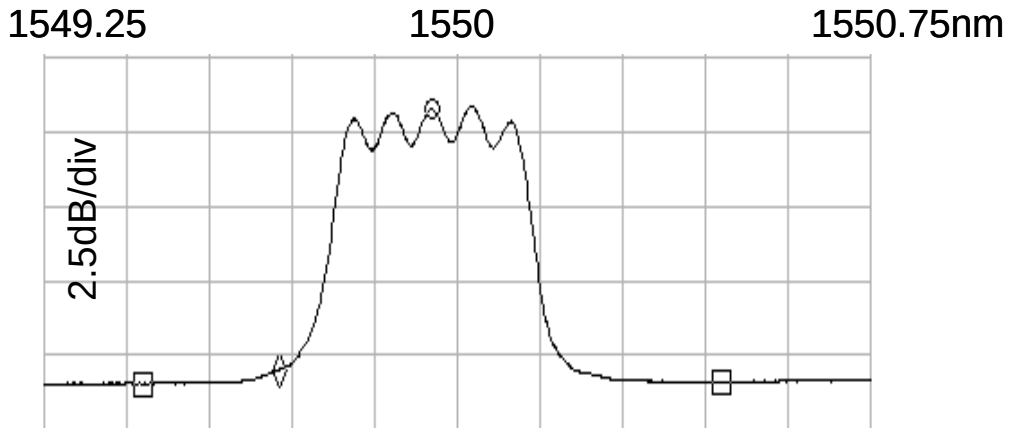

Figure 19. Optical spectrum of the 15 subband OFDM signal. The ripple is caused by the uneven power of 3 electrically modulated subband. The resolution bandwidth of this spectrum is 0.06 nm.

4.3 Digital signal processing in real-time CO-OFDM receiver

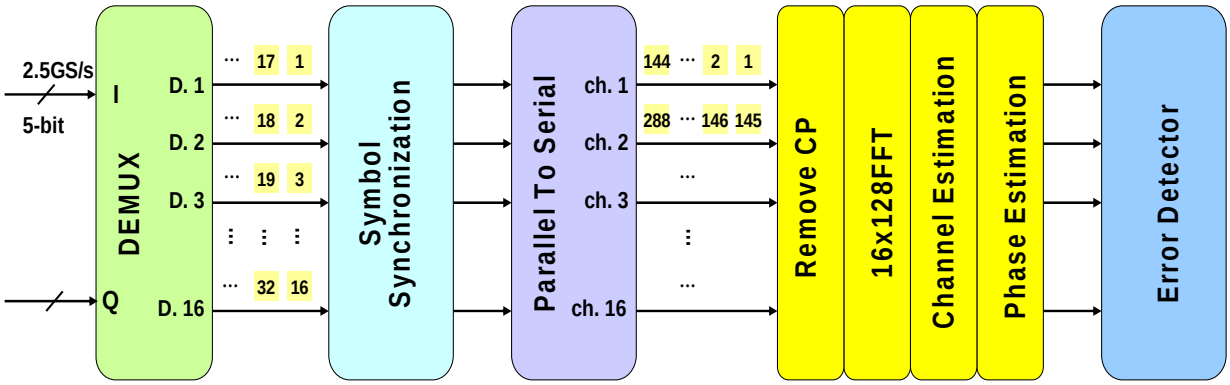

Figure 20. DSP diagram for real-time CO-OFDM receiver. The incoming samples are first de-multiplexed to 16 parallel channels followed by symbol synchronization, parallel-to-serial conversion, CP removal, FFT and channel and phase recovery before error detection is finally performed.

Figure 20 shows the block diagram of digital signal processing (DSP) in the real-time CO-OFDM receiver. 2.5 GS/s sampled data streams from I/Q channels were fed into FPGA through the high-speed serial ports. Although maximum speed of the FPGA clock rate exceeds 400 MHz, in order to meet timing closure of the design, the FPGA can only run at a clock rate of a few hundreds of megahertz. Thus the high-speed sampled digital signals were first de-multiplexed to 16 parallel channels, which lowered the required channel processing speed down to 156.25 MHz. The following procedure for OFDM was symbol synchronization. Traditional offline processing uses the Schmidl approach [87], where the auto-correlation of two identical patterns inserted at the beginning of each OFDM frame gives rise to a peak indicating the starting position of the OFDM frame and symbol. For the autocorrelation represented as,

$$P(d) = \sum_{k=0}^{L-1} r_{d+k}^{*} r_{d+k+L} \tag{20}$$

and a recursive equation can be found such that,

$$P(d+1) = P(d) + r_{d+L}^{*} r_{d+2L} - r_{d}^{*} r_{d+L} \tag{21}$$

An example of DSP implementation of equation (20) can be found in Figure 21, where L indicates the length of synchronization pattern, r_d indicates the complex samples and $P(d)$ indicates the autocorrelation term whose amplitude gives peak when the synchronization is found. The relatively simple equation (20) and the architecture in Figure 21, however, assumes that the incoming signal is a serial stream and this implementation only

works if the process clock rate is same as the sample rate. This is because the moving window for autocorrelation needs to be taken sample by sample while multiple samples need to be processed simultaneously at a parallel process clock cycle.

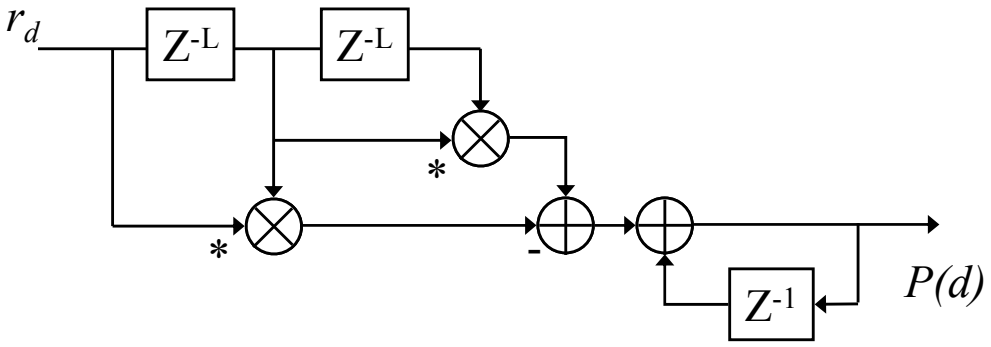

Figure 21. DSP block diagram of symbol synchronization based on autocorrelation taken on serial data samples.

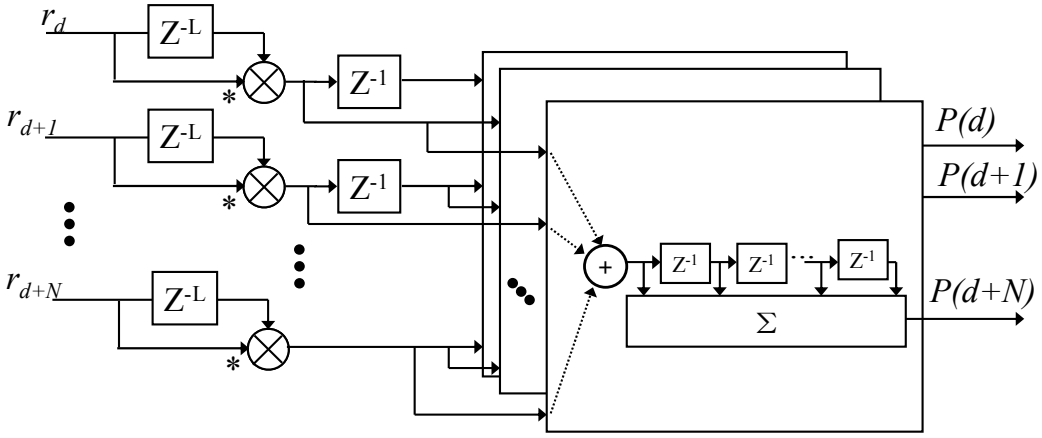

Figure 22. DSP block diagram of symbol synchronization for parallel process autocorrelation.

As there was no direct information available to indicate the frame starting point in the 16 parallel channels in our setup, locating the exact frame beginning would involve heavy computation that processes the data among all the channels. To illustrate this point, an implementation of the parallel autocorrelation can be constructed such that we can divide the autocorrelation of equation (20) by length N for the N parallel processing

$$P(d) = \sum_{k=0}^{(L/N)} \sum_{m=Nk}^{N(k+1)-1} \left(r_{d+m}^{*} r_{d+m+L} \right) \tag{22}$$

which does not have an apparent recursive equation, instead DSP realization can be presented in (21). As in equation (22) and Figure 22, by restricting the synchronization pattern length L to the integer multiplication of de-multiplexed bits N, a simple implementation of autocorrelation suitable for parallel processing is realized. However, for the case of N = 16 and L = 32, the processing resource required in this parallel implementation is estimated as

16 complex multipliers and 16 × 15 + 16 = 256 complex adders at each clock cycle. This indicates further efficiency improvement of symbol synchronization in parallel processing is desired.

To improve computation efficiency, we took a 2-step approach. In the first step, we set the cyclic prefix length to be equal to the number of the de-multiplexed channels, e.g., 16. This allows any of the first 16 points to be used as the starting point of an OFDM frame. In the second step, we replicated the synchronization pattern by number of the de-multiplexed channels, in this case 16, as well so that we can effectively down-sample the incoming signals by 16 and still can access to the synchronization pattern at any one of the de-multiplexed channel. This 2-step approach gives us the convenience of needing only one channel to perform the auto-correlation utilizing exactly the same scheme illustrated in Figure 21, without corrupting the following OFDM symbols. This dramatically reduces the computation effort. The detailed signal processing flow used for real-time CO-OFDM symbol synchronization is shown in Figure 23. The two identical synchronization patterns of length 32 (A1, A2,… An; A1, A2, …, An, n=32) were first replicated 16 times so that after the de-multiplexing, the synchronization patterns could be found in every parallel channel. The following 16 points were the cyclic prefix for the first OFDM symbol. By performing the auto-correlation of the sampled data in channel 1, the resulting strong peak indicates the beginning of each frame. Although this scheme can solve the critical computation resource issue, it is important to point out the scheme's drawbacks. First of all, the lengthened synchronization pattern, would not only reduce the spectrum efficiency, but also reduce the tolerance of the frequency offset correction capability if the method in [87] is used. Using the same synchronization pattern, frequency offset can be detected by estimating the phase of autocorrelation, and for our particular setup, maximum frequency offset that can be corrected is 4.9-MHz. Another issue is that since we don't have control over the starting location of the symbol within CP and a part of CP is essentially consumed for symbol offset correction, we expect the tolerance to CD and other ISI would be less than the ideal symbol window synchronization. With lower sampling speed at 1.4GS/s, successful implementation of frequency offset correction is reported in [26] using a technique based on Schmidl approach.

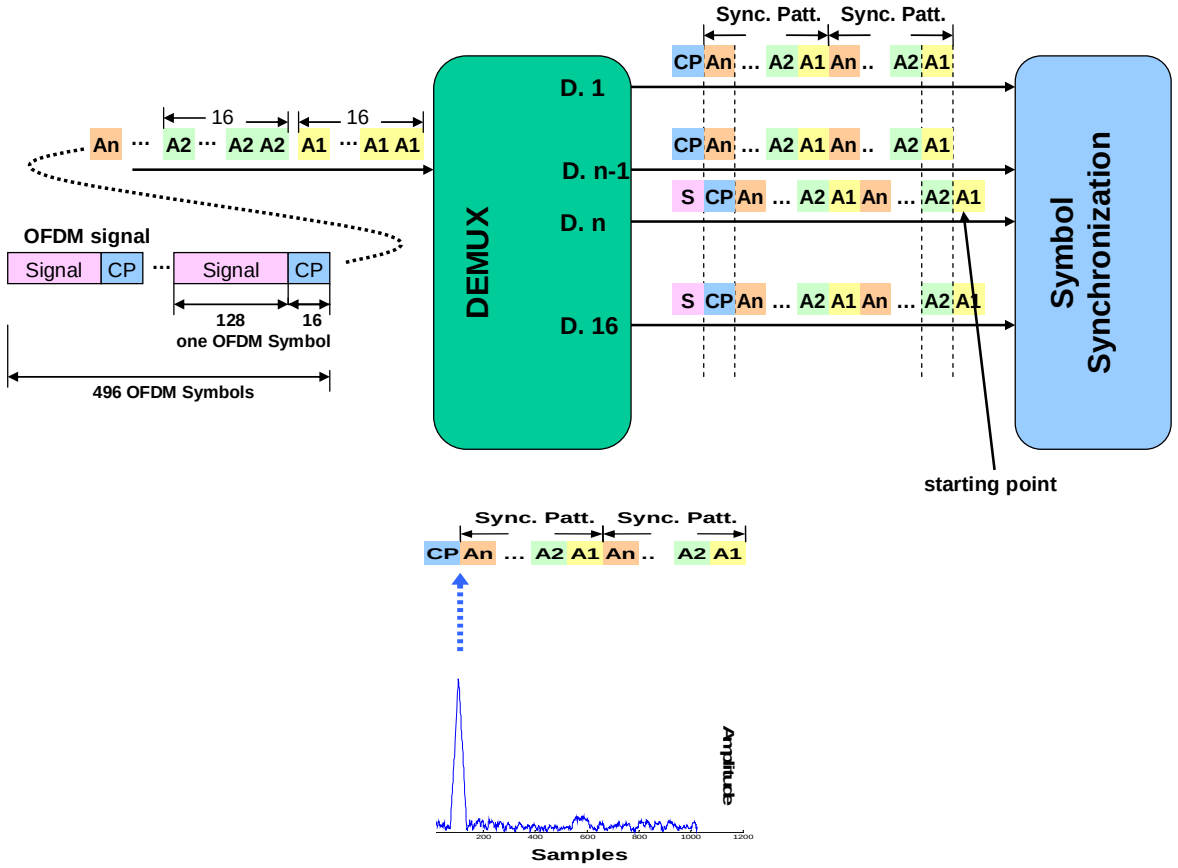

Figure 23. The symbol synchronization scheme applied in the real-time CO-OFDM receiver. The diagram indicates how the starting point of the synchronization pilot symbol can start anywhere in the 16 de-multiplexed channels. A measured auto-correlation trace is also shown on the right.

Since we have very small frequency offset tolerance, the same laser was split and used for both transmit and LO laser thus to avoid the necessity of frequency correction. Once this symbol synchronization was completed, a large proportion of FPGA's on-chip memory was used for first-in-first-out (FIFO) to convert the parallel data into the natural sample order for each parallel lane, and group every 144 points as an OFDM symbol. After removing the cyclic prefix, 128-point fast Fourier transform (FFT) for each channel was performed to convert the signal back to the frequency domain. In this work, we used Altera's built-in FFT function to perform such signal processing. We used 8 bits resolution for FFT and the number of real multipliers required for each 128-point FFT was 24.

Once in a frequency domain, we still need to estimate and compensate for the channel transfer and the random phase rotation caused by laser phase noise in much the same way as explained in detail [15]. This received signal in frequency domain at each subcarrier can be represented as,

$$R_d(k) = H(k) B_d(k) C_d(k) \tag{23}$$

where *k* indicates subcarrier indices and *d* indicates symbol number. $H(k)$ is a slow moving channel transfer function that we can assume constant for the entire frame of 512 symbols. $C_d(k)$ is the transmitted signal modulated in QPSK and $R_d(k)$ is the received signal. $B_d(k)$ is the Fourier transformed time variant random phase fluctuation that needs to be estimated and compensated for each symbol.

Channel transfer function can be estimated by comparing the received data with the pilot symbols and average over all pilot symbols per frame, we can estimate the inverse of the transfer function so that we can use it for later compensation such that,

$$\hat{H^{-1}}(k) = \frac{1}{M}\sum_{d=1}^{M} R_d^{*}(k) C_d(k) \tag{24}$$

where *M* is the number of pilot symbols per frame. The realization of this channel estimate can be done in a simple lookup table when subcarriers are modulated with QPSK as in Table 1 with no need for multipliers.

Table 4. Lookup table for channel and phase estimate

Message symbols of pilot	Modulated symbols of pilot	H^{-1} or B^{-1}	
		real	imaginary
0	*-1+j*	*-a-b*	*a-b*
1	*-1-j*	*-a+b*	*-a-b*
2	*1+j*	*a-b*	*a+b*
3	*1-j*	*a+b*	*-a+b*

Received signal is $R = a + jb$.

Figure 24 shows the diagram for real-time CO-OFDM channel estimation. Once the OFDM window is synchronized, an internal timer will be started, which is used to distinguish the pilot symbols and payload. Two steps are involved in this procedure, channel matrix estimation and compensation. In the time slot for pilot symbols, the received signal is multiplied with locally stored transmitted pilot symbols to estimate the channel response. The transmitted pattern typically has very simple numerical orientation. Thus, multiplication can be changed into addition/subtraction of real and imaginary parts of the complex received signal, which can give additional resource saving. Taking average of the estimated channel matrixes over time and frequency can be used to alleviate error due to the random noise. Then the averaged channel estimation will be multiplied to the rest of the received payload symbols

to compensate for the channel response. It is worthy pointing out that one complex multiplier can be comprised of only three (instead of four) real number multipliers.

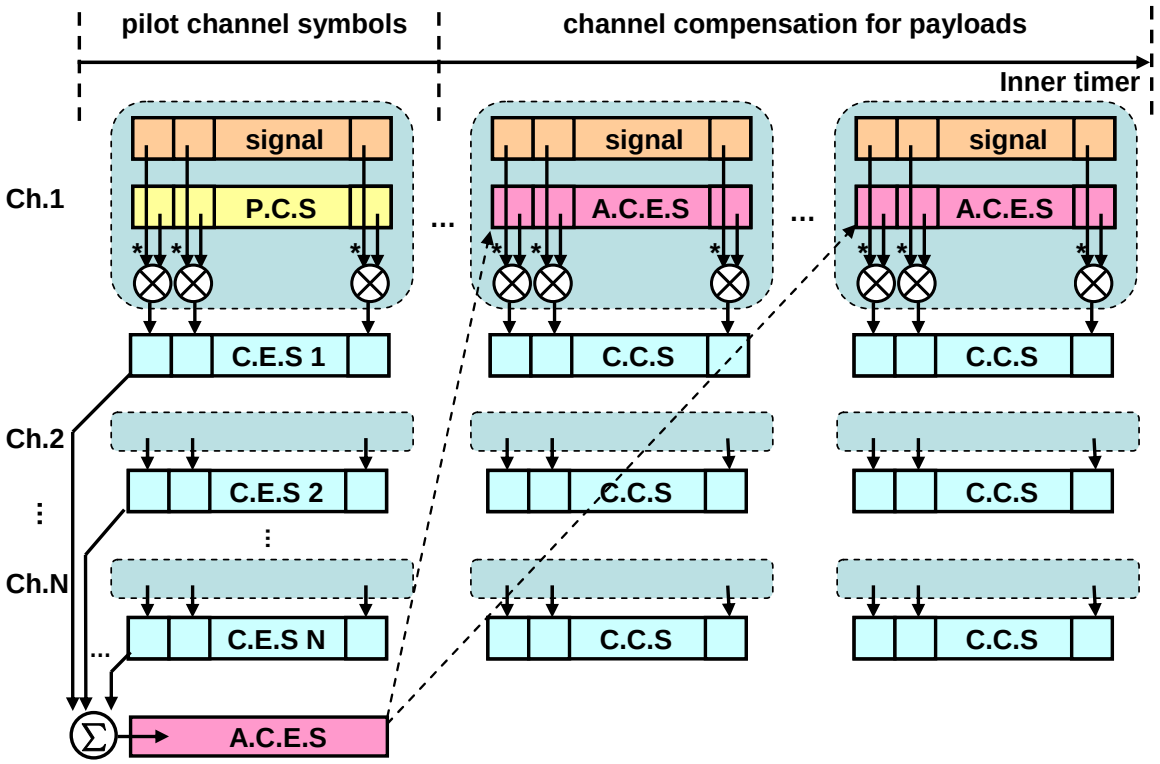

Figure 24. Channel estimation diagram. P.C.S: pilot channel symbol. C.E.S.: channel estimated symbol. A.C.E.S: averaged channel estimated symbol. C.C.S.: compensated channel symbol.

For phase noise estimation, among 115 filled subcarriers, 8 pilot subcarriers were evenly spaced across the OFDM spectrum for phase estimation. Figure 25 shows the location of the pilot subcarriers with respect to the subcarrier indices. Equation (24) can be slightly modified for phase estimation such that

$$\hat{B}_d^{-1} = \frac{1}{N_p}\sum_{k=1}^{N_p} R_d^{*}(k) C_d(k) \tag{25}$$

where N_p is the number of pilot subcarriers and 8 pilots are used in this case before data subcarriers are compensated. The implementation of the phase estimate can also be done by the lookup table in Table 4.

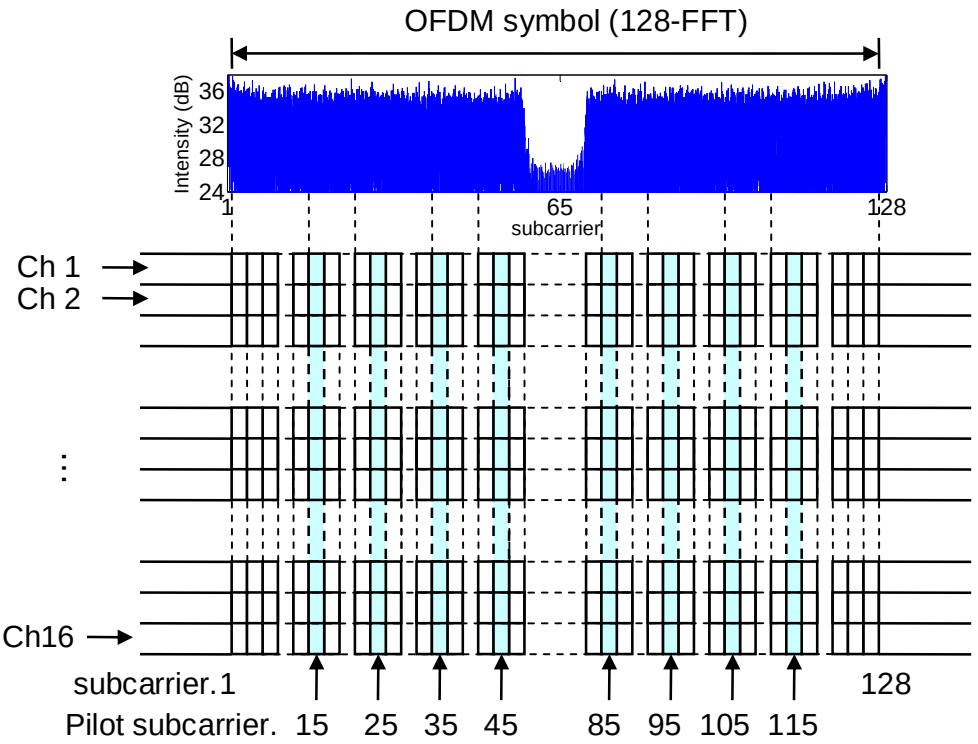

Figure 25. Above: Measured OFDM symbol amplitude with corresponding subcarriers indices. Below: Location of the pilot subcarriers in a symbol with 128 subcarriers.

Similar to channel estimation, phase estimation procedure can also be divided into estimation and compensation parts, which is shown in Figure 26. Pilot subcarriers within one symbol will be selected by the inner timer. These pilot subcarriers then are compared with local stored transmitted pattern to obtain the phase noise information. The same symbol is delayed, and then compensated with the estimated phase noise factor.

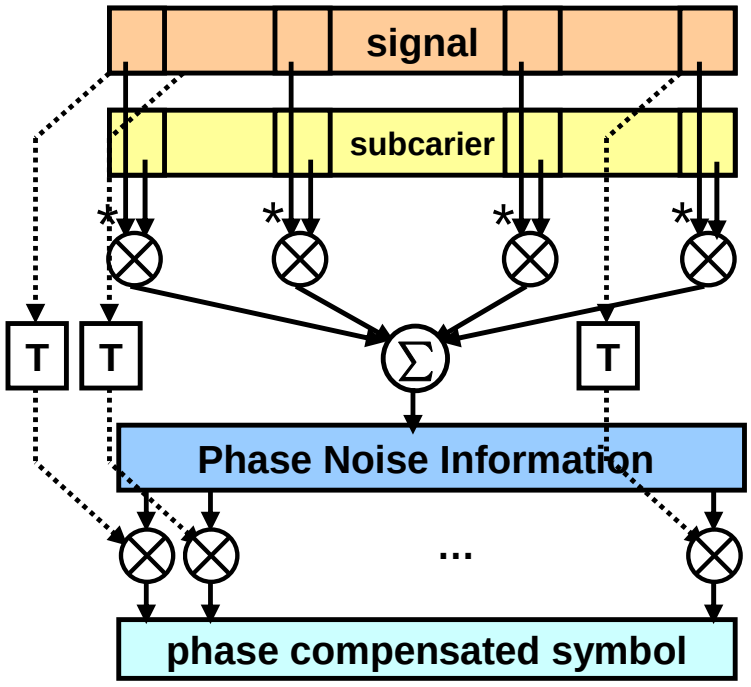

Figure 26. Phase estimation diagram.

Finally, the recovered data was compared with transmitted data inside the FPGA to identify the errors, and the error distribution over a span of continuous 512 OFDM frames was recorded and output periodically through SignalTap II which is an embedded logic analyzer of Altera FPGA.

4.4 Experimental results

As in offline processing measurements, many important parameters can be monitored in a real-time measurement as well through FPGA's on-chip random access memory. The Figure 23 shows the measured amplitude of the autocorrelation. The strong peak is observed and the peak index is successfully recovered to indicate the beginning of the frame and symbol. Figure 27 shows the measured transfer function of the channel. As previously explained, this channel estimate is obtained by the implemented FFT of finite resolution, i.e. 8 bits. Although the channel estimate from one symbol contains observable noise, averaged over 16 symbols the channel estimate remove most of the noise. Noticeable ISI is not added to this measurement, and the periodic fluctuation in the real part of the transfer function is due to the circular time shift of the sequence as the beginning of the FFT window is left arbitrary within CP, as explained previously on the employed symbol synchronization technique. The number of peaks corresponds to the number of circular sample shifts in the FFT window compared to the original OFDM symbol. More improvement in overhead efficiency is possible with the frequency domain averaging of the estimated channel as previously reported with high PMD channel [88]. Figure 28 shows the phase evolution of the OFDM symbols. Received 8 pilot subcarriers are compared to the locally stored patterns according to the previously described diagram and the results are averaged to obtain a less noisy phase estimate and the phase compensation is applied to the rest of subcarriers. In contrast to the blind phase detection such as Viterbi-Viterbi phase detection [89], often used in single-carrier digital coherent optical receiver [85], [24], the cycle slip of the phase is not a concern for the pilot assisted, i.e. pilot-aided phase detection which is naturally fit for OFDM.

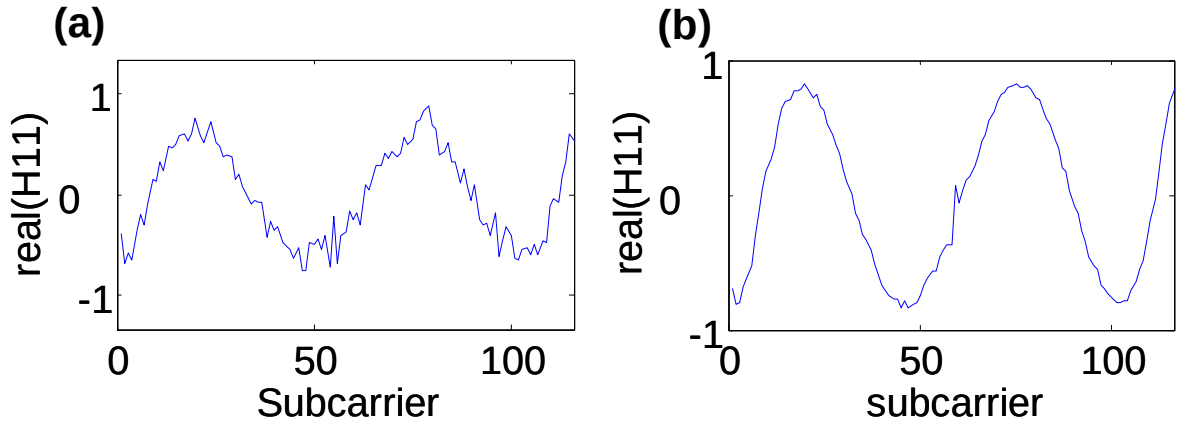

Figure 27. Measured channel transfer function estimated for each subcarrier. (a) One symbol out of 16 pilot symbols is used to estimate the channel. (b) All 16 symbols are averaged.

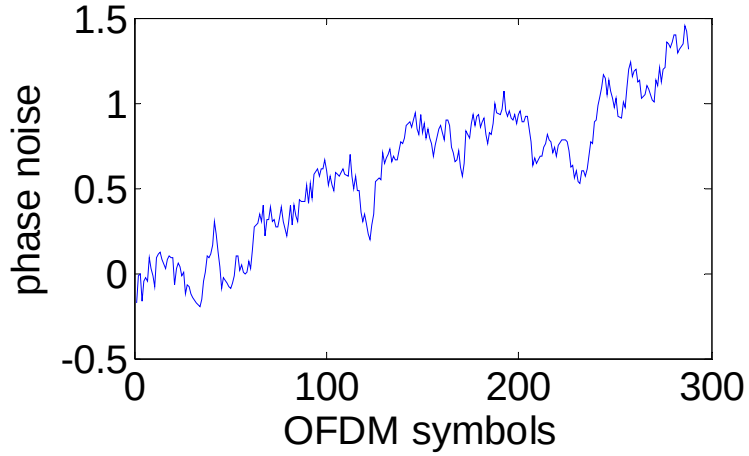

Figure 28. Measured phase evolution of the OFDM symbols. 8 out of 115 subcarriers are used as pilot to estimate and compensate for the detected phase.

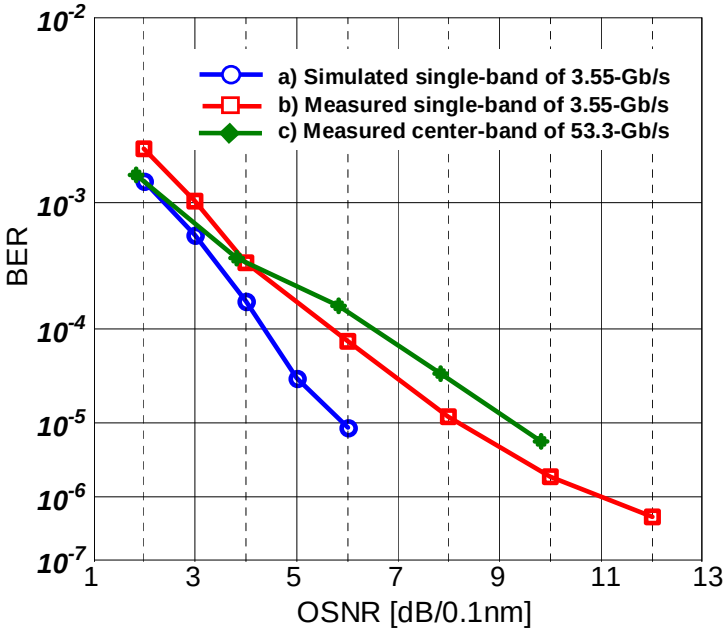

Figure 29. Simulated and measured BER vs. OSNR of the real-time coherent optical OFDM receiver. The curve (a) with circle dot indicates simulated result for the single-band of 3.55 Gb/s signal, (b) with empty square dot

indicates measured result for the single-band of 3.55 Gb/s and (c) with solid square dot is measured result for the center-band of 54Gb/s multi-subband experiment.

Figure 29 shows the simulated and measured BER as a function of OSNR for 3 cases: (a) a simulated single 3.55 Gb/s CO-OFDM signal (b) a measured single 3.55 Gb/s CO-OFDM signal; (c) the measured center subband of the 54 Gb/s multi-band signal. For a simulated curve, 100-kHz linewidth is assumed for both Tx and LO laser. In case (b), a BER better than 10^{-3} can be observed at OSNR of 3 dB. The OSNR is defined as the signal power in the subband under measurement over the noise power in a 0.1-nm bandwidth. In case (c), the required OSNR for BER 10^{-3} is 2.5 dB. There is virtually no penalty introduced by the band-multiplexing. The measured and simulated results agree closely at lower OSNR suggesting valid results are obtained in our measurement. The measured results, however, have slower slope of BER over OSNR than the simulated result and the discrepancy widens at higher OSNR. This can be attributed to the limited resolution of both ADC and DSP and more in-depth study is required to quantify these effects. Although we used the same laser source for both Tx and LO in the experiment due to the low tolerance to the frequency offset, the simulation result is obtained assuming 2 separate laser sources for Tx and LO and indicates no error floor. The overall measured BER however may have benefited from the same laser source for Tx and LO and can degrade if the separate laser source is used for intradyne measurement. There is also no apparent error floor observed in this measurement. Figure 29 shows two recorded BER measurements performed by the FPGA at high OSNR (of ~19 dB), (a) over a single OFDM frame and (b) over 512 OFDM frames. The horizontal scale of the figures indicates the different time span. The figure (a) shows the measurement result of a few symbols (16th and 17th symbol), although the error count in this figure is still recorded for the entire OFDM frame that contains those symbols. The figure (b) is recorded by a separate measurement taken for a longer time span of 512 frames. In the measurement (b), the measured error counts over 512 OFDM frames or $\sim 5.4\times10^{7}$ bits are 2, indicating a BER floor of 3.7×10^{-8}. To the best of our knowledge, this is the first report of BER under 10^{-7} for real-time CO-OFDM implementation. Further improvement can be expected if more bit resolution is employed. The overall data rate can potentially be increased with polarization-division multiplexing and/or higher level modulation format such as 16-QAM.

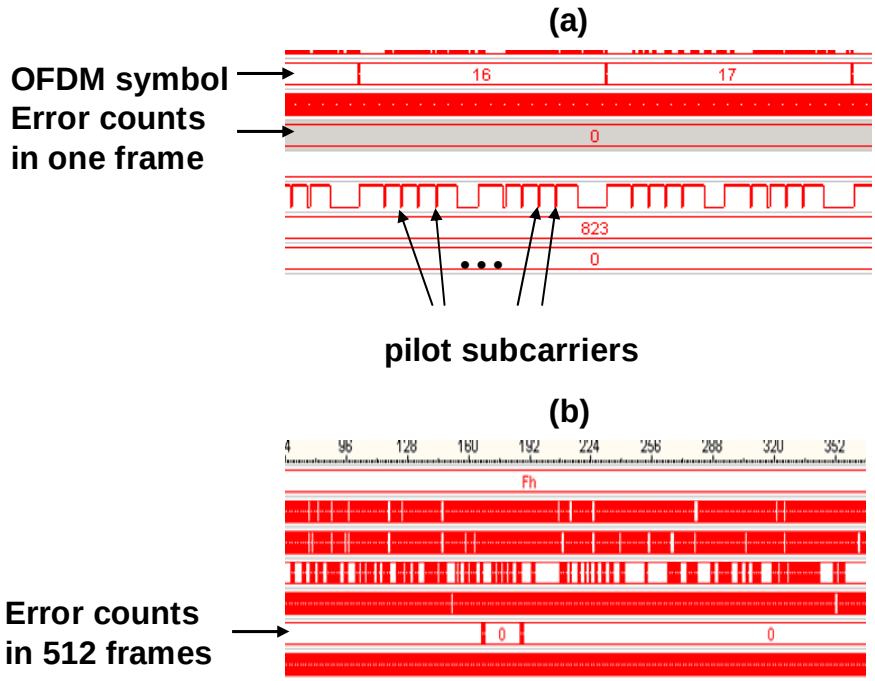

Figure 30. Recorded BER measurements from SignalTap II over (a) a single OFDM frame and (b) over 512 frames. Pilot subcarrier locations are indicated in the figure as bits with low level.

We should note that as opposed to the relatively simple frequency offset correction realizable in single-carrier coherent QPSK detection [90], the frequency offset correction of OFDM can require more FPGA resource and is not included in this real-time implementation. It is therefore desirable to move from the reported homodyne (Tx and LO share the same source) to a true intradyne detection in future work. Another challenge in CO-OFDM is the more stringent requirement in laser linewidth when the sampling speed is lower. One of the reason is that the narrower subcarrier bandwidth due to lower sampling speed has higher sensitivity to phase noise. This increased sensitivity to phase noise at lower sampling rate is also true for the single-carrier QPSK detection but the single-carrier QPSK is much more tolerant that the DFB laser of ~1-MHz linewidth can be successfully used to achieve low BER at 2.5 GS/s [91]. The aforementioned disadvantage of OFDM, however, becomes less significant as the sampling and bit speed increase.

In addition to the DSP algorithms that can be implemented, other important considerations for real-time optical OFDM are the hardware limitation, resource usage, and FPGA/ASIC capacity. The sampling speed/bandwidth of the ADC is one of the most critical limitations for the real-time implementation. Another most influential factor is the ADC bit resolution. Figure 31 shows a simulation result of the Q factor of 10 Gb/s QPSK CO-OFDM receiver as a function of bit-resolution of ADC outputs (curve with diamonds). 5-bit

resolution gives a Q penalty less than 0.8 dB. Moreover, the bit resolution of complex multipliers is also investigated. In the simulation shown in Figure 31 (curve with square), the ADC bit resolution is set to 5, and the bit resolution of multipliers increases from 3 to 10 bits. It can be seen that the system sensitivity improves with increased resolution and then saturates beyond 6-bit resolution. Typically, two kinds of commonly used DSP resources are 9-bit or 18-bit multipliers in FPGA. Thus, splitting a single 18-bit multiplier into two 9-bit multipliers can double the processor resources without degrading the system performance. Table 5 shows the multiplier resource usage in each procedure for the experiment in [26]. Frequency estimation with acceptable DSP precision will consume around 200 multipliers. Due to the limited resource, frequency estimation is not included in [26], but was implemented in a later experiment [92] where a larger capacity FPGA was used. Table II shows the compilation report on the resource usage and final estimated speed in Altera Stratix II GX FPGA.

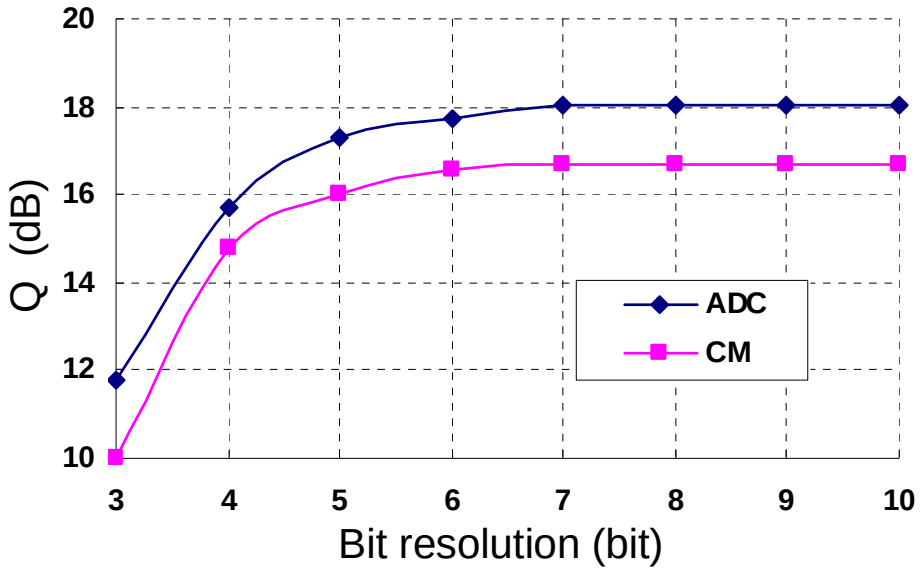

Figure 31. Q factor as a function of bit resolutions of ADC and complex multipliers. QPSK modulation is assumed. CM: complex multipliers (with 5-bit ADC resolution).

Table 5: FPGA 9-bit multipliers usage

Function	Multipliers	Channel
Auto-correlation	20	1
FFT	24	16
Channel estimation	3	16
Phase estimation	3	16
Total	500	

Table 6 : FPGA compilation report

Function	Consumed/Resource	Report
logic registers	77,797 / 106,032	88%
memory bits	626,671 / 6,747,840	9 %

9bit multipliers	500 / 504	99 %
Estimated Speed	152.21 MHz	

For optical OFDM FPGA implementation, multipliers are the most limited resource. The current FPGA technology can support over 2,500 multipliers. This implies it can ideally support dual polarization with up to 5 GS/s sampling rate per single DSPU. Designing with such FPGAs, 10 Gb/s and beyond is achievable. With CMOS ASIC design [6], the available number of multipliers and logic registers can be largely increased. Recently, a 40 Gb/s coherent QPSK transceiver implemented in 90 nm CMOS ASICs has been demonstrated in real-time, with four 6-bit 20GS/s ADCs [6]. Since CO-OFDM has lower computational complexity, the state-of-the-art silicon technology can potentially allow the real-time implementation for the reception of CO-OFDM at 40 Gb/s and beyond.

4.5 Conclusion

We have discussed detail architectures of the real-time implementation of a coherent optical OFDM receiver. The unique difficulties in high-speed signal processing of optically transmitted OFDM data are discussed and a few unique solutions and implementations were presented for OFDM symbol synchronization. The architectures were successfully implemented in a FPGA and demonstrated at 2.5 GS/s. The real-time receiver was used to receive a 53.3 Gb/s multi-band CO-OFDM signal with an error floor as low as 3.7×10^{-8}. Further possibilities of improving the computational efficiencies are discussed. With foreseeable improvement in ADC sampling speed and DSP resource, real-time reception of 100 Gb/s CO-OFDM can be expected.

5 Advanced Coding for CO-OFDM without Bandwidth Extending

Traditionally, advanced coding is used as forward error correction (FEC) technique to improve transmission system performance. For instance, the Reed–Solomon (RS) code with rate of (255,239) is widely used as first generation FEC code to correct the noised signal. This can help to completely recover the signal with bit error ratio (BER) under 2e-3 when the errors are evenly distributed. However, the codes in FEC usually introduce the overhead over the transmission rate. (255,239) RS coded will bring 7% overhead. This means the transmitted bandwidth has to be extended to fill in the coded signal. Moreover, the code with higher overhead will further improve the signal, while the signal bandwidth will become wider. Consequently the spectrum efficiency will reduce. Nowadays, the over Tb/s transmissions have been demonstrated, the signal bandwidth over the fiber media appears more costly. To save the transmission bandwidth, the advanced coding to improve system performance without the bandwidth extension is a promising technique. In this chapter, two approaches with different coding scheme for CO-OFDM are mainly discussed, trellis coded modulation (TCM) and low-density-parity-check (LDPC).

5.1. Trellis coded modulation for CO-OFDM

5.1.1 Introduction

100 Gb/s [16-18] and 1-Tb/s CO-OFDM transmission [19-21] has been recently demonstrated with polarization-division multiplexing (PDM) QPSK subcarrier modulation. To increase spectral efficiency, 16-QAM [93] and 32-QAM [94] subcarrier modulation has been applied to CO-OFDM transmission. The receiver sensitivities for these high-level QAM modulation formats, however, are much reduced as compared to QPSK. One method to efficiently increase the receiver sensitivity of a high-level QAM is through trellis-coded modulation (TCM) [95], a technique well known in wireless communication. In this scheme, the signal bandwidth remains the same, while the receiver sensitivity is much improved by convolutional coding over an expanded signal constellation. TCM was first proposed for optical communications by H. Buelow et al. [96], and was later investigated by other groups [97-99]. Through numerical simulations, single-carrier coded DQPSK with rate 1/2 was shown

to provide higher receiver sensitivity than uncoded DBPSK [96], and coded 8-ary DPSK with rate 2/3 was shown to provide higher sensitivity than uncoded DQPSK [97,98]. Recently, single-carrier coded 16-QAM with rate 3/4 was experimentally demonstrated with better performance than uncoded 8-ary PSK when bit error ratio (BER) became less than 10^{-5} [99]. Using TCM for subcarrier modulation in CO-OFDM was recently proposed and experimentally demonstrated with coded 8-PSK [100], showing 2.6 dB improvement in receiver sensitivity over uncoded QPSK at BER=10^{-3}. In this section, we demonstrate coded 32-QAM with rate 4/5 for subcarrier modulation in a 44 Gb/s PDM CO-QPSK signal occupying 7-GHz optical bandwidth. With the proposed TCM structure, coded 32-QAM improves the receiver sensitivities by 3.4 dB and 5.0 dB, respectively, at BER of 10^{-3} and 10^{-4}, as compared to uncoded 16-QAM with the same net data rate. As such, TCM may be an attractive approach for high spectral efficiency CO-OFDM systems where the receiver sensitivity becomes a critical issue.

5.1.2 CO-OFDM with Trellis-coded 32-QAM for subcarrier modulation

Figure 32 shows the digital signal processing (DSP) blocks used in CO-OFDM transmitter and receiver with trellis-coded 32-QAM for subcarrier modulation. The key new DSP blocks are the TCM encoder and decoder. The TCM encoder takes in 4 input bits, and output coded 5 bits, which are used for 32-QAM subcarrier modulation. The rate of the TCM is thus 4/5. Figure 33 shows the schematic of one implementation of the TCM encoder, which leaves the first two input bits uncoded, but convolutionally codes the last two input bits into three coded bits through a 128-state rate-2/3 convolutional encoder with 3 parity-check coefficients defined by G. Ungerboeck in [95], h^2=042, h^1=014, h^0=203, where $h^{0\text{-}2}$ is the multiplier coefficients for the three output coded bits in octal notation. The following parity-check equation is satisfied,

$$\sum_{i=0}^{2}\left(h_v^i z_{n-v}^i \oplus h_{v-1}^i z_{n-v+1}^i \oplus \ldots \oplus h_0^i z_n^i\right) = 0 \tag{26}$$

where $\oplus$ denotes modulo-2 addition, $\{Z_n\}$ is the code sequence, v is the constrain length, which is equal to 7 in the implementation shown in Figure 33. The asymptotic coding gain of the TCM at low BER is 7.37 dB. The coded subcarriers are then processed with regular OFDM operations, such as inverse fast Fourier transform (IFFT), parallel-to-serial formatting, cyclic prefix (CP) or guard interval (GI) insertion. At the receiver, the time-domain OFDM

signal in first converted into frequency domain by fast Fourier transform (FFT). Before that, two more procedures, namely OFDM window synchronization and CP removal, are performed. Channel and phase noise estimation and compensation are then conducted. Once the 32-QAM modulated subcarriers are recovered, they are fed into the TCM decoder, where Viterbi decoding algorithm is used. Two sorts of decoding schemes are performed, soft-decision and hard-decision decoding, with the earlier providing higher coding gain.

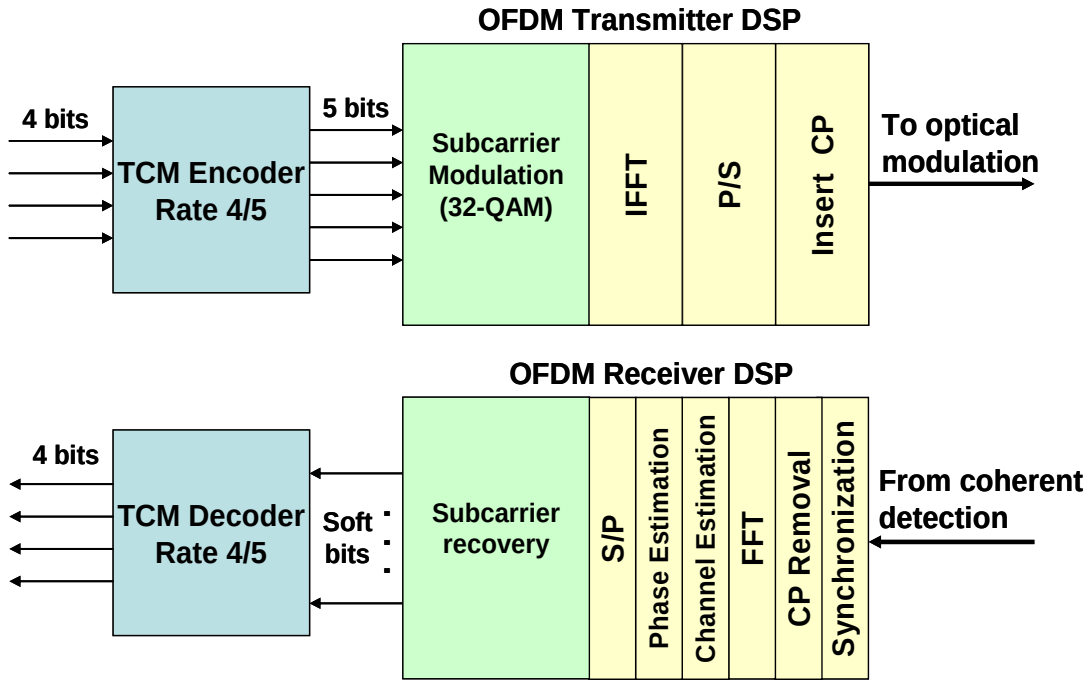

Figure 32. Transmitter and receiver DSP blocks in CO-OFDM trellis-coded 32-QAM encoder with trellis-coded 32-QAM for subcarrier modulation.

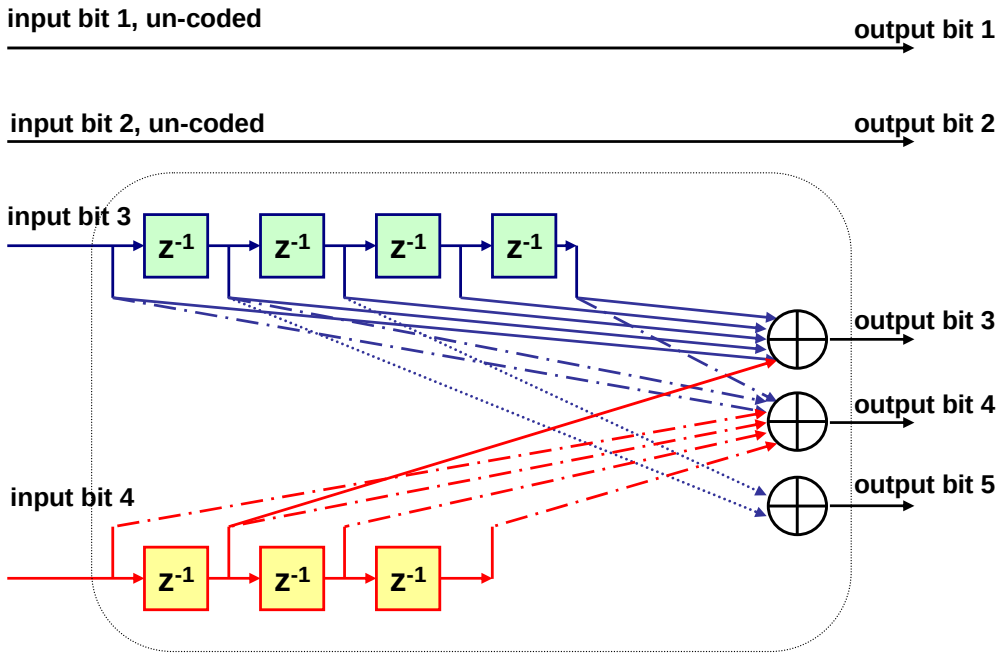

Figure 33. Schematic of a 0.8-rate with a 128-state rate-2/3 convolutional encoder

5.1.3 Experiment for TCM-CO-OFDM at back-to-back

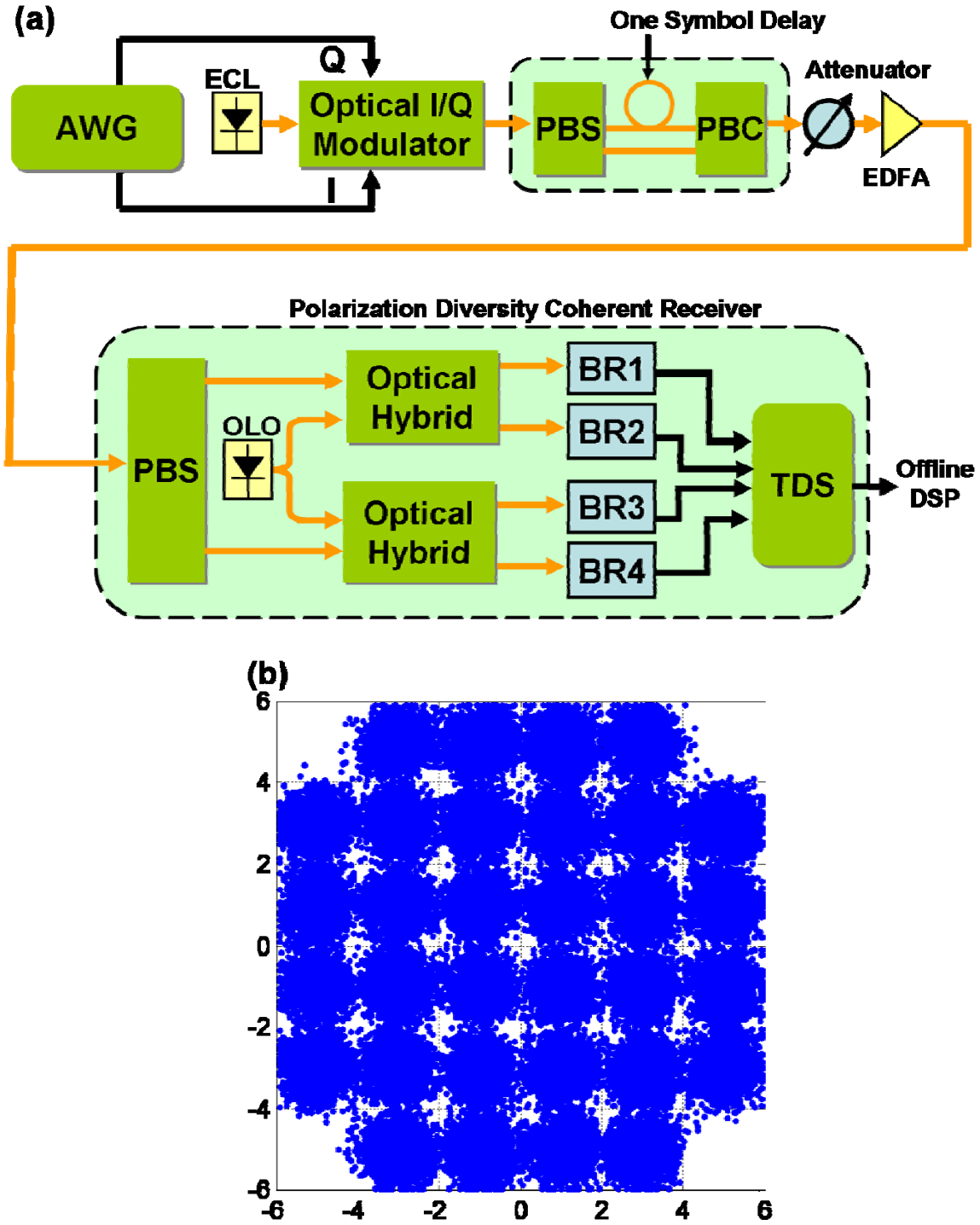

Figure 34. (a) Schematic of the experimental setup of a 44 Gb/s PDM CO-OFDM system. AWG: Arbitrary waveform generator. PBS(C): polarization beam splitter (combiner). BR: balanced receiver. TDS: Time-domain sampling scope. (b) Recovered 32-QAM constellation of the subcarriers in one polarization at OSNR=20 dB before TCM decoding.

Figure 34 (a) shows the experimental setup. At the transmitter, a data stream consisting of pseudo-random bit sequences of length 2^{15}-1 was first send into TCM encoder, where every 5-bit output is mapped with 32-QAM modulation. The coded signal in then filled onto 80 subcarriers. The data subcarriers, together with 8 pilot subcarriers and 20 unfilled subcarriers, were converted to the time domain via inverse Fourier transform (IFFT) with size 128. The unfilled subcarriers consisted of two center subcarriers, allocated to accommodate the frequency offset between the transmitter laser and the receiver optical local oscillator (OLO), and 18 edge subcarriers, used for over-sampling. A cyclic prefix of length 16 samples was used, resulting in an OFDM symbol size of 144. Four training symbols (TSs), consisting of two known correlated symbols [16], were inserted at the beginning of each OFDM frame that contains 1000 data symbols to facilitate frame synchronization and channel estimation. The real and imaginary parts of the OFDM symbol sequence were converted to analog waveforms by two digital-to-analog converters (DACs) operating at 10 GS/s, before being amplified and used to drive an optical I/Q modulator that was biased at null. The transmitter laser was an external-cavity lasers (ECLs) with 100-kHz linewidth, and for simplicity, the OLO shared the same laser as the transmitter laser. The maximum data rate of the signal after the optical modulation was 27.7 Gb/s. The optical signal was then split by a 3-dB coupler into two equal copies, which were then delayed by one symbol period with respect to each other and combined by a polarization beam splitter (PBS) to form a PDM-OFDM signal with a maximum data rate of 55.3 Gb/s before decoding. After the rate-4/5 TCM decoding, the net data rate became 44.3 Gb/s. The optical bandwidth of the PDM-OFDM signal is only ~7 GHz, which potentially allows for a spectral efficiency of up to 6.3 bit/s/Hz. Adjustable amount of optical noise was added by an optical pre-amplifier followed by an adjustable attenuator. At the receiver, the PDM-OFDM signal was detected by a digital coherent receiver consisting of a polarization-diversity optical hybrid, an OLO, and four analog-to-digital converters (ADCs), each operating at 50 GS/s. The effective resolution of the ADC's was about 5.5 bits. The digitized waveforms were stored and processed offline in a computer. The BER of the recovered data was obtained by direct error counting. A sample recovered constellation of the subcarriers before TCM decoding is shown in Figure 34 (b). Figure 35 shows the output BER from the soft-decision TCM decoder as a function of the input BER. Each data point corresponds to a measurement conducted on one OFDM frame for a given polarization. Remarkably, raw BER as high as 0.04 (or 4×10^{-2}) can be corrected to be below 10^{-3}. It remains to be seen if the trellis-coded 32-QAM can be applied together with a standard

forward error correction (FEC) code (with a moderate overhead of 7%) to obtain an overall coding gain that is close to the sum of the individual gains from the TCM and the FEC. Figure 36 shows the BER (averaged over the x- and y- polarizations) of the recovered 44 Gb/s PDM-OFDM signal as a function of the OSNR. The raw BER performance of 32-QAM exhibits a high error floor $>5\times10^{-2}$ for OSNR<21 dB. After the soft-decision TCM decoding, the required OSNRs at BER=10^{-3} and 10^{-4} become as low as 14.6 dB and 15.7 dB, respectively. As compared to uncoded 16-QAM (also shown in Figure 36), the required OSNR at BER=10^{-3} and 10^{-4} are lowered by 3.4 dB and 5.0 dB, respectively. The coding gain for BER smaller than 10^{-4} is larger than 5 dB. For OSNR higher than 16 dB, no errors were counted after decoding, indicating a BER much lower than 10^{-5}. The above measurements clearly show the effectiveness of the TCM in improving the receiver sensitivity (or OSNR performance).

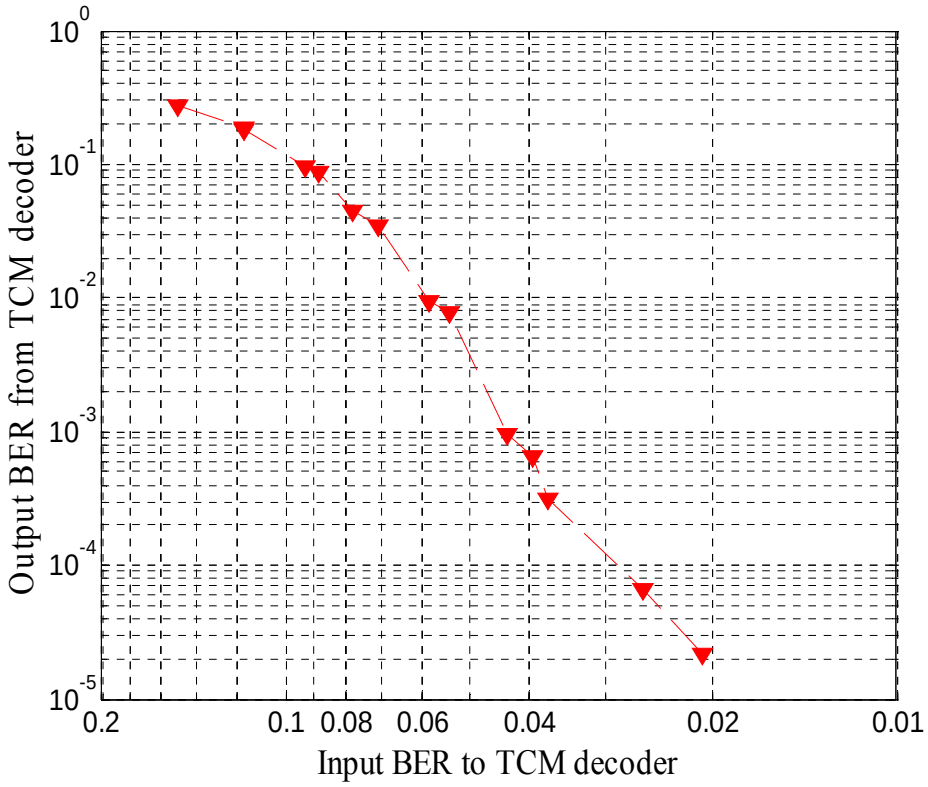

Figure 35. Output BER vs. input BER at the soft-decision TCM decoder.

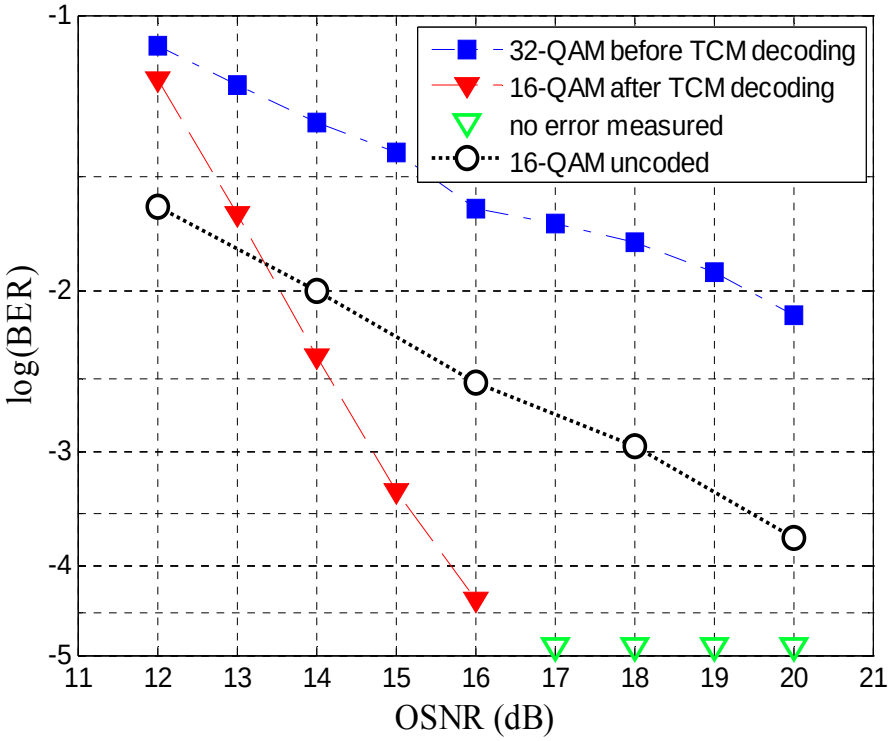

Figure 36. BER performance after the TCM decoding.

5.1.4 Experiment for TCM-CO-OFDM in long haul transmission

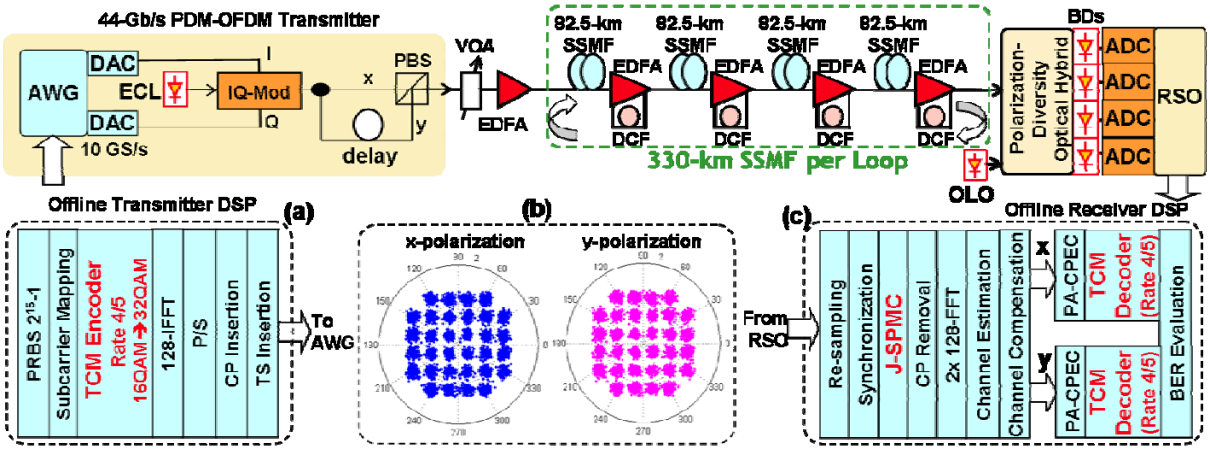

Figure 37. Schematic of the experimental setup of a 44 Gb/s PDM CO-OFDM transmission system. Insets: (a) transmitter-side offline DSP modules including a rate-4/5 32-QAM TCM encoder; (b) sample recovered constellations of trellis-coded 32-QAM subcarriers; and (c) receiver-side offline DSP modules including J-SPMC module and rate-4/5 32-QAM TCM decoder.

Figure 37 shows the schematic of the experimental setup. At the transmitter, offline digital signal processing (DSP), as shown in inset (a), was first performed to generate an OFDM waveform which was later stored in an arbitrary waveform generator (AWG). In the offline DSP, data stream consisting of pseudo-random bit sequences (PRBS) of length 2^{15}-1 was mapped on to 80 16-QAM modulated subcarriers, which were encoded by a rate-4/5 TCM encoder to generate 32-QAM modulated subcarriers. The TCM encoder initially left the first

two input bits uncoded, but coded the last two input bits into three coded bits through a 128-state rate-2/3 convolutional encoder with 3 parity-check coefficients defined by G. Ungerboeck in [95], h^2=042, h^1=014, h^0=203, where $h^{0\text{-}2}$ are the multiplier coefficients for the three coded bits in octal notation. The following parity-check equation was satisfied, $\sum_{i=0}^{2} h_v^i z_{n-v}^i \oplus h_{v-1}^i z_{n-v+1}^i \oplus ... \oplus h_0^i z_n^i = 0$, where $\oplus$ denotes modulo-2 addition, $\{Z_n\}$ is the code sequence, v is the constraint length, which was set to 7. The TCM encoder then mapped the total 5 bits onto trellis-coded 32-QAM, with an asymptotic coding gain of 6.02 dB as compared to un-coded 16-QAM [95].

The 80 coded subcarriers, together with 8 pilot subcarriers and 20 unfilled subcarriers, were converted to the time domain via inverse Fourier transform (IFFT) with size 128. The unfilled subcarriers consisted of two center subcarriers, allocated to accommodate the frequency offset between the transmitter laser and the receiver optical local oscillator (OLO), and 18 edge subcarriers, used for oversampling. After parallel-to-serial conversion (P/S), a cyclic prefix (CP) of length 16 samples was used, resulting in an OFDM symbol size of 144. To facilitate frame synchronization and channel estimation, four training symbols (TSs), [A A A –A], where A is a known OFDM symbol and –A is the inverted version of A, were inserted at the beginning of each OFDM frame that contained 1000 data symbols. The real and imaginary parts of the OFDM waveform were converted to analog waveforms by two digital-to-analog converters (DACs) operating at 10 GS/s, before being amplified and used to drive an optical I/Q modulator that was biased at null. The transmitter laser used an external-cavity laser (ECL) with 100-kHz linewidth. The maximum data rate of the signal after the optical modulation was 27.7 Gb/s. The optical signal was then polarization multiplexed with its one-symbol delayed copy through a polarization beam splitter (PBS) to form a PDM-OFDM signal with a maximum data rate of 55.3 Gb/s before decoding. Note that after the polarization multiplexing, the TSs at the beginning of each OFDM frame contained three dual-polarization (DP) symbols, [A/A, A/A, A/-A], where the symbol before (after) "/" is along x(y)-polarization. The first two DP symbols were thus identical to facilitate frame synchronization through autocorrelation, and the last two DP symbols were correlated in such as way that channel estimation can be readily performed while making the TS power equal to data symbol power [101].

The transmission fiber link was based on a loop setup consisted of four 82.5 km SSMF spans, each of which was followed by a dispersion compensating fiber (DCF) embedded in a 2-stage erbium-doped fiber amplifier (EDFA). The average loss of each span was 20 dB, and

the residual dispersion per span was ~42.5 ps/nm. At the receiver, the PDM-OFDM signal was detected by a digital coherent receiver consisting of a polarization-diversity optical hybrid, an OLO (different from the transmitter laser), and four 50-GS/s analog-to-digital converters (ADCs) embedded in a real-time sampling oscilloscope (RSO). The effective resolution of the ADC's was about 5.5 bits. The digitized waveforms were stored and processed offline. Sample recovered constellations of the subcarriers before TCM decoding in the back-to-back case are shown in inset (b). The receiver-side offline DSP blocks used are shown in inset (c). The other DSP modules used were similar to those described in [102]. Two key DSP modules are (1) joint SPMC (J-SPMC) module, as demonstrated in [103], to mitigate the nonlinear transmission penalty. The principle of J-SPMC is that the SPM effect on one polarization component not only has a contribution from the power of this polarization, but also has a contribution from the other polarization with a different scaling factor. So, to effectively compensate for the SPM effect for PDM-OFDM, the J-SPMC scheme can calculating and compensating phase modulation for each polarization by taking consideration of both polarization components; and (2) rate-4/5 32-QAM TCM decoder which used soft-decision Viterbi decoding algorithm. After TCM decoding, the net data rate became 44.3 Gb/s. The optical bandwidth of the signal was ~7 GHz, so this format potentially allows for a spectral efficiency up to 6.3 bit/s/Hz. The BER of the recovered data for each polarization was obtained by direct error counting.

Figure 38 (a) and (b) show the Q factor of the received 32-QAM signal, derived from the measured BER, after 330 km transmission as a function of signal launch power. The optimum signal power is increased from ~0 dBm without SPMC to ~1 dBm with SPMC. At the optimum powers, no error was measured after TCM decoding (for one entire OFDM frame containing 0.64 million bits), indicating a Q factor increase of >6 dB as compared to that before decoding. Figure 38 (c) shows the output BER as a function of input BER at the TCM decoder. Remarkably, an input BER of ~0.03 can be corrected to $<10^{-3}$ at the output.

Figure 39 shows the TCM decoder performance after 660 km transmission (or 2 loops). The optimum signal power is increased from -2 dBm without SPMC to 0 dBm with SPMC. At the optimum powers, the Q factor increase from TCM decoding is ~6 dB. The dependence of the output BER on the input BER at the TCM decoder again shows strong error correcting capability of the TCM decoder.

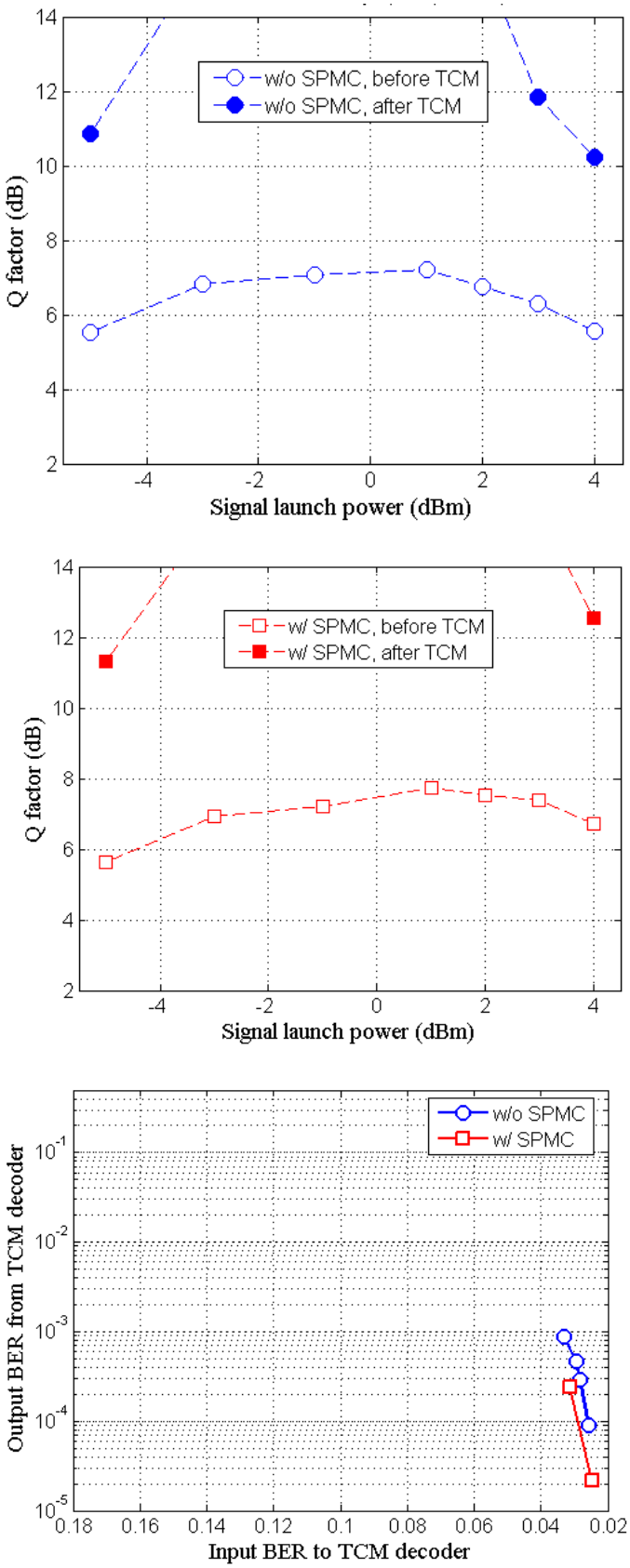

Figure 38. The signal Q factor (derived from BER) after 330 km transmission as a function of launch power without (a) and with (b) SPMC, and output BER vs. input BER at the soft-decision TCM decoder (c). Q values higher than 14 dB in the figure indicates that no error was counted in one OFDM frame.

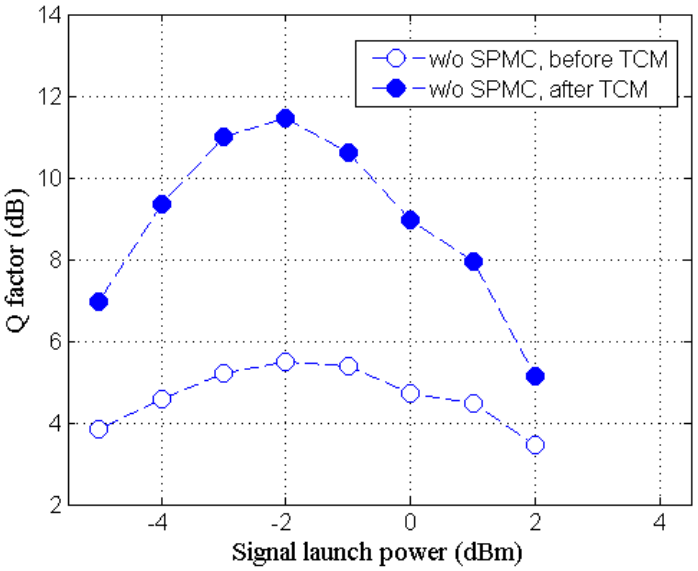
w/o SPMC, before TCM
w/o SPMC, after TCM
Q factor (dB)
Signal launch power (dBm)

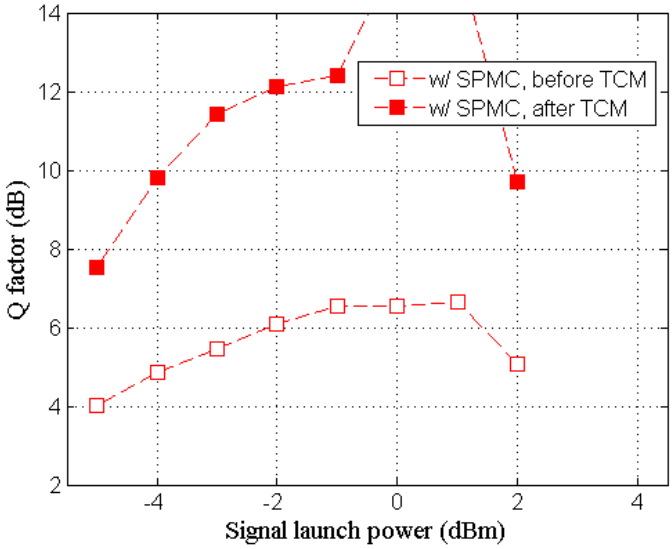
w/ SPMC, before TCM
w/ SPMC, after TCM
Q factor (dB)
Signal launch power (dBm)

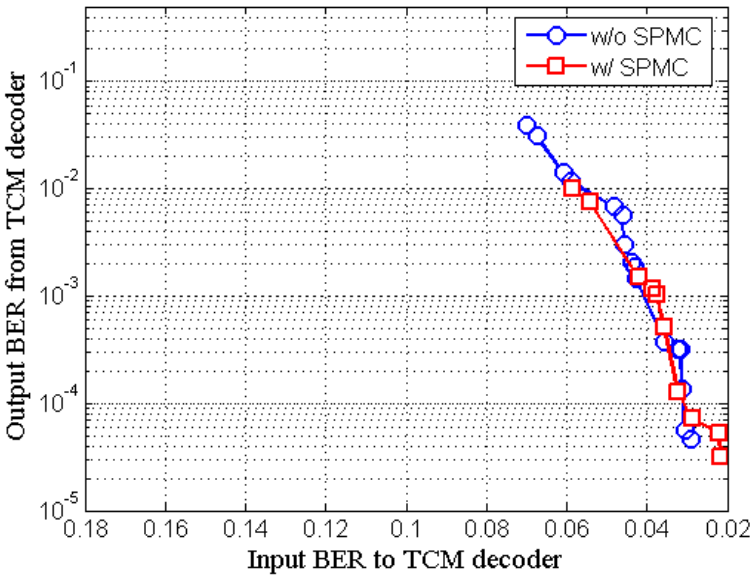
w/o SPMC
w/ SPMC
Output BER from TCM decoder
Input BER to TCM decoder

Figure 39. The signal Q factor (derived from BER) after 660 km transmission as a function of launch power without (a) and with (b) SPMC, and output BER vs. input BER at the soft-decision TCM decoder (c).

Figure 40 shows the TCM decoder performance after 990 km transmission (or 3 loops). The optimum signal power is increased from -3 dBm without J-SPMC to -1 dBm with J-SPMC. At the optimum powers, the Q factor increase from TCM decoding is ~2.5 dB for the case without SPMC, and ~5 dB for the case with SPMC. With SPMC and TCM, the optimal signal Q factor after the 990 km transmission is 11 dB, ~1.8 dB higher than the threshold of a typical enhanced FEC with 7% overhead. In addition, this performance is better than that of the uncoded 16-QAM CO-OFDM [103] after the same transmission link by ~2 dB. Finally, the output-input BER curve of TCM decoder shows uncompromised error correcting capability in this nonlinear transmission regime.

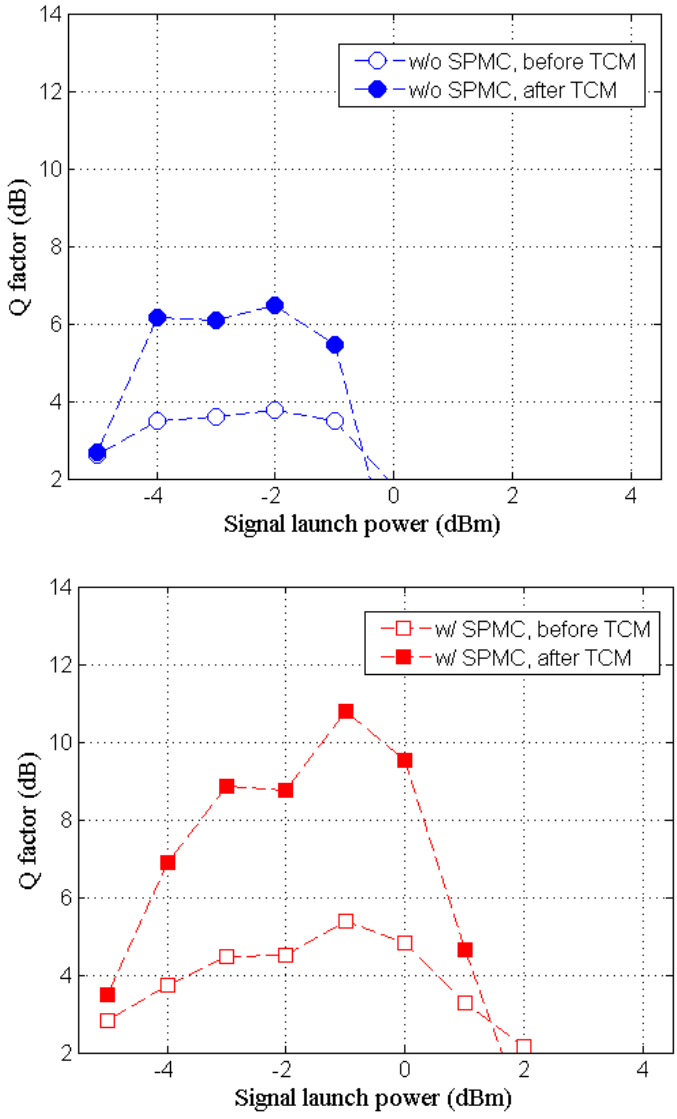

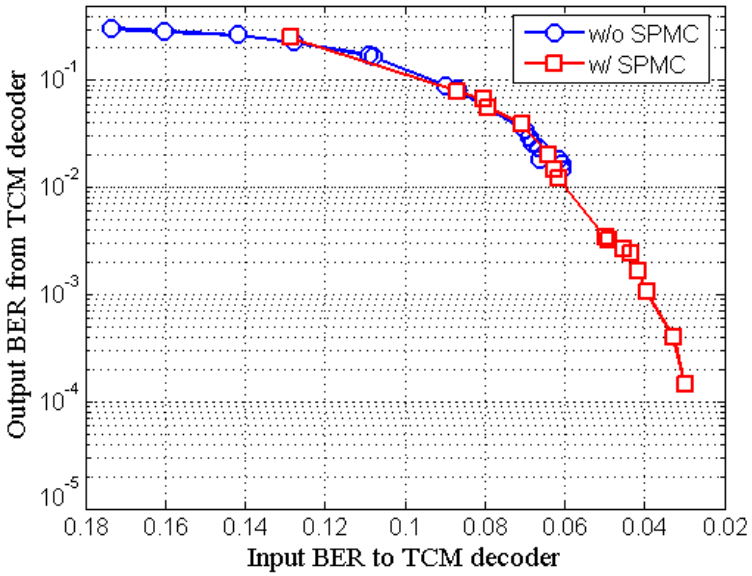

Figure 40. The signal Q factor (derived from BER) after 990 km transmission as a function of launch power without (a) and with (b) SPMC, and output BER vs. input BER at the soft-decision TCM decoder (c).

5.1.5 Conclusion

We have demonstrated long-haul transmission of a 44 Gb/s CO-OFDM signal with trellis-coded 32-QAM at back-to-back and 990 km dispersion-managed SSMF link. Experimental results at back-to-back were obtained with a 44 Gb/s PDM-CO-OFDM signal, showing receiver sensitivity improvements of 3.4 dB and 5.0 dB over its uncoded counterpart at BER of 10^{-3} and 10^{-4}, respectively. For long haul transmission, TCM, together with SPMC, substantially improves the transmission performance, showing its potential to assist high-SE and high-performance CO-OFDM transmission. The combination of TCM with high-level QAM modulation may be a promising technique to support high-spectral-efficiency and high-performance CO-OFDM transmission.

5.2. Low-density-parity-check for CO-OFDM

5.2.1. Introduction

A key approach to improve the reach of these high-speed systems is the use of high performance error correcting codes (ECC), among which low-density-parity-check (LDPC) has been recently pioneered by Djordjevic and Mizuochi [104 - 111] in the optical communication community. (LDPC) can achieve in theory as close as 0.0045dB to Shannon limit [112]. Compared to the first and second generations of forward error correction (FEC), LPDC as one of the main choices of the third generation FEC provides net coding gain around 10dB (at BER=10^{-13}) [111]. Increase overhead or use lower rate coding will further improve

the performance for LDPC codes, but it will also increase the bandwidth requirement for optoelectronic components and therefore the overall cost as is true for many other codes such as RS codes. So it is preferable that the coding gain can be achieved without increase of the signal bandwidth. This was investigated by Ungerboeck in his seminal work on Trellis coded modulation (TCM) [95]. In this section, following the similar spirit, we start with the conventional system with 4-QAM of 2 bits/symbol modulation, and expand the constellation to 16-QAM modulation of 4 bits/symbol that results in twice of data rate within the same electrical and optical bandwidth. The extra data rate (50%) is then used for rate ½ LDPC coding that results in the same net spectral efficiency as the conventional 4-QAM. The net effective coding gain of rate ½ LDPC coded 16-QAM modulation over conventional 4-QAM is demonstrated for the first time to the best knowledge of the authors, and the receiver OSNR sensitivity of 12.5 dB at data rate of 107 Gb/s is found, which is a record sensitivity for 100 Gb/s transmission experiment. Finally, we show the first 400 Gb/s LDPC coded 16-QAM CO-OFDM transmission over 960 km SSMF without Raman amplification. The results of this work show that CO-OFDM can be a potentially attractive candidate for 400 Gb/s or 1 Tb/s Ethernet long-haul transport over the installed link with the aid of high efficiency ECC. There are two relevant categories of publications prior to this work: one is to improve the transmission sensitivity by using stronger error correction codes, but requiring more overhead and electronic bandwidth [110]; the other is high spectral efficiency transmission by using higher order modulation, but requiring much higher OSNR and more stringent component specifications such as high resolution for ADC/DAC [6]. Our approach distinguishes from these two classes of the work in that we improve the sensitivity without a need for wider electrical bandwidth, and stringent ADC/DAC resolution, which may lead to an attractive solution for many applications.

5.2.2. Experiment setup and system configuration

The primary goal of this report is to demonstrate significant improvement of the receiver sensitivity through the use of LDPC without requiring higher optoelectronic bandwidth. Namely, we present a system design based on 16-QAM to provide coding overhead for LDPC, achieving enhanced receiver sensitivity while maintaining the same spectral efficiency of 3.3 bit/s/Hz as the uncoded 4-QAM modulation [7]. For ECC, we choose LDPC in this work as it provides flexibility of arbitrary rate coding compared to relatively rigid coding rate in TCM. Figure 41 shows the system configuration for 400 Gb/s LDPC coded 16-QAM CO-OFDM

system. Although longer block length can improve the coding performance, it also increases the hardware complexity. We use the practical length of LDPC code that is close to what have been demonstrated in real-time using state-of-art FPGA [109,110]. We use Reed-Solomon codes as outer code to eliminate possible error-floor in LDPC [112]. The data is first fed into RS (255, 239) and then the LDPC (4000, 2000) [113] encoder. In order to eliminate the influence of burst-errors, an interleaver is placed between the two serially-concatenated FEC codes [114], where the input signal is filled symbol by symbol, and output is sent subcarrier by subcarrier. The encoded data are then fed into 16-QAM OFDM base band generator to obtain digital OFDM time-domain signal, including procedures of serial-to-parallel conversion, data mapping to 16 QAM constellation, IDFT and guard interval insertion. The parameters for the OFDM baseband generation are as follows: 128 total subcarriers; guard interval is 1/8 of the symbol period. Middle 102 subcarriers out of 128 are filled, from which 4 pilot subcarriers are used for phase estimation. The middle two subcarriers are fed with zeros, where the frequency signal and local lasers are located. Polarization multiplexing doubles the raw rate to 53.3 Gb/s per band. After LDPC decoding, the net data rate is 26.7 Gb/s ($10\ \text{GHz} \cdot \log_2(16_{\text{QAM}}) \cdot 2_{\text{pols}} \cdot 96) / (128 \cdot 1.125_{\text{GI}}) \cdot 50\%_{\text{LDPC}}$), excluding the cyclic prefix, pilot tones, and unused middle two subcarriers. The real and imaginary parts of the OFDM waveforms are uploaded into an AWG operated at 10 GS/s to generate I/Q analog signals, and subsequently fed into I and Q ports of an optical I/Q modulator respectively. The optical input to the optical I/Q modulator is derived from a recirculating frequency shifter (RFS), essentially a recirculating loop including an I/Q modulator and optical amplifiers [19]. A multitone-source is generated by using a CW laser light replicated 16 times via the RFS, and is modulated into a 16-band CO-OFDM signal after being driven by a complex electrical OFDM signal, carrying a data rate of 428 Gb/s. The number of tones in the RFS is controlled by the bandwidth of the optical band-pass filter in the RFS loop, and the RF tone frequency is 7.96875 GHz, phase-locked with the AWG using a 10 MHz reference clock. This is to ensure that all the subcarriers across the entire OFDM spectrum are at the correct uniform frequency grids. There is no frequency guard band between each sub-band. The optical OFDM signal from the RFS is then inserted into a polarization splitter, with one branch delayed by one OFDM symbol period (14.4 ns) to emulate the polarization multiplexing, resulting in a total line rate of 856 Gb/s. The signal is then coupled into a recirculation loop comprising of 2×80 km SSMF fiber (span loss of 18.5 dB and 17.5 dB) and three EDFAs to compensate the loss. The signal is coupled out from the loop and received with a polarization diversity coherent

optical receiver [16,17]. The performance is detected on a per-band basis by aligning the local laser to the center of each band, and the detected RF signal is anti-alias filtered with a 7-GHz low-pass filter. The four RF signals for the two I/Q components are then input into a Tektronix Time Domain-sampling Scope (TDS) and are acquired at 20 GS/s and processed with a MATLAB program using 2×2 MIMO-OFDM models, which are detailed in [16,17]. Finally the complex symbol values are input to the LDPC soft-decoder for data recovery.

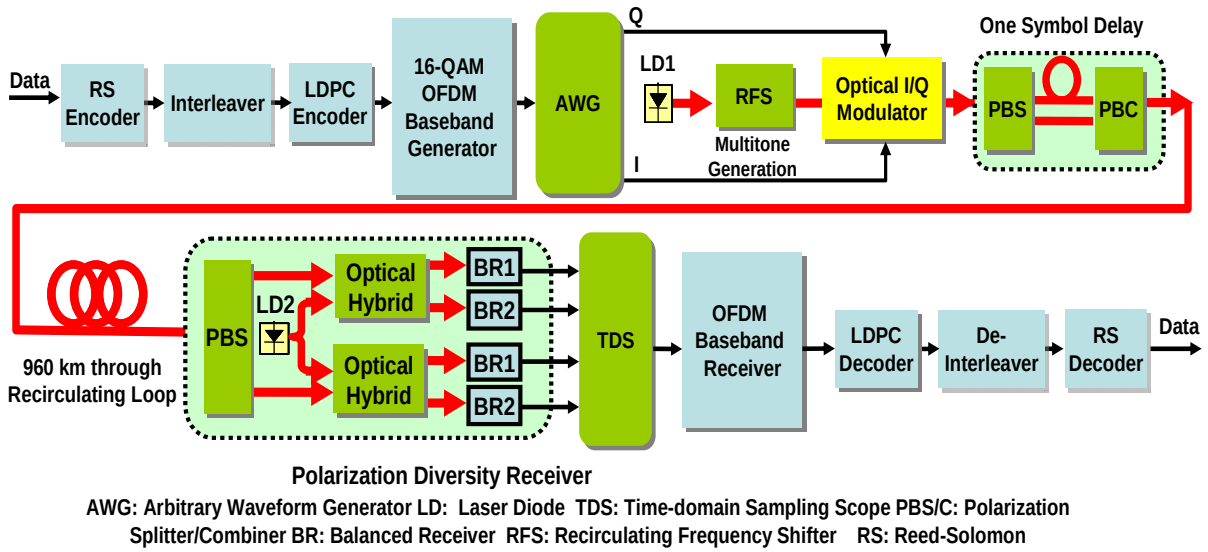

Figure 41. Experimental setup for 400 Gb/s LDPC coded CO-OFDM transmission.

LDPC codes was first invented by R. G. Gallager in 1960s [115], and rediscovered in 1990s by MacKay [116]. It was introduced to the optical communications during the last decade by Djordjevic and Mizuochi [104-111]. The soft-decision algorithm for LDPC can be best described using the Tanner graph [117]. The name of 'low density parity' is derived from the fact that the number of '1's in each column (or row) of the parity check matrix H (dimension of m times n) is very small compared to the block length. Tanner graph consists of m check nodes (the number of parity bits) and n variable nodes (the number of bits in a codeword) [104].The connection between c_i and f_j is made if the parity check matrix element $(H)_{ij}$ is a 1. Figure 42 shows a typical Tanner graph. The number of edges in the Tanner graph is equal to the number of ones in the parity-check matrix. The inserted H in the figure is the corresponding parity check matrix.

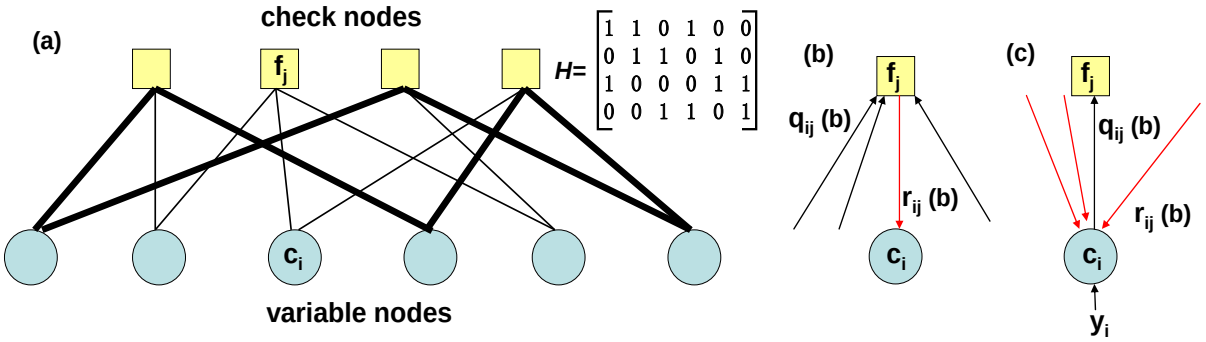

Figure 42. The Tanner graph representation of the parity-check matrix

The LDPC soft decoding algorithm is based on so-called belief propagation where the message is passed between the check and variable nodes [118]. The message sent by the variable node to the check node contains the pair of probability (q_{ij}) for the 'belief' that the variable node should be '0' or '1'. $q_{ij}(0)$ and $q_{ij}(1)$ stands for the two probabilities. Similarly, the message sent by the check node to the variable node also contains another probability (r_{ij}) for the 'belief' that the variable node should be '0' or '1'. At the beginning, the bit codes send their q_{ij} to check nodes. $q_{ij}(0)$ and $q_{ij}(1)$ stands for the amount of belief that received y_i is a 0 or 1. Then the check nodes will compute the response r_{ji} as

$$r_{ji}(0) = \frac{1}{2} + \frac{1}{2}\prod_{i' \in V_j \backslash i}(1 - 2q_{i'j}(1)), \qquad r_{ji}(1) = 1 - r_{ji}(0) \tag{27}$$

The variable nodes then will send the calculated response to bit node by

$$q_{ij}(0) = K_{ij}(1 - P_i)\prod_{j' \in C_j \backslash i} r_{j'i}(0), \qquad q_{ij}(1) = K_{ij}\prod_{j' \in C_j \backslash i} r_{j'i}(1) \tag{28}$$

where the K_{ij} is used to ensure that $q_{ij}(0) + q_{ij}(1) = 1$. The updating procedures of q_{ij} and r_{ij} are illustrated in Figure 42 (b) and (c). At this stage, the estimated $\hat{c}_j$ of the current variable c_j is using

$$Q_i(0) = K_i(1 - P_i)\prod_{j' \in C_i} r_{ji}(0), \qquad Q_i(1) = K_i P_i \prod_{j \in C_i} r_{ji}(1) \tag{29}$$

So if $Q_i(0) < Q_i(1)$, then $\hat{c}_j = 1$, and 0 vice versa. If the estimated codeword satisfies the parity check equation, then the decoding procedures terminates. Otherwise, it will continues in the next the iteration until the maximum number of iteration is exceeded. A convenient way to represent the probability is using log likelihood ratios (LLR). LLR allows the computation using sum and product operations, which is also used in our work. The details of updating equations are discussed in [117]. The dimension of the parity matrix is 2000×4000, and has

the weight of 3 [113]. We use log-domain sum-product decoding algorithm and number of iterations is set at 20. It is also worthy to point out that the used code from [113] will bring much complexity due to its randomness. One preferred option is using quasi-cyclic LDPC codes [109,110] with advantages of higher girth. The data after LDPC is input into a RS decoder for possible error-floor in LDPC and BER is computed. More comprehensive understanding of LDPC coding can be found in [104-111].

5.2.3. Experimental results and discussion

To identify net effective coding gain and the resultant improvement of the receiver sensitivity for the LDPC coded 16-QAM OFDM signal, we first measure the receiver performance for 107 Gb/s at back-to-back and the result is shown in Figure 43. Since we are comparing the two signals with the same net data rate, this coding gain is equivalent to the coding gain per bit if Figure 43 is re-plotted as BER versus SNR per bit Because of the sharp drop off of the BER after LDPC and maximum number of bits (1,500,000 bits per data point) measured, we defined the receiver sensitivity as the OSNR for the BER of 1×10^{-3} before RS decoding (BER of $1x10^{-3}$ or lower always results in zero error count after RS outer decoder in the experiment). Any error floor due to LDPC can be effectively eliminated by the interleaver / deinterleaver and RS FEC. It can be seen that the OSNR sensitivity for rate ½ LDPC coded 16-QAM signal is 12.5 dB OSNR compared with 15.5 dB OSNR in conventional 4-QAM signal, indicating a 3 dB improvement. We stress again this is achieved with the same electrical and optical bandwidth for all the optical and electrical components encountered. In contrast to the application of using high-order modulation for ultra-high spectral efficiency [94], the proposed rate ½ LDPC coded 16-QAM signal does not require higher OSNR, and the net coding gain could be utilized to increase transmission reach and/or reduce the required bit resolution for DAC/ADC compared to 4-QAM modulation case. The back-to-back 428 Gb/s BER performance is also shown at Figure 43 and the sensitivity is measured at 20.2 dB OSNR for LDPC coded 16-QAM. The inset shows for 16-QAM CO-OFDM signal at the OSNR of 19 dB.

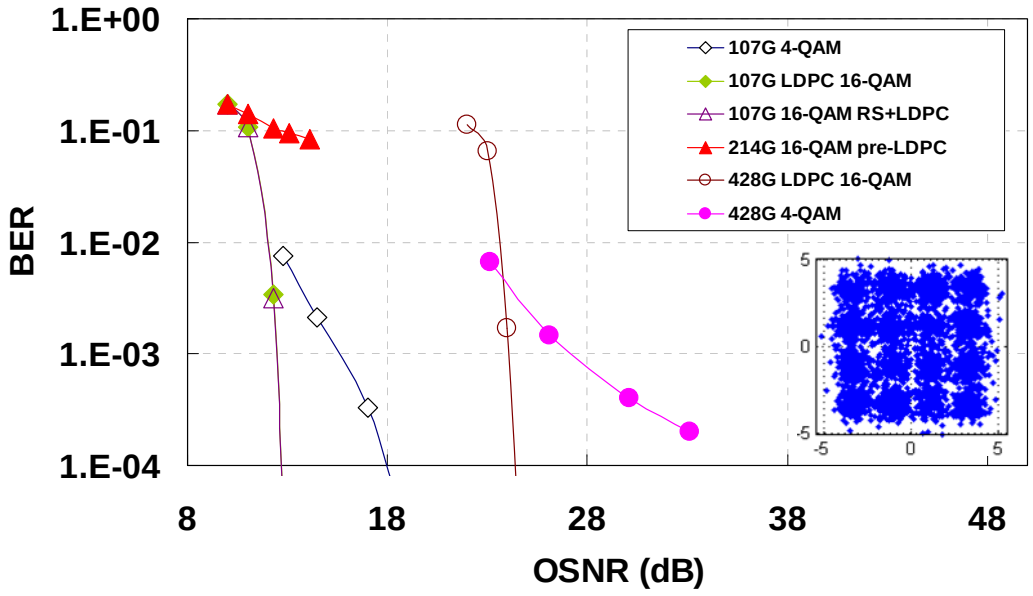

Figure 43. Back-to-back OSNR sensitivity for 107 Gb/s and 428 Gb/s signal. All the data rates shown are before 7 % RS FEC

Table 7. Detailed BER for the worst band of 428 Gb/s LDPC-coded 16-QAM signal at reaches of 960 km and 800 km.

Reach (km)	BER: raw (X-polarization)	BER: raw (Y-polarization)	BER: LDPC	BER: LDPC+RS
800	0.076993	0.077987	0	0
960	0.093084	0.094213	0	0

Table 7 shows the detailed BERs for 400 Gb/s LDPC-coded OFDM signal at different reaches. At the reach of 960 km with a launch power of 3dBm, only the performance of the worst band, the 8th band of the 400 Gb/s is shown including its raw BER for the 16-QAM signal or the input BER to LDPC decoder, BER after LDPC decoding, and BER after both LDPC and RS decoding. It can be seen that LDPC-coded 16-QAM signal can be received successfully (zero error counts for both polarizations) after 960 km transmission. We also measure transmission performance in various reaches below 960 km, all error-free after LDPC and RS decoding. Table 7 only shows one instance of the reach below 960 which is 800 km. Figure 44 shows the spectrum of the 400 Gb/s CO-OFDM signal at the reach of 960 km. Although each band is uniformly modulated with the same data, the chromatic dispersion induces rapid inter-band walk off and de-correlate the multi-band signal. In fact, the nonlinearity performance of such configuration is slightly conservative compared to the truly uncorrelated multiband signal [16]. We note this is the first experimental demonstration of

LDPC coding for long-haul transmission.

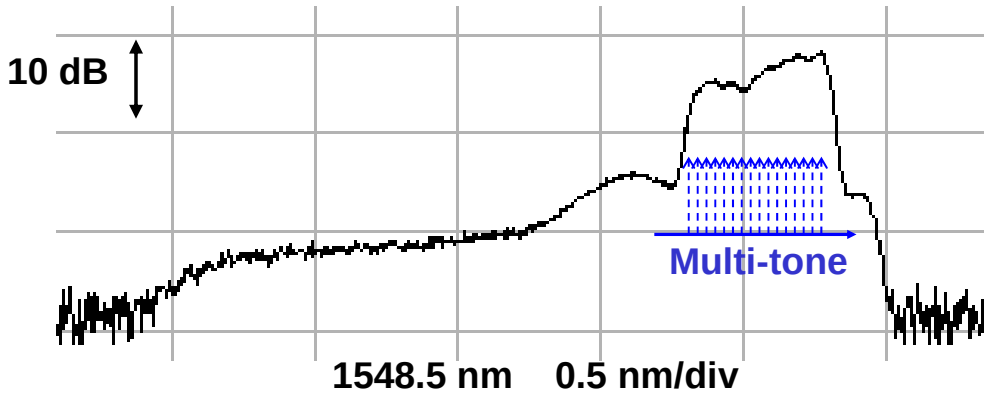

Figure 44. spectrum for 428 Gb/s LDPC-coded 16-QAM at reaches of 960 km.

5.2.4. Conclusion

We have shown record receiver sensitivity for 100 Gb/s CO-OFDM transmission via constellation expansion from 4-QAM to 16-QAM and rate 1/2 LDPC coding. As a result, transmission of 428 Gb/s single-channel CO-OFDM signal over 960 km SSMF is demonstrated without Raman amplification.

6 Some Advanced Techniques for CO-OFDM Based on Channel Estimation

In CO-OFDM, channel estimation is critical that affect the transmission system performance. And the transmission can also be verified to suit the channel if the channel information is obtained. In this chapter, we will show two advanced techniques in CO-OFDM based on channel estimation. The first scheme is called "Frequency-domain Averaging" algorithm, which can estimate the channel transfer information using one pair training symbol. This scheme can reduce the overhead caused by the traditional time-domain channel estimation algorithm. In second approach, we shifted the OFDM bit and power loading scheme from wireless onto fiber communication. Using bit and power loading, the transmission net rate can be improved according to the channel information.

6.1 Frequency-domain averaging based channel estimation

6.1.1 Introduction

Channel estimation is an important procedure in orthogonal frequency-division multiplexing (OFDM) based fiber transmission systems. With channel estimation, the physical effects of the fiber transmission link such as chromatic dispersion (CD) and polarization-mode dispersion (PMD) on the optical signal transmitted over the link are obtained, and subsequent channel equalization can be performed to restore the signal quality. In optically amplified long-haul transmission, the accuracy of the channel estimation is often limited by the presence of optical noise. To increase the channel estimation accuracy, a time-domain averaging method that averages the channel matrices estimated by multiple training symbols (TS's) for each frequency subcarrier is commonly used [16,17]. Recently, an intra-symbol frequency-domain averaging (ISFA) averaging based method was proposed [102] where the averaging is performed over the estimated channel matrices for multiple adjacent frequency subcarriers in the same TS. The ISFA method offers the benefits of overhead reduction and reaction speed improvement, and was recently demonstrated in a 40 Gb/s polarization-division-multiplexed (PDM) coherent optical OFDM system with PMD as large as 350 ps [119]. In this sub-chapter, we present the experimental demonstration in more detail, and compare the ISFA

performance with the time-domain averaging based channel estimation method. Moreover, the choice of the optimal averaging window size as a function of PMD is discussed.

6.1.2 ISFA-based channel estimation principle

Theoretical study on polarization-division multiplexed coherent optical OFDM was first proposed by [65]. The channel estimation in [16,17] was based on time-domain averaging. Since a number of subcarrier divides the OFDM spectrum into very narrow bandwidth, the response of each subcarrier can be treated as a constant. In the *i*th subcarrier, an optical OFDM signal can be expressed as

$$\begin{bmatrix} r_x(i) \\ r_y(i) \end{bmatrix} = \begin{bmatrix} h_{11}(i) & h_{12}(i) \\ h_{21}(i) & h_{22}(i) \end{bmatrix} \begin{bmatrix} s_x(i) \\ s_y(i) \end{bmatrix} \tag{30}$$

where the 2×1 vectors are the received and the transmitted OFDM signals, while the 2×2 matrix *H* is the channel transfer function for the *i*th subcarrier. To simplify the channel estimation, the time-multiplexed training symbols are sent in pairs across the two polarizations, namely, in the first symbol period t1, the only one polarization is transmitted OFDM signal, while another polarization is filled with zeros. In the following symbol period t2, the signal is transmitted in the inversed polarizations. Since only one polarization is used, to maintain the signal power in the whole transmission, the power of TS is doubled. In such a pair of the symbol period, the channel transfer function can be obtained as

$$\begin{bmatrix} h_{11}(i) & h_{12}(i) \\ h_{21}(i) & h_{22}(i) \end{bmatrix} = \begin{bmatrix} r_{1x}(i)/s_x(i) & r_{2x}(i)/s_y(i) \\ r_{1y}(i)/s_x(i) & r_{2y}(i)/s_y(i) \end{bmatrix} \tag{31}$$

where $r_{1x,y}$ and $r_{2x,y}$ are the received signal in the period t1, t2 respectively. The optical noise introduced fluctuation will highly affect the accuracy of the estimated channel matrix H. Traditionally, several such pairs of TS's are employed, and then averaged to obtain more accurate estimated matrix H.

$$H = \frac{1}{N}\sum_{i=1}^{N} H_{ti} \tag{32}$$

ti is the TS's time sequence index, N is the number of TS's. The TS's need to be inserted into OFDM symbols periodically in order to capture the dynamic channel behaviors. Normally, more than 2.5% of total OFDM symbols are used as TS's, which costs a large overhead on the net rate [16,17].

Compared to time-domain averaging methods, ISFA is the channel estimate method based on frequency-domain [102]. The channel behavior is usually highly related to adjacent subcarriers. To improve the accuracy of the channel estimation in presence of the optical noise, the ISFA estimates the ith subcarrier channel matrix by averaging the channel transfer function of itself and its multiple adjacent subcarriers. In effect, ISFA takes advantage of the fact that channel transfer function is usually highly correlated for adjacent subcarriers. For *i*th subcarrier, the averaging window is selected from the its m left neighbors to m right, or totally up to (2m+1) adjacent subcarriers.

$$H_i = \frac{1}{2m-1}\sum_{k=i-m}^{i+m} H_k \tag{33}$$

Different from equation(31), only one pair of Ts's is used in ISFA, which means much overhead caused by TS's can be reduced.

Two subcarrier regions need to be processed specially: (1) in the edge subcarriers, when the selected window size exceeds the bandwidth, namely, when i<m or i>M-m (M is the total number of subcarriers), the window size has to be narrowed to just keep the used subcarriers; (2) the subcarrier where the local oscillator is placed is usually highly affected by a strong DC component caused by the laser. In order to obtain the accurate channel matrix in subcarrier close to such affected subcarrier, this subcarrier needs to be excluded during the averaging.

6.1.3 Experimental setup and results

Figure 45 shows the experimental setup. At the transmitter, a data stream consisting of pseudo-random bit sequences of length 2^{15}-1 was first generated by Tektronix arbitrary waveform generator (AWG), each mapped onto 93 subcarriers with 8-QAM modulation. The data subcarriers, together with 7 pilot subcarriers and 28 unfilled subcarriers, were converted to the time domain via inverse Fourier transform (IFFT) with size 128. The unfilled subcarriers consisted of two center subcarriers, allocated to accommodate the frequency offset between the transmitter laser and the receiver optical local oscillator (OLO), and 26 unfilled edge subcarriers, used for over-sampling. A cyclic prefix of length 8 samples was used, resulting in an OFDM symbol size of 136. At least one TS pair, consisting of a known symbol and a zero symbol, was inserted into the OFDM symbol sequence before every 500 data symbols. The real and imaginary parts of the OFDM symbol sequence were converted to analog waveforms by two digital-to-analog converters operating at 10 GS/s, before being

amplified and used to drive an optical I/Q modulator that was biased at null. The transmitter laser and the OLO were external-cavity lasers (ECL's) with 100-kHz linewidth. The maximum net data rate of the signal after the optical modulation was 20.5 Gb/s. The optical signal was then split by a 3-dB coupler into two equal copies, which were then delayed by one symbol period with respect to each other and combined by a polarization beam splitter (PBS) to form a PDM-OFDM signal with a maximum net data rate of 41 Gb/s. The optical spectrum of the signal is also shown in Figure 45. The optical bandwidth of the 40 Gb/s PDM-OFDM signal is only ~8 GHz, which potentially allows for a spectral efficiency of higher than 3 bits/s/Hz. To assess the channel estimation performance under PMD, a polarization controller and two PMD emulators (PMDE's) were used. The first PMDE was a commercial PMDE capable of generating a differential group delay (DGD) ranging from 0 to 125 ps, and the second PMDE was a home-made PMDE capable of generating DGD as large as 500 ps. Adjustable amount of optical noise was added by an optical pre-amplifier followed by an adjustable attenuator. At the receiver, the PDM-OFDM signal was detected by a digital coherent receiver consisting of a polarization-diversity optical hybrid, an OLO, and four analog-to-digital converters (ADC's), each operating at 20 GS/s. The effective resolution of the ADC's was about 5 bits. The digitized waveforms were stored and processed offline in a computer. To increase the accuracy of the ISFA process under large frequency-dependent channel response, e.g., caused by high PMD, we halved the averaging window for 2m+1 edge subcarriers. Other signal processes needed to recover the original data were similar to those described in [16,17]. The bit-error ratio (BER) of the recovered data was obtained by direct error counting. Sample recovered signal constellations for both the x- and y-polarization components are shown as inset in Figure 45

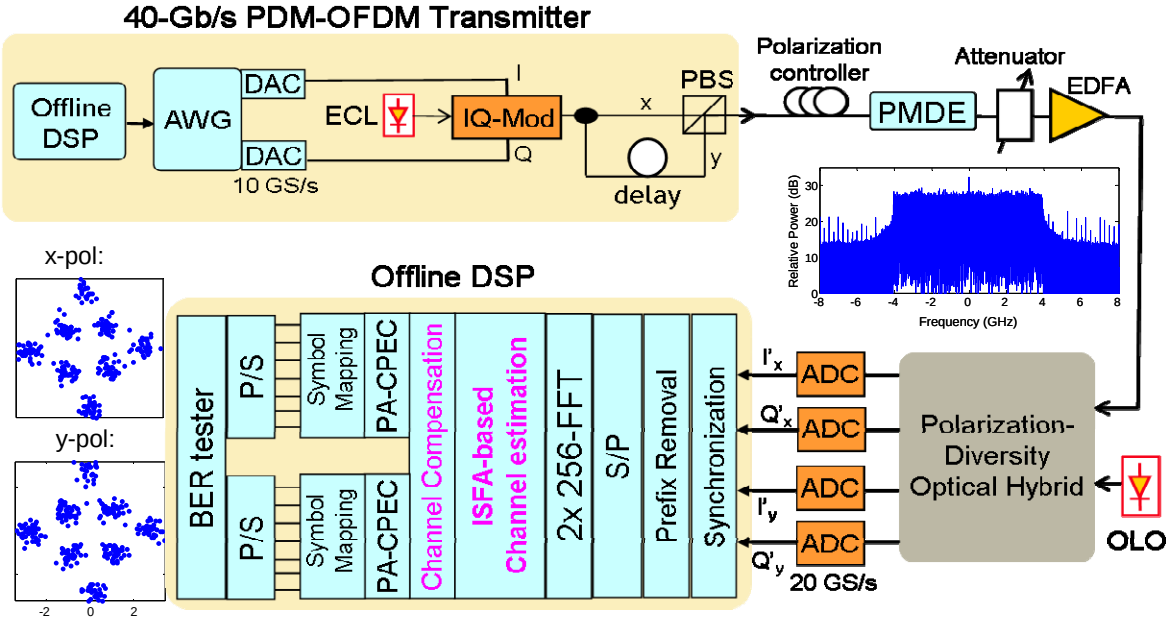

Figure 45. Experimental setup of a 40 Gb/s PDM CO-OFDM transmission system. Insets: sample recovered signal spectrum and constellations for the x- and y-polarization components. DSP: digital signal processing. PA-CPEC: pilot-assisted common-phase-error compensation.

Figure 46 shows the real part of channel matrix coefficient h_{xy} estimated without and with the ISFA process as a function of the modulated subcarrier index, under DGD values of 125 ps (provided by the 1st PMDE) and 350 ps (provided by the 2nd PMDE) and a splitting ratio of about 0.5. The m values used in the ISFA were 9 and 5 for the 125-ps and 350-ps DGD cases, respectively. Evidently, the estimated channel coefficient without the ISFA exhibits high-frequency fluctuations due to the presence of optical noise, and with ISFA, the noise-induced high-frequency fluctuations are removed.

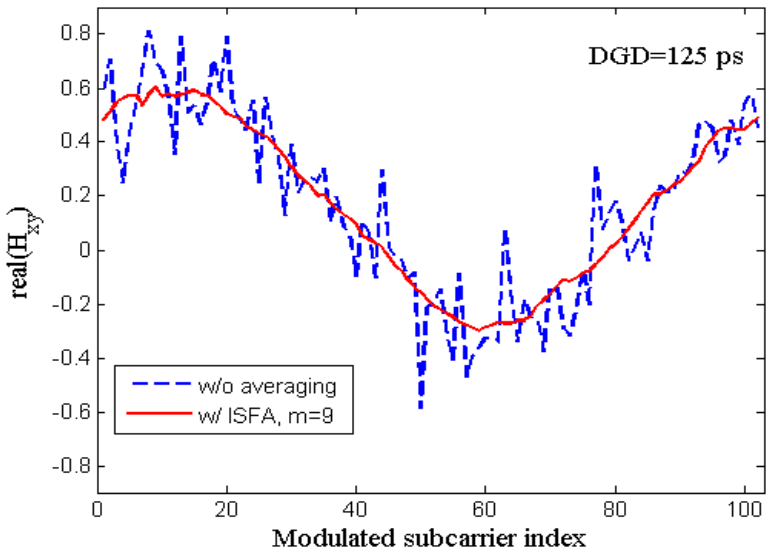

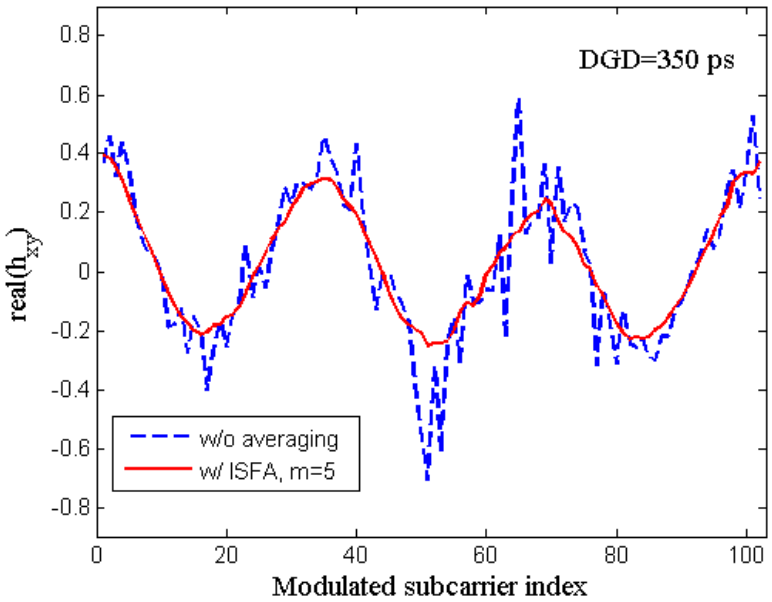

Figure 46. The real part of channel matrix coefficient hxy as a function of the modulated subcarrier index without and with ISFA for DGD=125 ps (left) and DGD=350 ps (right). OSNR=15 dB.

Figure 47 shows the BER of the recovered dual-polarization components of the 40 Gb/s PDM-OFDM signal as a function of the OSNR without averaging and with the ISFA having m equal to 9 under a DGD of 125 ps. Without averaging, there is a high error floor of ~10-2. With the ISFA, the BER performance is much improved. The required OSNR for a BER of 10-3 is ~15 dB. The absolute OSNR performance could be further improved by using ADC's with a higher resolution. The Moreover, the ISFA performance is slightly better than that obtained with the time-domain averaging based channel estimation using 10 TS's or N=5 times as large an overhead as in the ISFA case. The overhead caused by TS's is reduced from 2% using time-domain averaging algorithm to only 0.4% using ISFA.

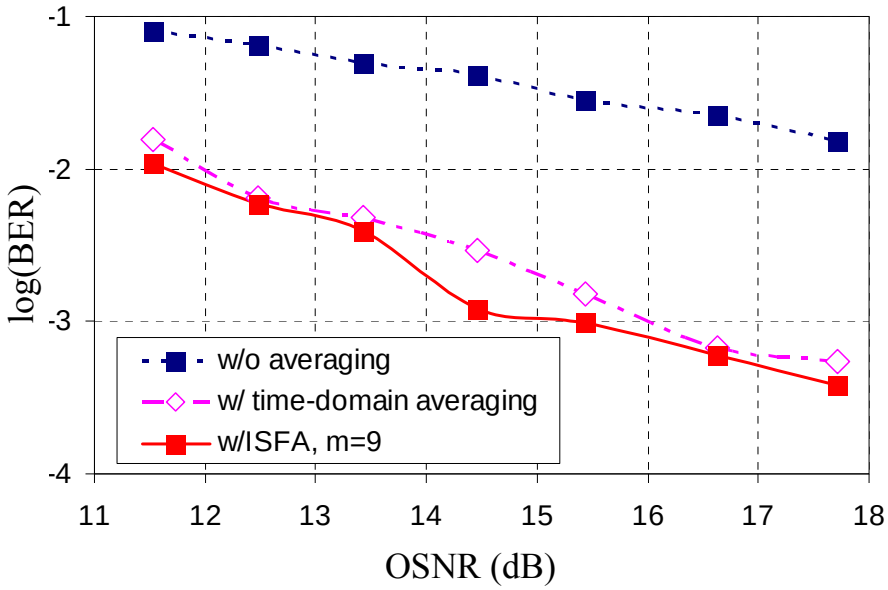

Figure 47. BER of the recovered dual-polarizations of the 40 Gb/s PDM-OFDM signal as a function of the OSNR without averaging and with the ISFA under DGD of 125 ps. The results obtained with time-domain averaging based channel estimation using 10 TS's are also plotted for comparison.

Figure 48 shows the recovered signal Q factor, derived from the BER, as a function of the size of the averaging window, with a DGD of 125 ps and an OSNR of 15 dB. The signal Q factor increases quickly when m is increased from 0 to 5, and reaches ~10 dB at m of 9. As expected, the Q factor gradually decreases with further increase of m, due to the loss of frequency resolution in the channel estimation. Figure 49 shows the signal Q factor as a function of DGD (generated by the 2nd PMDE) with different window size. For a Q penalty of 0.3 dB, the tolerable DGD is ~200 ps with m of 9, and is ~350 ps with m of 5. Under 200 ps, the Q factor with large averaging window (m of 7 and 9) is slightly better than m of 5. With optimum window averaging, the Q performance is better than other schemes, especially when the DGD is lager than 300 ps.

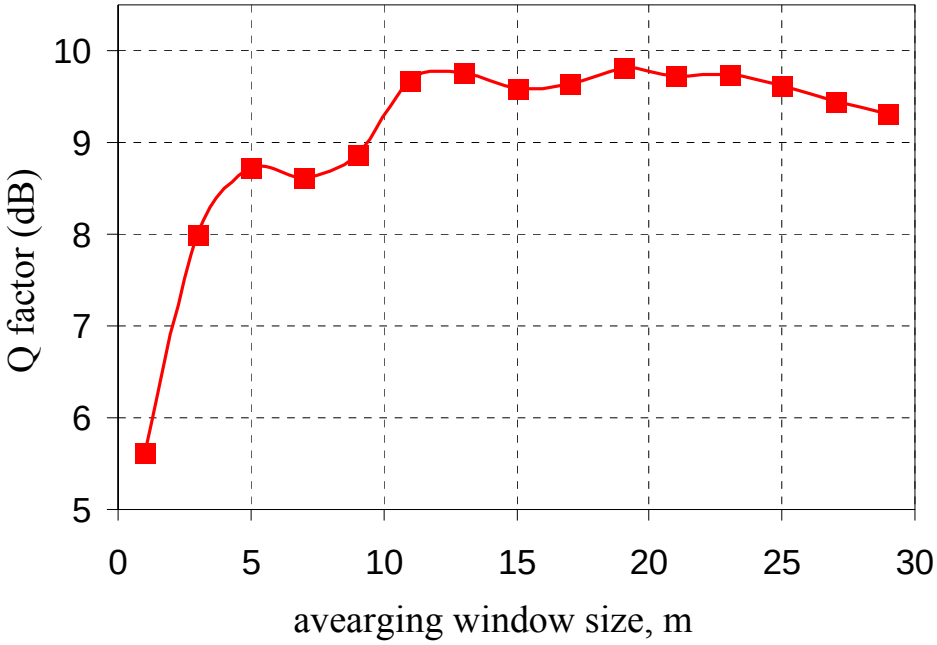

Figure 48. Signal Q factor vs. the size of the averaging window in the ISFA process under DGD of 125 ps, and OSNR of 15 dB.

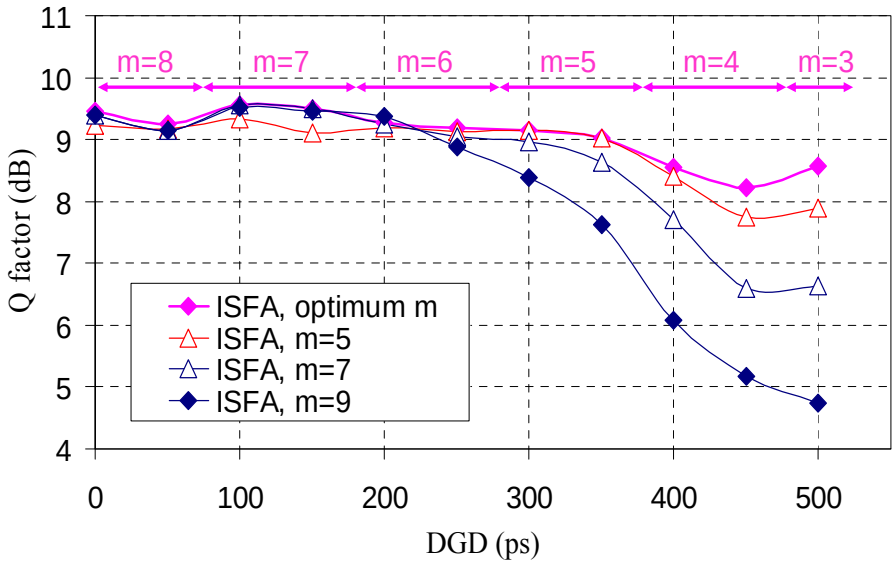

Figure 49. Signal Q factor vs. DGD when the ISFA-based channel estimations with different window size. The label above the curves shows the size range with optimized averaging window size.

6.1.4 Conclusion

We have presented the experimental demonstration of the ISFA-based channel estimation in a 40 Gb/s PDM-OFDM system with PMD as large as 350 ps. Compared to time-domain averaging, ISFA shows comparable performance with much reduced overhead. ISFA can also be employed with other OFDM modulation formats, such as 16QAM, 32QAM, to achieve higher spectral efficiency.

6.2 Bit and power loading for CO-OFDM

6.2.1 Introduction

Orthogonal frequency-division multiplexing (OFDM) is a special form of multicarrier modulation in which the signal data stream is transmitted over many orthogonal lower bit rate subcarriers. One of the distinctive advantages of OFDM over single-carrier counterpart is that the system is managed according to the individual subcarrier. Once the channel condition of each subcarrier is known, the system performance can be improved through proper manipulation of the individual subcarriers. One of the most simple and effective ways, called bit loading, is done by optimally allocating different modulation scheme across all the subcarriers [120]. In particular, the signal-to-noise ratio (SNR) of each subcarrier can be monitored through channel estimation, and the subcarriers with high SNR value will be loaded with higher number of bits per subcarrier. As a result, the overall data rate is maximized. Another commonly used method is power loading. In such scheme, different frequency tones are loaded with an optimal power [121]. In so doing, the system performance, such as bit error ratio can be improved. It is noted that bit and power loading has been demonstrated in multi-mode fiber using discrete multi-tone modulation [122].

This capability of CO-OFDM transceiver to support variable bit rate through bit loading is an attractive feature for reconfigurable optical network. The benefits are two folds. First, it allows one receiver capable of supporting multiple data rate [123], preferably through software; second, the data rate of each dynamically established connection can be adjusted according to the 'quality' of the channel. We would like to point out two boundary conditions for such an optical variable data rate manipulation. First, the electrical and optical bandwidth for the signal is preferred to be constant. This is desirable as no hardware adjustment is required, namely, neither the optical filter bandwidth nor the electrical filter bandwidth adjustment is needed; Second, the power of each wavelength channel should not be modified even the data rate is varied. Otherwise, modifying the individual wavelength power as a result of dynamic data rate adjustment will affect the gain and tilt of the other channels that share the same optical amplifier and co-propagate in the same fiber link with the channel being adapted. This will inevitably incur degrading performance to other channels. In this sub-chapter, we show the first experiment of CO-OFDM systems with bit and power loading. In particular, we show a proportion of the OFDM subcarriers is loaded with 8-QAM from original uniform 4-QAM. The data rate is subsequently increased from 10.7 Gb/s to 13.3 Gb/s without modifying

the channel bandwidth and launch power. The system performance can be further improved through optimal power loading into each modulation band. The bit and power loading are performed after 1000 km transmission over SSMF fiber without optical dispersion compensation. Our work demonstrates that CO-OFDM may potentially become an attractive choice of modulation format for future reconfigurable optical networks.

6.2.2 Principle of bit and power loading for CO-OFDM

There are wealth of literatures on the optimal algorithm for bit and power loading in OFDM systems [120,121]. We start by formally laying out the generic bit/power loading optimization problem as follows [121]:

$$\max\left(R\right) = \max\left(\sum_{k=1}^{Nsc} R_k\right) \tag{34}$$

Under the constraint given by

$$\sum_{i=1}^{N_{sc}} P_i = P_0 \tag{35}$$

where Nsc is the number of subcarriers, R and R_k are the composite data rate and individual subcarrier data rate, respectively, P_0 and P_i are the composite total power and individual subcarrier power. (34) and (35) show that under the condition of constant total power, the order of modulation (bit loading) and the power of each subcarrier (power loading) can be adjusted, namely, data rate can be maximized by such 'bit-loading' according to the system margin provided by the SNR of the channel. Compared with the wireless systems where the subcarrier SNR varies by tens of dB due to multi-path fading, the optical channel is relatively benign. However, the imperfection in electrical and optical response, fiber nonlinearity, polarization mode dispersion (PMD), and polarization dependent loss (PDL) could result in large diversity of SNR cross the OFDM spectrum. The bit/power loading will inevitably improve the system performance. In this work, we limit the granularity of R to the multiple OC-48 rates. The bit-loading can be simply performed by assigning higher-order modulation to the subcarriers with high SNR. Once the bit-loading is finalized, the power loading can be employed to minimize the overall BER or maximize the system margin. The formulation similar to (34) under the same constraint (35) is given by

$$\min\left(Err\right)=\min\left(\sum_{k=1}^{Nsc}Err_k\right) \tag{36}$$

where Err and Errk are respectively the total errors, and the errors from individual subcarriers.

6.2.3 Experimental setup and results

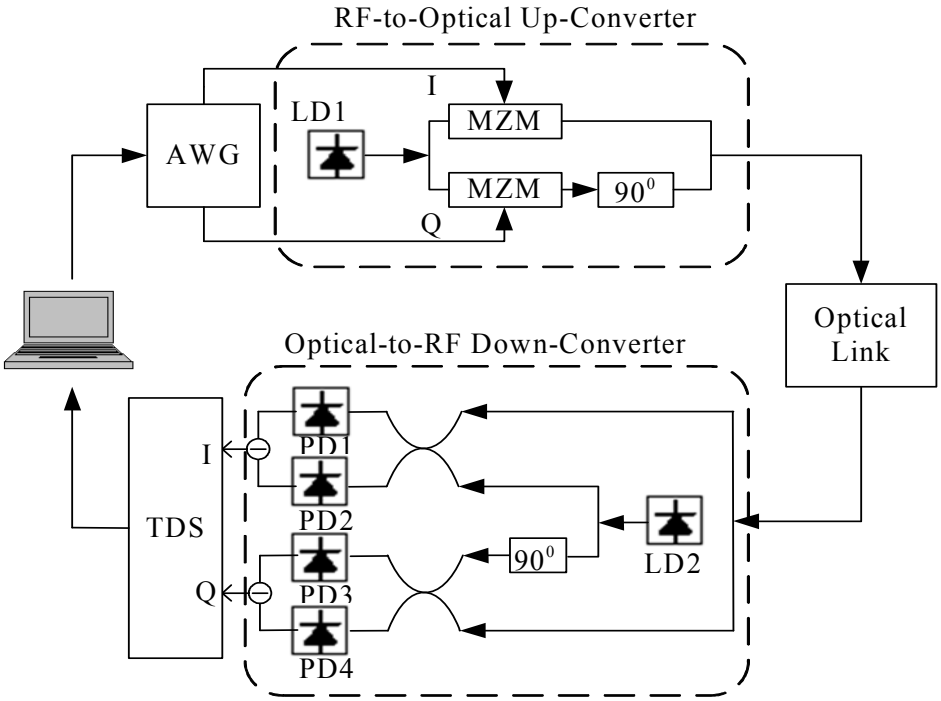

Figure 50. Experimental setup for bit and power loading in CO-OFDM systems (AWG: Arbitrary Waveform Generator LD: Laser Diode MZM: Mach-Zenhder Modulator PD: Photodiode TDS: Time Domain-sampling Scope)

Figure 50 shows the experimental setup for verifying the transmitter with bit and power loading scheme, in direct up/down conversion architecture [72]. The transmitted signal is generated by Matlab program originated from 2^{15}-1 pseudo random binary sequence （PRBS）, then mapped to either uniform 4-QAM, or a mixture of 4-QAM and 8-QAM. The time domain signal is formed after inverse fast Fourier transform (IFFT) operation, and then inserted with guard interval. The I and Q components of the time signal is uploaded onto Tektronix Arbitrary Waveform Generator (AWG), which will produce the analog signals at 10 GS/s. The total number of OFDM subcarriers is 128, and guard interval is 1/8 of the observation window. Only 89 subcarriers out of 128 are filled, and 12 of them are used for phase estimation. The resultant data rate in the uniform loading of 4-QAM transmissions is 10.7 Gb/s. The optical I/Q modulator comprised of two Mach-Zehnder modulators (MZM) with 900 phase shift, directly up-converts OFDM baseband signals from RF domain to optical

domain. The optical OFDM signal is launched into multi-span of fiber link emulated with a recirculation loop. The recirculation loop consists of 100 km SSMF fiber and an erbium-doped fiber amplifier (EDFA) to compensate the link loss. At the receiver side, direct optical-to-RF down-conversion is employed. We tune the local oscillator (LO) laser frequency close to that of the incoming signal. Both signal and LO are fed into an optical 900 hybrid. Two balanced receivers are used to detect the I and Q components. The detected RF signals are then sampled with a Tektronix Time Domain-sampling Scope (TDS) at 20 GS/s. The sampled data is processed with a Matlab program to perform receiver signal processing, involving (i) FFT window synchronization using Schmidl format to identify the start of the OFDM symbol, (ii) software down-conversion of the OFDM RF signal to base-band to remove residual frequency offset, (iii) phase estimation and channel estimation, and (iv) constellation construction for each carrier and BER computation.

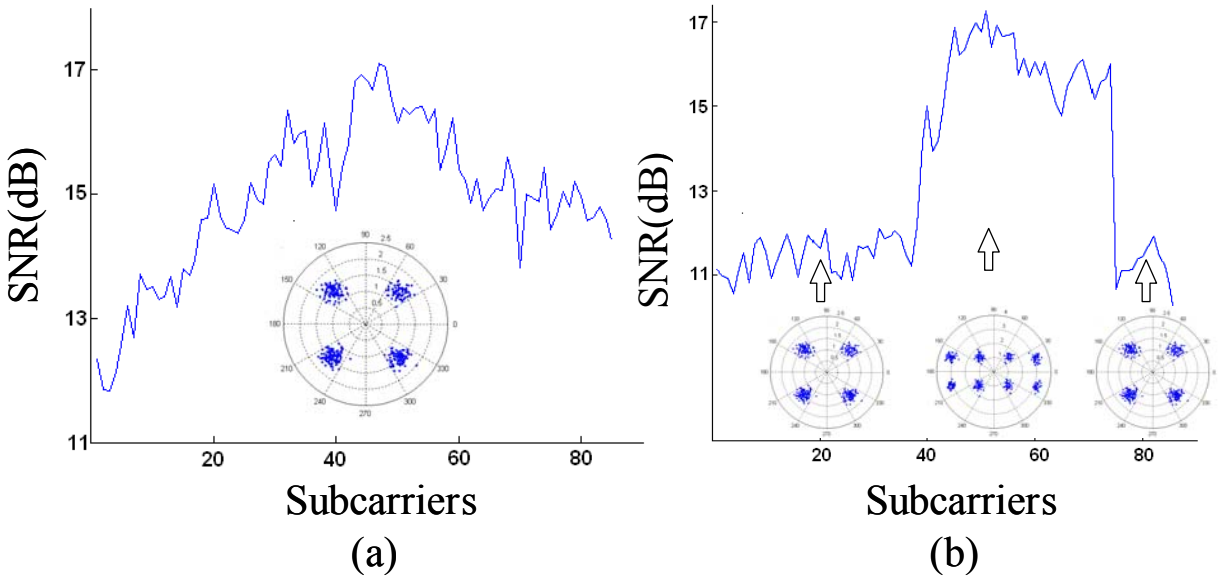

Figure 51. The SNR of OFDM subcarriers for (a) uniform loading, and (b) mixed loading.

The first experiment conducted is 10.7 Gb/s CO-OFDM transmission over 1000 km SSFM fiber, with uniform 4-QAM loading. The distribution of the SNR across the subcarriers is shown in Figure 51 (a), obtained through OFDM receiver signal processing. The SNR values of the middle subcarriers are greater than those at two sides. It seems that most of the subcarriers with high SNR can be further upgraded to high-order QAM. This corresponds to the optical network operation scenarios, at the beginning of the system life, there may be ample system margin to spend, or for a new connection at shorter reach, which both will produce the high SNR for the OFDM subcarriers. Because of the excessive SNR margin, we are able to load an additional data into the OFDM signal, to be exact, another OC-48 traffic

onto original OC-192 one. In order to achieve that, a nominal 50 % of the subcarriers should be loaded with 8-QAM from original 4-QAM. The data rate increases from 10.7 Gb/s to 13.3Gb/s. Figure 51 (b) shows the SNR of the OFDM subcarriers with a mixture of 4-QAM and 8-QAM loading, with 8-QAM filled in the middle of OFDM spectrum. The insets show the constellation diagrams associated with each bit-loading band. The clear constellations show that additional data rate has been successfully carried onto this OFDM transmission system. Note that we have achieved this by using the same optical and electrical bandwidth and the same of launch power of -3.5 dBm. The adjustment only involves the software embedded in the transceiver without a need for hardware adjustment. Therefore, this adaptive date rate manipulation is hidden from the other wavelength channels, that is, there is no need for any adjustment from neighboring channels.

We then measure the sensitivity performance of this variable bit-loading system, at different percentages of the OFDM subcarriers loaded with 8-QAM, and the results are shown in Figure 52. It can be seen that as more subcarriers are loaded with higher-order QAM, the sensitivity degrades. Specifically, when the data rate is increased by an additional OC-48, the optical Signal-to-Noise Ratio (OSNR) penalty is degraded by 2.5 dB at the BER of 10^{-3}. The penalty will increase when higher-order modulation such as 16-QAM bit-loading is employed, signifying that the bit-loading is ultimately limited by the available system margin.

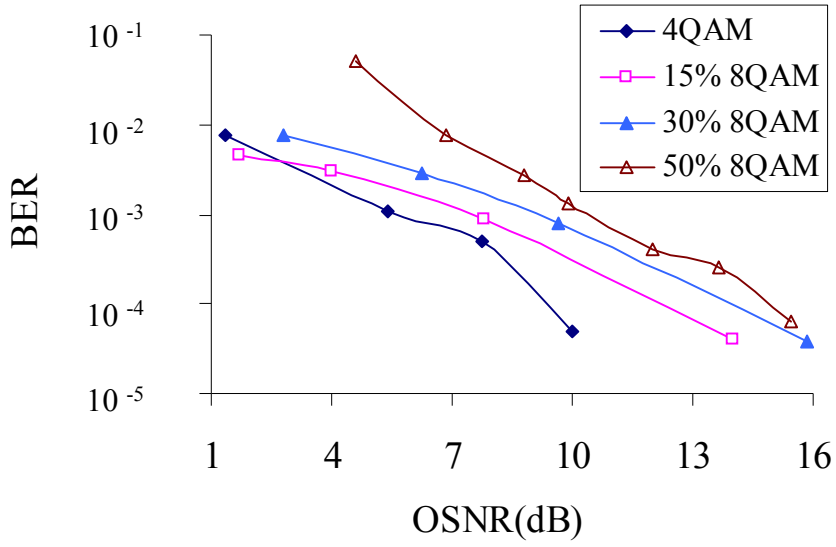

Figure 52. BER performance with varying percentage of the 8-QAM after 1000 km transmission.

We also carry out the measurement of the OSNR sensitivity performance for bit-loading of 50 % of 8-QAM at reach of 600 km and 1000 km. Figure 53 shows that OSNR penalty at 600 km and 1000 km is respectively about 0.4 dB and 1 dB, compared with back-to-back transmission.

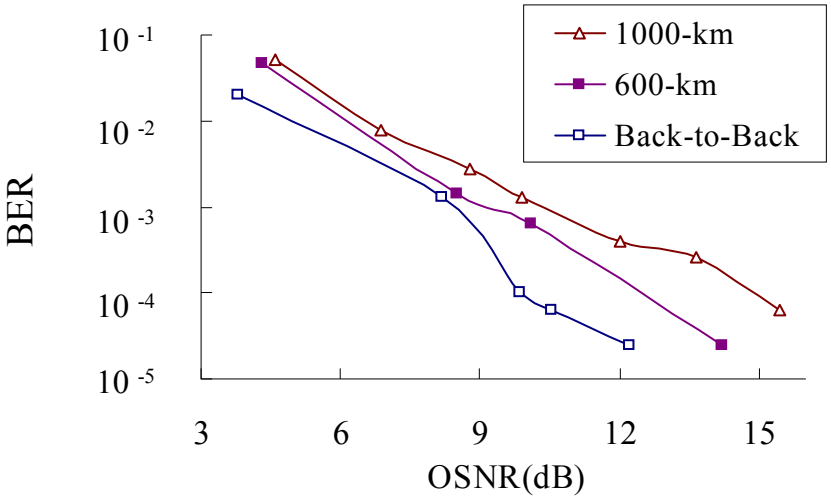

Figure 53. BER performance at reach of 600 km and 1000 km

Once an additional OC-48 is loaded onto the original data rate, the remaining manipulation is power loading, namely, the optimal power partition between 4-QAM and 8-QAM subcarriers. To obtain the optimal power loading, we adjusted ratio of the power of 8-QAM to the overall signal power, but we still keep the launch power as a constant at -3.5 dBm. In such a low power, the influence of nonlinearity is negligible. But nonlinear effect should be considered if a higher power is used. We characterize the overall system performance for 1000 km transmission. Figure 54 (a) shows the BER as the function of the percentage of the power consumed by 8-QAM subcarriers. The measurement is done with noise loading to an OSNR of 12.5 dB at the receiver, so that the minimum BER can be measured. It can be seen that the optimal power loaded onto 8-QAM is around 50-55 %. Figure 54 (b) shows the sensitivity comparison between the optimal power loading of 50 % and the non-optimal power loading of 70 %. The optimal loading has a 1 dB OSNR advantage over the non-optimal loading.

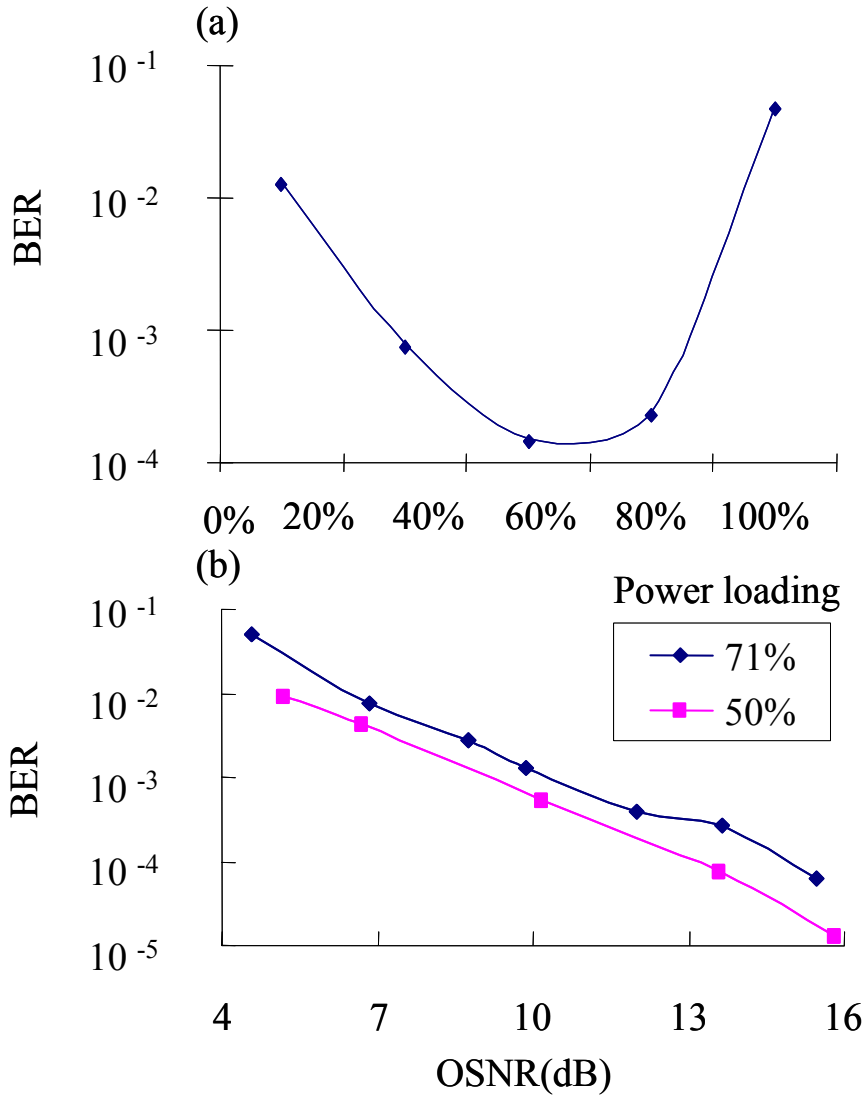

Figure 54. (a) BER as a function of percentage of the power for 8-QAM, and (b) BER performance at different power loading

6.2.4 Conclusion

We have shown the first experiment of CO-OFDM systems with bit and power loading, in particular, without modifying the channel bandwidth and launch power. The system performance is further improved through optimal power loading into each modulation band. Our work shows that CO-OFDM may potentially become an attractive choice of modulation format for future.

7 Conclusions

In this thesis, we have numerically and experimentally analyzed and demonstrated the high-speed optical transmission system using coherent optical orthogonal frequency-division multiplexing (CO-OFDM). A few key topics have been addressed including (i) the demonstration of 107 Gb/s CO-OFDM over long-haul transmission, (ii) real-time demonstration for CO-OFDM, (iii) advanced coding to improve the CO-OFDM transmission performance is presented in the third part, and (iv) novel channel technique for CO-OFDM.

7.1 107 Gb/s CO-OFDM long haul transmission

In chapter 3, we have proposed and elucidated the principle of orthogonal-band-multiplexed OFDM (OBM-OFDM) to subdivide the entire OFDM spectrum into multiple orthogonal bands. As a result, the DAC/ADCs do not need to operate at extremely high sampling rate. We show the proof-of-concept transmission experiment through optical realization of OBM-OFDM. A numerical simulation for both single channel and WDM transmission is conducted to verify the feasibility of the demonstrated OBM-OFDM experiment system. Back-to-back OSNR sensitivity of 15.8 dB at the data rate of 107 Gb/s for a BER of 10^{-3} was achieved. The demonstrated system employs 2×2 MIMO-OFDM signal processing and achieves high electrical spectral efficiency of 3.3 bit/s/Hz.

7.2 Real-time CO-OFDM implementation

We have discussed detail architectures of the real-time implementation of a coherent optical OFDM receiver. The unique difficulties in high-speed signal processing of optically transmitted OFDM data are discussed and a few unique solutions and implementations were presented for OFDM symbol synchronization. The architectures were successfully implemented in a FPGA and demonstrated at 2.5 GS/s. The real-time receiver was used to receive a 53.3 Gb/s multi-band CO-OFDM signal with an error floor as low as 3.7×10^{-8}. Further possibilities of improving the computational efficiencies are discussed. With foreseeable improvement in sampling speed of ADCs and DSP resource of FPGAs, real-time reception of 100 Gb/s CO-OFDM can be realized in near future.

7.3 Advanced coding for CO-OFDM without bandwidth extending

We have demonstrated long-haul transmission of a 44 Gb/s CO-OFDM signal with trellis-coded 32-QAM at back-to-back and 990 km dispersion-managed SSMF link. Experimental results at back-to-back were obtained with a 44 Gb/s PDM-CO-OFDM signal, showing receiver sensitivity improvements of 3.4 dB and 5.0 dB over its uncoded counterpart at BER of 10^{-3} and 10^{-4}, respectively. For long haul transmission, TCM, together with SPMC, substantially improves the transmission performance, showing its potential to assist high-SE and high-performance CO-OFDM transmission. The combination of TCM with high-level QAM modulation may be a promising technique to support high-spectral-efficiency and high-performance CO-OFDM transmission. We have also shown record receiver sensitivity for 100 Gb/s CO-OFDM transmission via constellation expansion from 4-QAM to 16-QAM and rate 1/2 LDPC coding. As a result, transmission of 428 Gb/s single-channel CO-OFDM signal over 960 km SSMF is demonstrated without Raman amplification.

7.4 Some advanced techniques for CO-OFDM based on channel estimation

We have presented the experimental demonstration of the ISFA-based channel estimation in a 40 Gb/s PDM-OFDM system with PMD as large as 350 ps. Compared to time-domain averaging, ISFA shows comparable performance with much reduced overhead. ISFA can also be employed with other OFDM modulation formats, such as 16QAM, 32QAM, to achieve higher spectral efficiency. Based on channel estimation, we also demonstrate the experiment of CO-OFDM systems with bit and power loading, in particular, without modifying the channel bandwidth and launch power. The system performance is further improved through optimal power loading into each modulation band.

All our demonstrations have shown that coherent optical OFDM is a powerful technique, which is promising for the next generation networks.

References

[1] J.-L. Beylat, “How will optical networks continue to transform the way the world communicates?” in Proc. APOC 2007, Plenary Presentation, Wuhan, China, 2007.

[2] D. B. Keck, "Optical fiber spans 30 years," Lightwave 17, 2000.

[3] G. Raybon and P. Winzer, "100 Gb/s Challenges and Solutions," in Proc. Optical Fiber Communication (OFC) Conference 2008, paper OTuG1, 2008.

[4] M. Duelk, “Next generation 100 G Ethernet,” in European Conference on Optical Communication 2005, paper Tu3.1.2, Glasgow, Scotland, 2005.

[5] Marciniak, M., "100 Gb Ethernet over fibre networks- reality and challenges," ICTON Mediterranean Winter Conference, 2007. ICTON-MW 2007 , vol., no., pp.1-6, 6-8 Dec. 2007

[6] H. Sun, K. -T. Wu, and K. Roberts, “Real-time measurements of a 40 Gb/s coherent system,” Opt. Express **16**, 873-879, 2008.

[7] W. Shieh, Q. Yang, and Y. Ma, "107 Gb/s coherent optical OFDM transmission over 1000-km SSMF fiber using orthogonal band multiplexing," Opt. Express **16**, 6378-6386, 2008.

[8] http://www.micram.com/index.php/products/vega

[9] J. M. Kahn and K.-P. Ho, “Spectral efficiency limits and modulation/detection techniques for DWDM Systems,” J. Sel. Top. Quantum Electron. **10**, 259–271, 2004.

[10] Winzer, P.J., and Essiambre, R.J., "Advanced Optical Modulation Formats," Proceedings of the IEEE , vol.**94**, no.5, pp.952-985, May 2006

[11] Q. Pan and R. J. Green, "Bit-error-rate performance of lightwave hybrid AM/OFDM systems with comparison with AM/QAM systems in the presence of clipping impulse noise," IEEE Photon. Technol. Lett. **8**, 278-280, 1996.

[12] W. Shieh and C. Athaudage, “Coherent optical orthogonal frequency division multiplexing,” Electron. Lett., vol. **42**, pp. 587-589, 2006

[13] A. J. Lowery, L. Du, and J. Armstrong, “Orthogonal frequency division multiplexing for adaptive dispersion compensation in long haul WDM systems,” in Proc. Optical Fiber Communication (OFC) Conference 2006, paper PDP 39, 2006.

[14] I. B. Djordjevic and B. Vasic, “Orthogonal frequency division multiplexing for high-speed optical transmission,” Opt. Express, vol. **14**, pp. 3767–3775, 2006.

[15] W. Shieh, X. Yi, Y. Ma, and Q. Yang, "Coherent optical OFDM: has its time come? [Invited]," J. Opt. Netw. **7**, 234-255, 2008

[16] Q. Yang, Y. Ma, and W. Shieh, "107 Gb/s coherent optical OFDM reception using orthogonal band multiplexing", in Proc. Optical Fiber Communication (OFC) Conference 2008, PDP 7, 2008.

[17] S. Jansen, I. Morita, T. Schenk, and H. Tanaka, "121.9 Gb/s PDM-OFDM transmission with 2b/s/Hz Spectral Efficiency over 1000km of SSMF," J. Lightwave Technol. **27**, 177-188, 2009.

[18] E. Yamada, A. Sano, H. Masuda, E. Yamazaki, T. Kobayashi, E. Yoshida, K. Yonenaga, Y. Miyamoto, K.Ishihara, Y. Takatori, T. Yamada, and H.Yamazaki, "1Tb/s (111Gb/s/ch × 10ch) no-guard-interval COOFDM transmission over 2100 km DSF," in Opto-Electronics and Communications (OECC) Conference, paper PDP6, 2008.

[19] Y. Ma, Q. Yang, Y. Tang, S. Chen, and W. Shieh, "1-Tb/s per Channel Coherent Optical OFDM Transmission with Subwavelength Bandwidth Access," in Proc. Optical Fiber Communication (OFC) Conference 2009, paper PDPC1, San Diego, USA, 2009.

[20] R. Dischler, and F. Buchali, "Transmission of 1.2 Tb/s Continuous Waveband PDM ‐OFDM ‐FDM Signal with Spectral Efficiency of 3.3 bit/s/Hz over 400 km of SSMF," in Proc. Optical Fiber Communication (OFC) Conference 2009, paper PDP C2, San Diego, USA, 2009.

[21] S. Chandrasekhar et al., "Transmission of a1.2Tb/s 24-carrier No-guard-interval Coherent OFDM Superchannel over 7200km of Ultra-large-area Fiber," in European Conference on Optical Communication 2009, paper no. PD 2.6, 2009.

[22] K. Roberts, "Electronic dispersion compensation beyond 10 Gb/s" in Technical Digest, LEOS Summer Topical Meeting (IEEE, 2007), paper MA2.3, 2007.

[23] J. Sitch, "Implementation aspects of high-speed DSP for transmitter and receiver signal processing," in Technical Digest, LEOS Summer Topical Meeting (IEEE, 2007), paper MA4.3, 2007.

[24] A. Leven, N. Kaneda, and Y.-K. Chen, "A real-time CMA-based 10Gb/s polarization demultiplexing coherent receiver implmented in an FPGA," in Proc. Optical Fiber Communication (OFC) Conference 2008, San Diego, CA, 2008.

[25] T. Pfau, R. Peveling, J. Hauden, N. Grossard, H. Porte, Y. Achiam, S. Hoffman, S. K. Ibrahim, O. Adamczyk, S. Bhandare, D. Sandel, M. Porrman, and R. Noe, "Coherent digital polarization diversity receiver for real-time polarization-multiplexed QPSK transmission at 2.8 Gb/s," Photon. Technol. Lett., vol.**19**, pp. 1988-1990, Dec. 2007.

[26] Q. Yang, N. Kaneda, X. Liu, S. Chandrasekhar, W. Shieh, Y. K. Chen, "Real-time coherent optical OFDM receiver at 2.5 GS/s for receiving a 54 Gb/s multi-band signal," in Proc. Optical Fiber Communication (OFC) Conference 2009, paper PDPC5, 2009.

[27] S. Chen, Q. Yang, Y. Ma, and W. Shieh, "Multi-gigabit real-time coherent optical OFDM receiver," in Proc. Optical Fiber Communication (OFC) Conference 2009, paper OTuO4, 2009.

[28] D. Qian, T. T. Kwok, N. Cvijetic, J. Hu, and T. Wang, "41.25 Gb/s Real-Time OFDM Receiver for Variable Rate WDM-OFDMA-PON Transmission," in Proc. Optical Fiber Communication (OFC) Conference 2010, paper PDPD9, 2010.

[29] R. P. Giddings, X. Q. Jin, E. Hugues-Salas, E. Giacoumidis, J. L. Wei, and J. M. Tang, "Experimental demonstration of a record high 11.25Gb/s real-time optical OFDM transceiver supporting 25km SMF end-to-end transmission in simple IMDD systems," Opt. Express **18**, 5541-5555, 2010

[30] Hillerkuss, D.; Schellinger, T., Schmogrow, R., Winter, M., Vallaitis, T., Bonk, R., Marculescu, A., Li, J., Dreschmann, M., Meyer, J., Ben Ezra, S., Narkiss, N., Nebendahl, B., Parmigiani, F., Petropoulos, P., Resan, B., Weingarten, K., Ellermeyer, T., Lutz, J., Möller, M., Hübner, M., Becker, J., Koos, C., Freude, W., Leuthold, J.: "Single source optical OFDM transmitter and optical FFT receiver demonstrated at line rates of 5.4 and 10.8 Tbit/s," in Proc. Optical Fiber Communication (OFC) Conference 2010, paper PDPC1

[31] T. Pfau, S. Hoffmann, R. Peveling, S. Bhandare, S. Ibrahim, O. Adamczyk, M. Porrmann, R. Noé, and Y. Achiam, "First real-time data recovery for synchronous QPSK transmission with standard DFB lasers," IEEE Photon. Technol. Lett., vol. **18**, no. 18, pp. 1907–1909, Sep. 15, 2006.

[32] A.Leven, N. Kaneda, A. Klein, U.-V. Kco, and Y.-K. Chen, "Real-time implementation of 4.4 Gbit/s QPSK intradyne receiver using field programmable gate array," Electron. Lett., vol. **42**, no. 24, pp. 1421–1422, Nov. 23, 2006.

[33] A. Sano, H. Masuda, T. Kobayashi, M. Fujiwara, K. Horikoshi, E. Yoshida, Y. Miyamoto, M. Matsui, M. Mizoguchi, H. Yamazaki, Y. Sakamaki, and H. Ishii, "69.1-Tb/s (432 x 171-Gb/s) C- and Extended L-Band Transmission over 240 Km Using PDM-16-QAM Modulation and Digital Coherent Detection," in Proc. Optical Fiber Communication (OFC) Conference 2010, paper PDPB7, 2010.

[34] X. Zhou, J. Yu, M. Huang, Y. Shao, T. Wang, L. Nelson, P. Magill, M. Birk, P. I. Borel, D. W. Peckham, and R. Lingle, "64-Tb/s (640x107-Gb/s) PDM-36QAM Transmission over 320km Using Both Pre- and Post-Transmission Digital Equalization," in Proc. Optical Fiber Communication (OFC) Conference 2010, paper PDPB9, 2010.

[35] Masato Yoshida, Hiroki Goto, Keisuke Kasai, and Masataka Nakazawa, "64 and 128 coherent QAM optical transmission over 150 km using frequency-stabilized laser and heterodyne PLL detection," Opt. Express **16**, 829-840, 2008.

[36] A. J. Lowery, L. Du, and J. Armstrong, "Orthogonal frequency division multiplexing for adaptive dispersion compensation in long haul WDM systems," in Proc. Optical Fiber Communication (OFC) Conference 2006, paper PDP 39, 2006.

[37] I. B. Djordjevic and B. Vasic, "Orthogonal frequency division multiplexing for high-speed optical transmission," Opt. Express, vol. **14**, pp. 3767–3775, 2006.

[38] U.S. patent 174,465, "Improvement in Telegraphy," Alexander Graham Bell, Mar. 7, 1876.

[39] R. W. Chang, "Synthesis of band-limited orthogonal signals for multichannel data transmission," Bell Sys. Tech. J., vol. **45**, pp. 1775-1796, 1966.

[40] S. B. Weinstein and P. M. Ebert, "Data transmission by frequency division multiplexing using the discrete Fourier transform," IEEE Trans. Communications, vol. **19**, issue: 5, pp. 628-634, Oct. 1971.

[41] A. Peled and A. Ruiz, "Frequency domain data transmission using reduced computational complexity algorithms," In Proc. IEEE International Conference on Acoustics, Speech, and Signal Processing, volume **5**, pp. 964-967, April 1980.

[42] L.J. Cimini, "Analysis and simulation of a digital mobile channel using orthogonal frequency division multiplexing," IEEE Trans. on Communications, vol. COM-**33**, pp. 665-675, July 1985.

[43] B. J. Dixon, R. D. Pollard, and S. Iezekiel, “Orthogonal frequency-division multiplexing in wireless communication systems with multimode fiber feeds,” IEEE Trans. Microwave Theory Tech. 49, 1404-1409, 2001.

[44] A.J. Lowery, L. Du, and J. Armstrong, “Orthogonal frequency division multiplexing for adaptive dispersion compensation in long haul WDM systems,” in Proc. Optical Fiber Communication (OFC) Conference 2006, paper PDP39, 2006.

[45] I. B. Djordjevic and B. Vasic, “Orthogonal frequency-division multiplexing for high-speed optical transmission,” Opt. Express, vol. **14**, pp.3767–3775, May, 2006.

[46] W. Shieh, X. Yi and Y. Tang, “Transmission experiment of multi-gigabit coherent optical OFDM systems over 1000km SSMF fibre,” IEE Electron. Lett., vol. **43**, pp. 183-185, Feb, 2007.

[47] R. You, and J. M. Kahn, “Average power reduction techniques for multiple-subcarrier intensity-modulated optical signals”, IEEE Transaction on Communications, vol. **49**, pp. 2164-2171, 2001.

[48] N. E. Jolley, H. Kee, R. Rickard, and J. Tang, “Generation and propagation of a 1550 nm 10 Gbit/s optical orthogonal frequency division multiplexed signal over 1000 m of multimode fibre using a directly modulated DFB,” in Proc. Optical Fiber Communication (OFC) Conference 2005, paper OFP3, 2005.

[49] A. J. Lowery and J. Armstrong, “Orthogonal-frequency-division multiplexing for dispersion compensation of long-haul optical systems,“ Optics Express, vol. **14**, no. 6, pp.2079-2084, Mar, 2006.

[50] S. Chen, Y. Ma, and W. Shieh, "110-Gb/s Multi-Band Real-Time Coherent Optical OFDM Reception after 600-km Transmission over SSMF Fiber," in Proc. Optical Fiber Communication (OFC) Conference 2010, paper OMS2, 2010.

[51] R. R. Mosier, and R. G. Clabaugh, “Kineplex, a bandwidth-efficient Binary transmission system,” AIEE Transaction, vol. **76**, pp. 723-728, 1958.

[52] M.S. Zimmerman, and A. L. Kirsch, “AN/GSC-10 (KATHRYN) variable rate data modem for HF radio,” AIEE Transaction, vol. **79**, pp. 248-255, 1960.

[53] R. W. Chang, “Synthesis of band-limited orthogonal signals for multichannel data transmission,” Bell Sys. Tech. J., vol. **45**, pp. 1775-1796, 1966.

[54] P. Duhamel and H. Hollmann, “Split-radix FFT algorithm,” IET Elect. Lett., vol. **20**, pp. 14-16, 1984.

[55] S. Hara and R. Prasad, Multicarrier Techniques for 4G Mobile Communications, Artech House, Boston, 2003.

[56] L. Hanzo, M. Munster, B. J. Choi, and T. Keller, OFDM and MC-CDMA for Broadband Multi-User Communications, WLANs and Broadcasting, Wiley, New York, 2003.

[57] Hara, S., and Prasad, R., Multicarrier techniques for 4G mobile communications. Boston, Artech House, 2003.

[58] L. Hanzo, M. Muenster, B. Choi, and T. Keller, OFDM and MC-CDMA for Broadband Multi-User Communications, WLANs and Broadcasting.Wiley, 2003.

[59] J. M. Tang and K. A. Shore, "Maximizing the transmission performance of adaptivelymodulated optical OFDM signals in multimode-fiber links by optimizing analog-to-digital converters," J. Lightwave Technol. **25**, 787-798, 2007.

[60] X. Q. Jin, J. M. Tang, P. S. Spencer, and K. A. Shore, "Optimization of adaptively modulated optical OFDM modems for multimode fiber-based local area networks [Invited]," J. Opt. Networking, vol. **7**, pp.198-214, 2008.

[61] W. Shieh and I. Djordjevic, OFDM for Optical Communications. Amsterdam, The Netherlands: Elsevier, 2009.

[62] W. Shieh, X. Yi, Y. Ma, and Y. Tang, "Theoretical and experimental study on PMD-supported transmission using polarization diversity in coherent optical OFDM systems," Opt. Express, vol. **15**, pp. 9936-9947, 2007.

[63] S. L. Jansen, I. Morita, N. Takeda, and H. Tanaka, "20-Gb/s OFDM transmission over 4,160-km SSMF enabled by RF-Pilot tone phase noise compensation," in Proc. Optical Fiber Communication (OFC) Conference 2007, paper PDP15, Anaheim, CA, USA, 2007.

[64] E. Yamada, A. Sano, H. Masuda, T. Kobayashi, E. Yoshida, Y. Miyamoto, Y. Hibino, K. Ishihara, Y. Takatori, K. Okada, K. Hagimoto, T. Yamada, and H. Yamazaki, "Novel no-guardinterval PDM CO-OFDM transmission in 4.1 Tb/s (50 88.8-Gb/s) DWDM link over 800 km SMF including 50-GHz spaced ROADM nodes" in Proc. Optical Fiber Communication (OFC) Conference 2008, paper PDP8, San Diego, CA, USA, 2008.

[65] W. Shieh, X. Yi, and Y. Tang, "Transmission experiment of multi-gigabit coherent optical OFDM systems over 1000 km SSMF fiber," Electron. Lett., **43**, 183-185, 2007.

[66] P. J. Winzer, G. Raybon, and M. Duelk, "107-Gb/s optical ETDM transmitter for 100 G Ethernet transport," in European Conference on Optical Communication 2005, Paper Th4.1.1, Glasgow, Scotland 2005.

[67] C. R. S. Fludger, T. Duthel, D. van den Borne, C. Schulien, E-D. Schmidt, T. Wuth, E. de Man, G. D. Khoe, and H. de Waardt, "10 x 111 Gbit/s, 50 GHz Spaced, POLMUX-RZ-DQPSK Transmission over 2375 km Employing Coherent Equalisation," in Proc. Optical Fiber Communication (OFC) Conference 2007, paper PDP22, Anaheim, CA 2007.

[68] W. Shieh, H. Bao, and Y. Tang, "Coherent optical OFDM: theory and design," Opt. Express **16**, 841-859, 2008.

[69] A. D. Ellis and F. C. G. Gunning, "Spectral density enhancement using coherent WDM," IEEE Photon. Technol. Lett., **17**, 504-506, 2005.

[70] A. Sano, E. Yoshida, H. Masuda, T. Kobayashi, E. Yamada, Y. Miyamoto, F. Inuzuka, Y. Hibino, Y. Takatori, K. Hagimoto, T. Yamada, Y. Sakamaki, "30 x 100-Gb/s all-optical OFDM transmission over 1300 km SMF with 10 ROADM nodes," in European Conference on Optical Communication 2007, Paper PD 1.7, Berlin, Germany, 2007.

[71] T. Kobayashi, A. Sano, E. Yamada, Y. Miyamoto, H. Takara, and A. Takada, "Electro-optically subcarrier multiplexed 110 Gb/s OFDM signal transmission over 80 km SMF without dispersion compensation" Electron. Lett., **44**, 225-226, 2008.

[72] Y. Tang, W. Shieh, X. Yi, and R. Evans, "Optimum design for RF-to-optical up-converter in coherent optical OFDM systems," IEEE Photon. Technol. Lett., **19**, 483 – 485, 2007.

[73] S. L. Jansen, I. Morita, N. Takeda, and H. Tanaka, "20-Gb/s OFDM Transmission over 4,160-km SSMF Enabled by RF-Pilot Tone Phase Noise Compensation, " in Proc. Optical Fiber Communication (OFC) Conference 2007, paper PDP15, 2007.

[74] B.R. Washburn, S.A. Diddams, N.R. Newbury, J.W. Nicholson, M.F. Yan, and C.G. Jorgensen, "Phaselocked, erbium-fiber-laser-based frequency comb in the near infrared," Optics Lett. **29**, pp. 250-252, 2004.

[75] Y. Wang, Z. Pan, C. Yu, T. Luo, A. Sahin, and A.E. Willner, "A multi-wavelength optical source based on supercontinuum generation using phase and intensity

modulation at the line-spacing rate," in European Conference on Optical Communication 2003, Paper Th3.2.4, Rimini, Italy, 2003.

[76] W. Shieh, "Coherent optical MIMO-OFDM for optical fibre communication systems," workshop 5, European Conference on Optical Communication, 2007.

[77] S. L. Jansen, I. Morita and H. Tanaka, "16x52.5-Gb/s, 50-GHz spaced, POLMUX-CO-OFDM transmission over 4,160 km of SSMF enabled by MIMO processing KDDI R&D Laboratories," in European Conference on Optical Communications, paper PD1.3, 2007.

[78] J. Armstrong, "Analysis of new and existing methods of reducing intercarrier interference due to carrier frequency offset in OFDM," IEEE Transactions on Communications, vol. **47**, pp. 365-369, 1999.

[79] X. Yi, W. Shieh, and Y. Ma, "Phase Noise Effects on High Spectral Efficiency Coherent Optical OFDM Transmission," J. of Lightwave Technology, vol. **26**, pp. 1309-1316, 2008.

[80] F. Derr, "Coherent optical QPSK intradyne system: concept and digital receiver realization," J. Lightwave Technol., vol. **10**, pp. 1290-1296, Sept. 1992

[81] L. G. Kazovsky, "Phase- and polarization-diversity coherent optical techniques," J. Lightwave Technol., vol. **7**, pp. 279-292, Feb. 1989.

[82] M. G. Taylor, "Coherent detection method using DSP for demodulation of signal and subsequent equalization of propagation impairments," Photon. Technol. Lett., vol.**16**, pp. 674-676, Feb. 2004.

[83] R. Noe, "Phase noise-tolerant synchronous QPSK/BPSK baseband-type intradyne receiver concept with feedforward carrier recovery," J. Lightwave Technol., vol. **23**, pp. 802-808, Feb. 2005.

[84] S. Savory, "Digital filters for coherent optical receivers," Optics Express, vol. **16**, pp. 804-817, Jan. 2008.

[85] N. Kaneda and A. Leven, "Coherent polarization-division-multiplexed QPSK receiver with fractionally spaced CMA for PMD compensation," Photon. Technol. Lett., vol.**21**, no. 4, pp. 203-205, Feb. 2009.

[86] Wireless LAN medium access control (MAC) and physical layer specifications (PHY), IEEE Standard 802.11a, 1999.

[87] T. M. Schmidl and D. C. Cox, “Robust frequency and timing synchronization for OFDM,” IEEE Trans. Commun., vol. **45**, pp. 1613–1621, Dec. 1997.

[88] Q. Yang, N. Kaneda, X. Liu, and W. Shieh, “Demonstration of frequency-domain averaging based channel estimation for 40-Gb/s CO-OFDM with high PMD,” in Proc. Optical Fiber Communication (OFC) Conference 2009, paper OWM6, 2009.

[89] A. J. Viterbi, and A. M. Viterbi, “Nonlinear Estimation of PSK-Modulated Carrier Phase with Application to Burst Digital Transmission,” IEEE Trans. Inform. Theory, vol. **29**, pp 543-551, Jul. 1983.

[90] A. Leven, N. Kaneda, U. -T. Koc, and Y. -K. Chen, “Frequency estimation in intradyne reception,” Photon. Technol. Lett., vol.**19**, no. 6, pp. 366-368, Mar. 2007.

[91] N. Kaneda, A. Leven, and Y.-K. Chen, “Block length effect on 5.0 Gbit/s real-time QPSK intradyne receivers with standard DFB laser,” Electron. Lett., vol. **43**, pp. 1106-1107, Sep, 2007.

[92] Simin Chen, Qi Yang, Yiran Ma, and William Shieh, "Real-Time Multi-Gigabit Receiver for Coherent Optical MIMO-OFDM Signals," J. Lightwave Technol. **27**, 3699-3704, 2009.

[93] H. Takahashi et al., “8x66.8-Gbit/s coherent PDM-OFDM transmission wover 640 km of SSMF at 5.6-bit/s/Hz spectral efficiency,” in European Conference on Optical Communication 2008, post-deadline paper Th.3.E.4, 2008.

[94] H. Takahashi et al., “DWDM transmission with 7.0-bit/s/Hz spectral efficiency using 8x65.1-Gb/s coherent PDM-OFDM signals,” in Proc. Optical Fiber Communication (OFC) Conference 2009, post-deadline paper PDPB7, 2009.

[95] G. Ungerboeck, “Trellis-coded modulation with redundant signal sets part I/II”, IEEE Commun. Mag. **25**, 5-22, 1987.

[96] H. Buelow, G. Thielecke, and F. Buchali, “Optical trellis coded modulation (oTCM),” in Proc. Optical Fiber Communication (OFC) Conference 2004, Paper WM5.

[97] H. Zhao, E. Agrell, and M. Karlsson, “Trellis-coded modulation in PSK and DPSK communications,” in European Conference on Optical Communication 2006, paper We.3.P.93, 2006.

[98] M. S. Kumar, H. Yoon, and N. Park, “Performance evaluation of trellis code modulated oDQPSK using the KLSE method,” IEEE Photon. Technol. Lett. **16**, 1245-1247, 2007.

[99] T. Sakamoto, A. Chiba, I. Morhashi, and T. Kawanishi, "Optical trellis-coded modulation with multi-parallel MZM," in European Conference on Optical Communication 2009, paper P.3.17, 2009.

[100] Qi Yang, Yiran Ma, and William Shieh, "1-Tb/s Signal-channel Coherent Optical OFDM Transmission with Trellis-coded Modulation", Electronics Letters, pp 1045 - 1047, 2009

[101] X. Liu and F. Buchali, "Novel channel estimation method for PDM-OFDM enabling improved tolerance to WDM nonlinearity," in Proc. Optical Fiber Communication (OFC) Conference 2009, paper OWW5, 2009.

[102] X. Liu and F. Buchali, "Intra-symbol frequency-domain averaging based channel estimation for coherent optical OFDM," Opt. Express **16**, 21944-21957, 2008.

[103] X. Liu, S. Chandrasekhar, A. H. Gnauck, and R. W. Tkach, "Experimental demonstration of joint SPM compensation in 44-Gb/s PDM-OFDM transmission with 16-QAM subcarrier modulation," in European Conference on Optical Communication 2009, paper 2.3.4, 2009.

[104] I. B. Djordjevic, M. Cvijetic, L. Xu, and T. Wang, "Using LDPC-coded modulation and coherent detection for ultra high-speed optical transmission," IEEE/OSA J. Lightwave Technol., **25**, pp. 3619-3625, 2007.

[105] I. B. Djordjevic, H. G. Batshon, Lei Xu and T. Wang, "Coded polarization-multiplexed iterative polar modulation (PM-IPM) for beyond 400 Gb/s serial optical transmission," in Proc. Optical Fiber Communication (OFC) Conference 2010, Paper No. OMK2, 2010.

[106] I. B. Djordjevic, and Vasic, B. "Multilevel Coding in M-ary DPSK/Differential QAM High-Speed Optical Transmission with Direct Detection," IEEE/OSA J. Lightw. Technol., vol. **24**, pp. 420-428, Jan. 2006.

[107] M. Arabaci, I. B. Djordjevic, R. Saunders, and R. M. Marcoccia, "Non-binary Quasi-Cyclic LDPC based coded modulation for beyond 100 Gb/s transmission," IEEE Photon. Technol. Lett., vol. **22**, no. 6, pp. 434 - 436, March 15, 2010.

[108] I. B. Djordjevic, Lei Xu, and Ting Wang, "Beyond 100 Gb/s optical transmission based on polarization multiplexed coded-OFDM with coherent detection," J. Opt. Commun. Netw. **1**, 50-56, 2009.

[109] I. B. Djordjevic, M. Arabaci, and L. Minkov, "Next generation FEC for high-capacity communication in optical transport networks," J. Lightw. Technol., **27**, no. 16, pp. 3518–3530, 2009.

[110] Mizuochi, T., Konishi, Y., Miyata, Y., Inoue, T., Onohara, K., Kametani, S., Sugihara, T., Kubo, K., Yoshida, H., Kobayashi, T., and Ichikawa, T., "Experimental demonstration of concatenated LDPC and RS codes by FPGAs emulation," Photonics Technology Letters, IEEE, **21**, no.18, pp.1302-1304, 2009.

[111] Mizuochi, T., "Next Generation FEC for optical communication," Optical Fiber communication/National Fiber Optic Engineers Conference, 2008. OFC/NFOEC 2008. Conference on , vol., no., pp.1-33, 24-28 Feb. 2008.

[112] S.Y. Chung, G. D. Forney, T. J. Richardson, and R. Urbanke, "On the design of low-density parity-check codes within 0.0045 dB of the Shannon limit," IEEE Commun. Lett., vol. 5, pp. 58–60, Feb. 2001.

[113] D.J.C. Mackay. Ldpc database. Available at http://www.inference.phy.cam.ac.uk/mackay/codes/data.html.

[114] A. Tychopoulos, "FEC in optical communications," IEEE Circuits Devices Mag., **22**, no. 6, pp. 79–86, Nov./Dec. 2006.

[115] R. G. Gallager, Low Density Parity Check Codes, MIT Press, Cambridge, Mass., 1963.

[116] D. J. C. MacKay and R. M. Neal,"Near Shannon limit performance of low density parity check codes," Electronics Letters **32** (18): 1645-1646, 1996.

[117] S. J. Johnson., S. R. Weller, "Low-density parity-check codes: design and decoding", Wiley Encyclopedia of Telecommunications, John Wiley and Sons, 2003.

[118] Bernhard M. J. Leiner, "LDPC codes - a Brief Tutorial," April 2005.

[119] Q. Yang, N. Kaneda, X. Liu, and W. Shieh "Demonstration of frequency-domain averaging based channel estimation for 40-Gb/s CO-OFDM with high PMD," in Proc. Optical Fiber Communication (OFC) Conference 2009, paper OWM6, 2009.

[120] Y. George, O.Amrani, "Bit loading algorithms for OFDM", ISIT 2004.Chicago, pp. 388, 2004.

[121] B. S. Krongold, K. Ramchandran, D.L. Jones, "Computationally efficient optimal-power allocation algorithms for multicarrier communication systems," IEEE Trans. on Com. **48**, pp. 23-27,2000.

[122] S.C.J. Lee, F. Breyer, S. Randel, J. Zeng, F. Huijskens, H. P. A. van den Boom1, A. M. J. Koonen, and N. Hanik, "24-Gb/s Transmission over 730 m of Multimode Fiber by Direct Modulation of an 850-nm VCSEL Using Discrete Multi-Tone Modulation," in Proc. Optical Fiber Communication (OFC) Conference 2007, paper PDP 6, 2007.

[123] L. Christen, Y.K. Lize, S. Nuccio, J.-Y. Yang, N. Jayachandran, P. Ebrahimi, A.E. Willner, R. Kashyap, and Loukas Paraschis, "Multi-format Continuously Variable Bitrate DPSK/OOK Demodulating Receiver Design," in European Conference on Optical Communications (ECOC), paper Tu3.2.4, Cannes, France, 2006.

Appendix A

Acronyms

ADC	analog-to-digital converter
ASIC	application-specific integrated circuit
AWG	Arbitrary Waveform Generator
BER	bit error ratio
CD	chromatic dispersion
CMOS	complementary metal–oxide semiconductor
CO-OFDM	coherent optical OFDM
CP	cyclic prefix
CP	cyclic prefix
DAC	digital-to-analog converter
DCF	dispersion compensating fiber
DD	direct detection
DGD	differential group delay
DSP	digital signal processing
ECL	external-cavity laser
EDFA	erbium-doped fiber amplifier
FDM	frequency division multiplexing
FFT	fast Fourier transform
FIFO	first-in-first-out
FPGA	field-programmable gated array
GI	guard interval
IBI	inter-band interference
IC	integrated circuit
IM	intensity modulation
ISI	inter symbol interference
LD	Laser Diode
MZM	Mach-Zenhder Modulator

OFDM	orthogonal frequency-division multiplexing
OLO	optical local oscillator
OSNR	optical signal noise ratio
P/S	parallel-to-serial conversion
PAPR	peak-to-average power ratio
PBS	polarization-beam splitter
PD	Photodiode
PIN-TIA	transimpedance amplifier
PMD	polarization mode dispersion
PRBS	pseudo-random bit sequences
RSO	real-time sampling oscilloscope
SSMF	standard signal mode fiber
TCM	trellis-coded modulation
TDS	Time Domain-sampling Scope
TS	training symbol
VGA	variable gain amplifier
WDM	wavelength division multiplexing
XC-OFDM	cross-channel OFDM